Effects of High Temperature Treatment on Curl And Microstructure of Heavily Boron Doped Silicon

by

Denise M. Bruce, Capt, USAF

Degree Awarded: Master of Science (Materials Science and Engineering)
Institution: Massachusetts Institute of Technology, Cambridge, MA
Year of Degree Award: 1997
Number of Pages: 110

ABSTRACT

An experimental study was performed to investigate the effects of high temperature treatment on the microstructure and curling behavior of heavily boron-doped silicon structures. Cantilever structures were created from p++ boron diffused silicon wafers. The post-diffusion high temperature "anneal" treatment temperature was varied while the anneal time remained constant. The micromechanical cantilevers were analyzed for curl as a function of the anneal temperature using an optical profiler. Bulk sections from the wafers were analyzed to obtain boron concentration using secondary ion mass spectroscopy (SIMS) and to obtain the distribution of lattice constant using x-ray diffraction. Microstructure of plan-view and cross-section samples was investigated with the transmission electron microscope (TEM).

Results of the curl measurements revealed that all non-annealed cantilever structures were curled in one direction, and those annealed for 90 minutes above 1100°C were all curled in the other direction, with an apparent transition temperature of about 1050°C.

SIMS analysis confirmed that boron concentration becomes more uniform through the wafer thickness with increasing anneal temperature. X-ray diffraction revealed that the magnitude of the smallest lattice constant present in a wafer increases with increasing anneal temperature. TEM observations showed that dislocation and precipitate density do not change with anneal temperature.

REPORT DOCUMENTATION PAGE

Form Approved
OMB No. 0704-0188

1. AGENCY USE ONLY *(Leave blank)*	2. REPORT DATE	3. REPORT TYPE AND DATES COVERED
	17 Apr 97	

4. TITLE AND SUBTITLE
Effects of High Temperature on Curl and Microstructure of Heavily Boron Doped Silicon

5. FUNDING NUMBERS

6. AUTHOR(S)
Denise M. Bruce

7. PERFORMING ORGANIZATION NAME(S) AND ADDRESS(ES)
Massachusetts Institute of Technology, Cambridge MA

8. PERFORMING ORGANIZATION REPORT NUMBER
97-015

9. SPONSORING/MONITORING AGENCY NAME(S) AND ADDRESS(ES)
DEPARTMENT OF THE AIR FORCE
AFIT/CI
2950 P STRRET
WRIGHT-PATTERSON AFB OH 45433-7765

10. SPONSORING/MONITORING AGENCY REPORT NUMBER

11. SUPPLEMENTARY NOTES

12a. DISTRIBUTION AVAILABILITY STATEMENT

12b. DISTRIBUTION CODE

13. ABSTRACT *(Maximum 200 words)*

14. SUBJECT TERMS

15. NUMBER OF PAGES
110

16. PRICE CODE

17. SECURITY CLASSIFICATION OF REPORT	18. SECURITY CLASSIFICATION OF THIS PAGE	19. SECURITY CLASSIFICATION OF ABSTRACT	20. LIMITATION OF ABSTRACT

CSDL-T-1279

EFFECTS OF HIGH TEMPERATURE TREATMENT ON CURL AND MICROSTRUCTURE OF HEAVILY BORON DOPED SILICON

by

Denise M. Bruce

February 1997

Master of Science Thesis
Massachusetts Institute of Technology

The Charles Stark Draper Laboratory, Inc.
555 Technology Square, Cambridge, Massachusetts 02139-3563

Effects of High Temperature Treatment on Curl and Microstructure of Heavily Boron Doped Silicon

by

Denise M. Bruce

B.S. Mechanical Engineering
The Ohio State University, 1992

Submitted to the Department of Materials Science and Engineering
in Partial Fulfillment of the Requirements for the Degree of
Master of Materials Science and Engineering

at the
Massachusetts Institute of Technology
February 1997

Signature of Author Denise M Bruce
Department of Materials Science and Engineering
January 17, 1997

Approved by Kaplesh Kumar
Kaplesh Kumar
Technical Supervisor, Draper Laboratory

Certified by Eugene A. Fitzgerald
Eugene A. Fitzgerald
Thesis Advisor

Accepted by
Linn W. Hobbs
John F. Elliott Professor of Materials
Chairman, Department Committee on Graduate Students

Effects of High Temperature Treatment on Curl And Microstructure of Heavily Boron Doped Silicon

by

Denise M. Bruce

Submitted to the Department of Materials Science and Engineering
on January 17, 1997 in Partial Fulfillment of the Requirements for
the Degree of Master of Materials Science and Engineering

ABSTRACT

An experimental study was performed to investigate the effects of high temperature treatment on the microstructure and curling behavior of heavily boron-doped silicon structures. Cantilever structures were created from p++ boron diffused silicon wafers. The post-diffusion high temperature "anneal" treatment temperature was varied while the anneal time remained constant. The micromechanical cantilevers were analyzed for curl as a function of the anneal temperature using an optical profiler. Bulk sections from the wafers were analyzed to obtain boron concentration using secondary ion mass spectroscopy (SIMS) and to obtain the distribution of lattice constant using x-ray diffraction. Microstructure of plan-view and cross-section samples was investigated with the transmission electron microscope (TEM).

Results of the curl measurements revealed that all non-annealed cantilever structures were curled in one direction, and those annealed for 90 minutes above 1100°C were all curled in the other direction, with an apparent transition temperature of about 1050°C.

SIMS analysis confirmed that boron concentration becomes more uniform through the wafer thickness with increasing anneal temperature. X-ray diffraction revealed that the magnitude of the smallest lattice constant present in a wafer increases with increasing anneal temperature. TEM observations showed that dislocation and precipitate density do not change with anneal temperature.

Thesis Advisor: Eugene A. Fitzgerald

Title: Associate Professor of Materials Science and Engineering

TABLE OF CONTENTS

	Page
ABSTRACT	2
TABLE OF CONTENTS	3
LIST OF FIGURES	5
LIST OF TABLES	6
ACKNOWLEDGMENTS	7
1. INTRODUCTION	8
2. BACKGROUND THEORY AND LITERATURE REVIEW	10
2.1 Diffusion Theory and Studies	10
2.2 Microstructural Theory and Studies	12
2.2.1 Dislocation Theory	12
2.2.2 X-Ray Theory	14
2.3 Annealing Theory and Studies	15
3. EXPERIMENTAL PROCEDURE	19
3.1 General Approach	19
3.2 Wafer Layout	19
3.3 Tablet Tracking	20
3.4 WYKO Tablet (Cantilever Structures) Design	21
3.5 Wafer Fabrication Process	22
3.6 Test Methods and Equipment	27
3.6.1 WYKO Tablet Cantilever Deflection	27
3.6.2 X-ray Diffraction	28
3.6.3 Transmission Electron Microscopy (TEM)	28
3.6.4 Secondary Ion Mass Spectroscopy (SIMS)	30

TABLE OF CONTENTS (Continued)

	Page
4. RESULTS AND DISCUSSION	32
4.1 Cantilever Structures	32
4.1.1 CS01 Results	33
4.1.2 CS02 Results	35
4.1.3 Comparison of CS01 and CS02	36
4.2 X-ray Diffraction	38
4.3 TEM Observations	41
4.4 SIMS Analysis	42
5. CONCLUSIONS	44
5.1 Cantilever Structures	44
5.2 X-Ray Diffraction	45
5.3 TEM Observations	45
5.4 SIMS Analysis	46
5.5 Correlation Between Microstructural Observations and Curl Reversal	46
6. RECOMMENDATIONS FOR FUTURE WORK	48
APPENDIX A: DERIVATION OF EQUATIONS	49
APPENDIX B: WYKO DATA	52
APPENDIX C: X-RAY DATA	71
APPENDIX D: TEM PHOTOGRAPHS	86
APPENDIX E: SIMS DATA	91
REFERENCES	109

LIST OF FIGURES

		Page
Figure 1:	Diamond Cubic Slip System	13
Figure 2:	Wafer Tablet Layout	20
Figure 3:	WYKO Tablet Layout	22
Figure 4:	Pictorial Representation of Wafer Processing	25
Figure 5:	Comparison of Beam Tip Deflections for CS01 Wafers	33
Figure 6:	Linear Trendlines for Beam Tip Deflections for CS01 Wafers	34
Figure 7:	Prediction of Curl Reversal Anneal Temperature	35
Figure 8:	Comparison of Beam Tip Deflections for CS02 Wafers	36
Figure 9:	Comparison of Tip Deflections for CS01 and CS02 1100°C Annealed Wafers	37
Figure 10:	Comparison of Control Wafer Tip Deflections with Theory	38
Figure 11:	Normalized θ - 2θ Scan Plots	39
Figure 12:	Comparison of Boron Profiles for CS02 Control and 1100°C Wafers	43
Figure 13:	CS02-A Cross-Section Sample Dislocations	86
Figure 14:	CS02-F Cross-Section Sample Dislocations	87
Figure 15:	CS02-A Plan-View Sample Kikuchi Pattern	88
Figure 16:	CS02-A Plan-View Sample Dislocations and Precipitates	88
Figure 17:	Plan-View Sample Precipitate-Free Region (CS01-1175°C Test Wafer)	89
Figure 18:	Plan-View Sample Dislocations and Precipitates (CS01-1175°C Test Wafer)	89
Figure 19:	Plan-View Sample Precipitates -- Boxed Region of Figure 18 (CS01-1175°C Test Wafer)	90

LIST OF TABLES

	Page
Table 1: Primary Lattice Constants	40
Table 2: Cross-Section TEM Sample First Dislocation Depth	41

ACKNOWLEDGMENTS

Special thanks to my Draper Laboratory advisor, Kaplesh Kumar, for convincing me that this project was a worthwhile endeavor and to my MIT advisor, Gene Fitzgerald, for spending so much time getting me up to speed on the previous work, and for teaching me how to get something useful from the TEM! I would also like to thank Connie Cardoso of Draper Laboratory for her endless patience and help with getting my experimental wafers fabricated, Ken Wu of MIT for teaching me TEM sample preparation, Mayank Bulsara of MIT for running my x-ray diffraction samples, Bill Lampert and Jim Solomon of Wright Laboratory for running my SIMS samples, and the Air Force for making me a reasonably well-paid graduate student. Last, but far from least, many thanks to my husband, Jeff, for inspiring me to get started on the writing and supporting me through long hours of homework, ion milling, TEM work, and more writing.

This thesis was prepared at The Charles Stark Draper Laboratory, Inc. with funding provided by a Draper Independent Research and Development project.

January 17, 1997

Chapter 1: INTRODUCTION

Heavy boron doping is routinely used in the fabrication of silicon structures for micromechanical applications. Boron increases the resistance of silicon to some etchants, thus allowing fabrication of thin structures, such as cantilevers and membranes [1]. The high boron concentration ($\sim 10^{20}$ cm^{-3}) has the unfortunate side effect of contracting the pure silicon lattice [2]. Non-uniform concentrations of boron through the thickness of a micromechanical structure lead to unwanted curl due to the stresses associated with the compositional variations.

A typical process for creating micromechanical structures involves creating mesas (elevated regions) on the front (shiny) surface of a silicon wafer by masking the areas to become mesas and etching away a few microns from the rest of the front surface. Next, boron is diffused into the wafer from the front surface. Then, the wafer is subjected to a high temperature "anneal" treatment to achieve greater uniformity in boron concentration. Structures are formed by masking the wafer with the structure pattern and performing a deep etch of the front surface. A glass wafer can then be bonded to the silicon wafer using the mesas as bond points. The final step releases the structures by etching away all silicon that does not contain enough boron to stop the etchant. Since the highest boron concentrations will be near the front surface, this final step will etch away silicon from the back surface until the etch-stop boron concentration is reached.

Since the anneal step is performed to reduce the curl of the final micromechanical structures, it would be best to anneal after the structure has been released. However, this

is not always practically possible, due to other processing temperature limitations. For example, the silicon-to-glass bond cannot withstand the high temperatures required for annealing. In this case, the anneal is performed before structure release, which makes optimizing the anneal process very difficult. An additional difficulty is the possibility of causing a structure initially curled in one direction to curl in the opposite direction with the annealing process.

It is the goal of this thesis to postulate an ideal anneal treatment and to understand the different effects that may contribute to the curl-reversal behavior. Three parameters are investigated under several different anneal conditions, namely: 1) change in lattice constant, 2) dislocation movement, and 3) actual boron distribution. These effects are correlated with anneal temperature and observations of physical curling in cantilever structures.

Chapter 2: BACKGROUND THEORY AND LITERATURE REVIEW

The literature revealed substantial interest in curling of micromechanical silicon structures, since it is a significant problem in many applications. However, no experimental work was found which carried out a complete study of the effects of different high temperature treatments on microstructure and correlated those results with measurements of physical structural curling. To conduct this study, it was important to understand several key concepts. Diffusion, microstructure, and annealing are reviewed below along with discussions of applicable literature.

2.1 Diffusion Theory and Studies

Boron is diffused into silicon wafers from the front surface during processing in order to create an etch-stop to define structure thickness. The boron concentration required for an ethylenediamine-pyrazene-catechol (EDP) etch-stop in silicon is about $7x10^{19}cm^{-3}$, which results in even higher front surface concentrations.

Normal diffusion follows Fick's Second Law, which is:

$$\frac{\partial C(x, t)}{\partial t} = \frac{\partial}{\partial x}\left(D \frac{\partial C}{\partial x}\right). \qquad (1)$$

In the above equation, D is the diffusion coefficient which changes according to substrate and diffused elements, and diffusion conditions. The variables C, t, and x stand for diffused species concentration, diffusion time, and diffusion depth respectively. Solving this equation for a solid source diffusion into a semi-infinite slab gives equation (2) [3].

$$C(x, t) = C_s \operatorname{erfc}\left(\frac{x}{2\sqrt{Dt}}\right) \qquad (2)$$

In equation (2), C_s is surface concentration and erfc is the complementary error function. Unfortunately, for high concentration ($>10^{19}$ cm^{-3}) diffusions of boron in silicon, this simple model does not correctly predict the actual diffusion.

At high doping densities, the diffusion coefficient is not constant, but exhibits a dependence on local boron concentration [4, 5]. In 1969, Thai [4] proposed a theoretical model for diffusion of boron in silicon that incorporated a concentration dependent diffusion coefficient. He postulated that dislocation multiplication and movement caused an increase in local vacancy concentration. In 1975, Fair [5] described the concentration dependence of boron diffusivity in silicon, and created theoretical high concentration boron diffusion profiles in silicon for diffusions performed in non-oxidizing ambients. An oxidizing environment also affects boron atom mobility [6], and further complicates a prediction of boron concentration profile.

Secondary ion mass spectroscopy (SIMS) data of deep boron diffusion profiles with no anneal show that variation in boron concentration from about 1μm depth to the etch-stop ($7x10^{19}cm^{-3}$ in EDP) is reasonably linear [7]. To obtain a simple model for the curling expected in an as-diffused cantilever structure, a linear gradient of boron will be assumed. Furthermore, it will be assumed that no relaxation of the lattice has occurred. Equation (3) gives vertical deflection, v, for a linear boron gradient through the thickness of a rectangular cantilever structure. See Appendix A for the derivation of equation (3).

$$\boxed{v = \frac{\alpha_T - \alpha_B}{2\, h\, \alpha_{Si}}\, y^2} \qquad (3)$$

In the above equation, α_T is the lattice constant at the top surface, α_B is the lattice constant at the bottom surface, α_{Si} is the lattice constant of pure silicon, h is the cantilever beam height, and y is the distance along the length of the cantilever beam. Positive values of v indicate downward deflections.

2.2 Microstructural Theory and Studies

Dislocation and x-ray theory are discussed in this section.

2.2.1 Dislocation Theory

When boron diffuses into silicon, it primarily enters substitutional sites in the silicon structure. Since the boron atom is smaller than the silicon atom, its presence will shrink the region it occupies, resulting in a tensile stress within the material. When the strain energy present exceeds the energy required to form a dislocation (dislocation energy) a dislocation will form to introduce plastic relaxation of the material [8]. These dislocations are called misfit dislocations. With higher boron concentration, strain energy becomes higher, and more dislocations are created.

Pure silicon has a diamond cubic crystal structure, which has a primary slip system (slip plane / slip direction) of {111} / <110>, as shown in Figure 1. Misfit dislocations of 60° type would be expected with this slip system. However, 60° dislocations may combine to form edge dislocations.

In 1964, Washburn, Thomas, and Queisser [9] examined misfit dislocations caused by phosphorus diffusion in silicon. They used the transmission electron microscope (TEM) to observe dislocations, and found primarily edge dislocations. They also observed that dislocation lines were often decorated by precipitates.

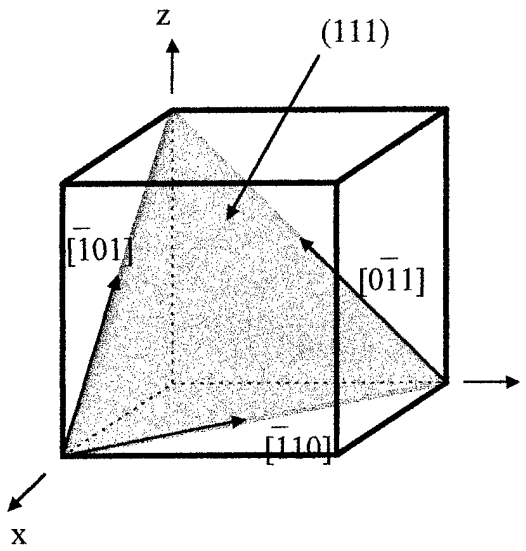

Figure 1: Diamond Cubic slip system.

A plan-view and cross-sectional TEM study of dislocations in heavily boron-doped silicon was done by Ning and Pirouz in 1991 [10]. They showed a dislocation free zone near the surface, with a layer containing dislocations beneath. Thicknesses of the dislocation-free zone and the layer of dislocations were found to be functions of diffusion time. Dislocations were found to be mostly of 60° type with some screw. The Burgers vector was determined to be ½<110>. Another TEM study was done by Ning, Pirouz, Mehregany, and Chu in 1991 [11] which compared the microstructures of heavily boron-doped silicon subjected to thermal oxidation or having a surface layer of borosilicate glass. Their cross-sectional TEM work did not reveal significant differences.

After dislocation glide has removed the lattice mismatch stress, the dislocations will not move without some sort of external stress. The stress required to cause dislocation motion decreases with increasing temperature. Presence of obstructions, such as precipitates, will increase the required stress.

When the temperature of a wafer is raised in the anneal process, boron diffusion occurs. Changing the boron concentration in a relaxed lattice will introduce a stress. If the stress and temperature combination is high enough, dislocations may move by glide or climb.

In 1970, Erofeev and Nikitenko [12] studied mobility of dislocations in silicon containing impurities, and observed that the activation energy for dislocation motion decreases with increasing electrically active impurity concentration. The effect for donor impurities was stronger than for acceptor.

2.2.2 X-Ray Theory

A relaxed boron-silicon lattice will have a lattice constant smaller than that of pure silicon. In 1991, Baribeau and Rolfe [13] determined variation of the lattice constant of boron-doped silicon as a function of dopant concentration using SIMS and x-ray diffraction. They found a linear relationship between boron concentration and lattice constant. In 1992, Holloway and McCarthy [2] did a thorough review of previous work in determination of lattice contraction of boron-doped silicon.

X-ray diffraction is often used to determine lattice constants associated with a crystalline material using Bragg's law, given in equation (4).

$$n\lambda = 2\,d\sin(\theta_B) \qquad (4)$$

In the Bragg equation, n is an integer, λ is the x-ray beam wavelength, d is the interplanar spacing and θ_B is the Bragg angle. The lattice constant, α, is related to the interplanar spacing, d, of the (hkl) plane by equation (5).

$$\alpha = d\sqrt{h^2 + k^2 + l^2} \qquad (5)$$

A "triple axis θ - 2θ" scan is often used to determine lattice constants with x-ray diffraction. When the x-ray beam leaves the emitter, it passes through a "first crystal" and a narrow slit to minimize $\Delta\lambda$ and to collimate the beam. It then reflects from the sample and passes through another collimator before entering the detector. The term "triple axis" comes from the fact that the beam is redirected at three points: the first crytal, the sample, and the final collimator.

In x-ray diffraction, the Bragg angle, θ_B, is the angle between the incident x-ray beam and the sample surface normal. The diffracted beam will leave the sample at twice the Bragg angle from the incident beam, or $2\theta_B$. While scanning the sample, the x-ray emitter is stationary while the sample rotates to change θ_B. For the detector to receive the diffracted beam, it must rotate by 2θ for every θ rotation of the sample. This procedure explains the term "θ - 2θ scan."

A triple axis θ - 2θ scan will show a narrow peak for the silicon lattice, and other peaks for other lattice constants. The plot of this scan uses seconds (1/3600 of a degree) for the abscissa. The Bragg angle associated with a given reflection in pure silicon is known, and the difference in seconds from the silicon peak to other peaks can be measured. Therefore, the Bragg angles for the other peaks can be computed, and thus the lattice constants determined.

2.3 Annealing Theory and Studies

A high temperature anneal treatment is often used to reduce curl in micromechanical structures by creating a more uniform boron distribution through the structure thickness.

In 1990, Ding, Ko, and Mansour [14] created cantilever beams from boron-diffused silicon. They presented optimum anneal conditions for beam flatness with annealing before and after beam release. They did not observe any curl reversal after annealing, but that may have been due to the short beam lengths (600μm) or limitations of the measurement method used. The method used to measure curl was not discussed.

In 1993, Chu and Mehregany [15] investigated the effect of thermal oxidation (an oxidizing anneal) on the residual stress distribution through the thickness of heavily boron-doped silicon films. They looked at as-diffused and thermally oxidized cantilever beam structures, and observed a curl reversal after thermal oxidation at 1100°C for 50 minutes. Also in 1993, Holloway [16] proposed a theoretical solution for curvature of a structure strained by substitutional doping with an arbitrary concentration profile. He postulated that there would be a tendency for curvature with the opposite sense if conditions occurred where diffusion of the dopant was not accompanied by migration of misfit dislocations.

In 1994, Wang, Xu, Lu, Sun, and Wang [17, 18] reported on the effects of rapid thermal annealing of heavily boron-doped silicon. Rapid anneals were done with ten second durations and ~200°C/second heating and cooling rates. They observed that boron atoms can be present in interstitial sites and boron-rich silicon precipitates if the boron concentration exceeds the solid solubility limit in bulk silicon material, which affects lattice distortion. They found that lattice mismatch was proportional to substitutional boron concentration rather than total doping concentration in the range 7.5×10^{19} cm^{-3} to 3.1×10^{20} cm^{-3}. Randomly distributed precipitates cause inhomogeneous strain which results in broadening of the x-ray Bragg reflection peak. They also observed

that boron-rich precipitates dissociate at anneal temperatures above 1100°C and further contract the lattice parameter.

Most recently, in 1995, Cabuz, Fukatsu, Kurabayashi, Minami, and Esashi [19] investigated characteristics of heavily boron-doped silicon mechanical structures. They observed a curl reversal in annealed structures. They explained this behavior by proposing that during the post-diffusion anneal process, low-doped regions experience increasing boron concentration and thus develop tensile stress, while highly-doped regions experience decreasing boron concentration and thus develop compressive stress. They also suggested that a potential solution would be to eliminate formation of dislocations during initial boron diffusion. However, this solution is impractical since it is not possible to prevent dislocations from forming with high concentration boron doping.

The theory presented by Cabuz, et. al. could be tested by investigating boron concentration profiles, lattice constants and dislocations in both as-diffused (curled in one direction) and annealed (curled in the opposite direction) structures. The following results would support the theory.

1) Boron concentration profile becomes more flat after annealing. - The boron gradient through the thickness of an as-diffused wafer causes diffusion of boron when the wafer temperature is elevated during the anneal process. This diffusion will cause the boron distribution to become more uniform.

2) Smallest lattice constants disappear after annealing. - The areas of highest boron concentration before annealing exhibit the smallest lattice constants. During the anneal

treatment, these areas will experience a decrease in boron concentration due to diffusion. A decrease in boron concentration will cause an increase in lattice constant.

3) Dislocations do not move during annealing. - If the dislocations cannot move, areas of increasing boron concentration will develop a tensile stress, while areas of decreasing boron concentration will develop a compressive stress. These stresses would be relaxed if dislocation motion were to occur.

Chapter 3: EXPERIMENTAL PROCEDURE

3.1 General Approach

Several different methods were used to gain information about the effects of different anneal (high temperature treatment) temperatures on micromechanical structures fabricated from heavily boron-doped silicon. Eleven wafers were fabricated by identical processing except for anneal temperature. Two wafers did not undergo the anneal step at all. The other nine wafers were annealed: one at 900°C, one at 950°C, one at 1000°C, one at 1050°C, two at 1100°C, two at 1150°C, and one at 1175°C.

3.2 Wafer Layout

Each 3-inch diameter wafer was designed to contain 44 tablets. Each tablet was 9mm square and contained a specimen for one of five test methods. The five test methods used were optical measurement (WYKO) of cantilever structure deflections, X-ray diffraction, cross-section TEM, plan-view TEM, and Secondary Ion Mass Spectroscopy (SIMS). The corresponding five types of tablets were called WYKO (W), X-ray (X), cross (C), plan (P) and SIMS (S) respectively. The particular placement shown in Figure 2 was chosen to accomplish maximum number of specimens from each wafer, and allow an automated wafer sawing procedure to efficiently produce the specimens.

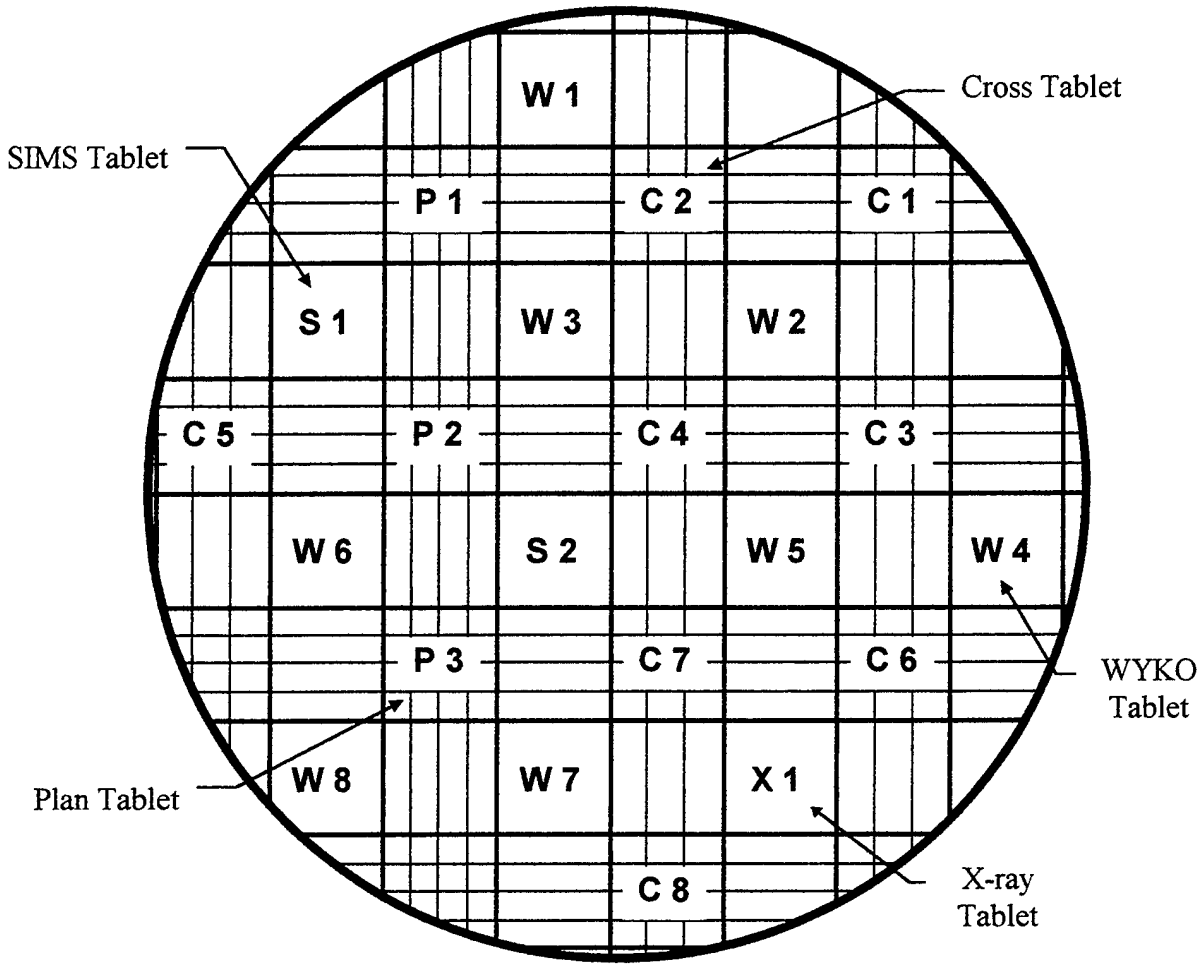

Figure 2: Wafer tablet layout.

3.3 Tablet Tracking

It was important to keep track of the original tablet position on the wafer because previous experimental data had shown that within-wafer variation of properties can be significant. Wafer position designations are included in Figure 2. Each WYKO tablet (cantilever structures) was fabricated with a number on it. X-ray and SIMS tablets were scribed on the back with appropriate numbers before placing them in containers. Tablets

of plan-view and cross-section specimens were placed in separate boxes, which were labeled with appropriate wafer designation and position. WYKO, plan-view and cross-section TEM, and SIMS tablet data from different wafers were only compared when the tablets came from the same wafer positions.

3.4 WYKO Tablet (Cantilever Structures) Design

The WYKO tablets were fabricated with four sets of cantilever beams and two reference structures on each tablet. Each of the four sets of beams had different widths, in particular 30μm, 60μm, 150μm, and 400μm. Several beams of each width were fabricated with various lengths from about 30μm up to about 3700μm. The longest beam length was chosen based on the imaging capability of the WYKO instrument. Each individual beam was attached to glass in the anodic bond processing step by a bond pad. The bond pads were placed such that the beam tips were aligned at a distance of 20μm from a reference structure. The reference structures were fabricated as very short (30μm) ledges protruding from a rectangular bond pad. These ledges were constructed to be too short to allow any measurable curl, and therefore could be used as a common reference point for beam tip measurements. Figure 3 shows the WYKO tablet layout.

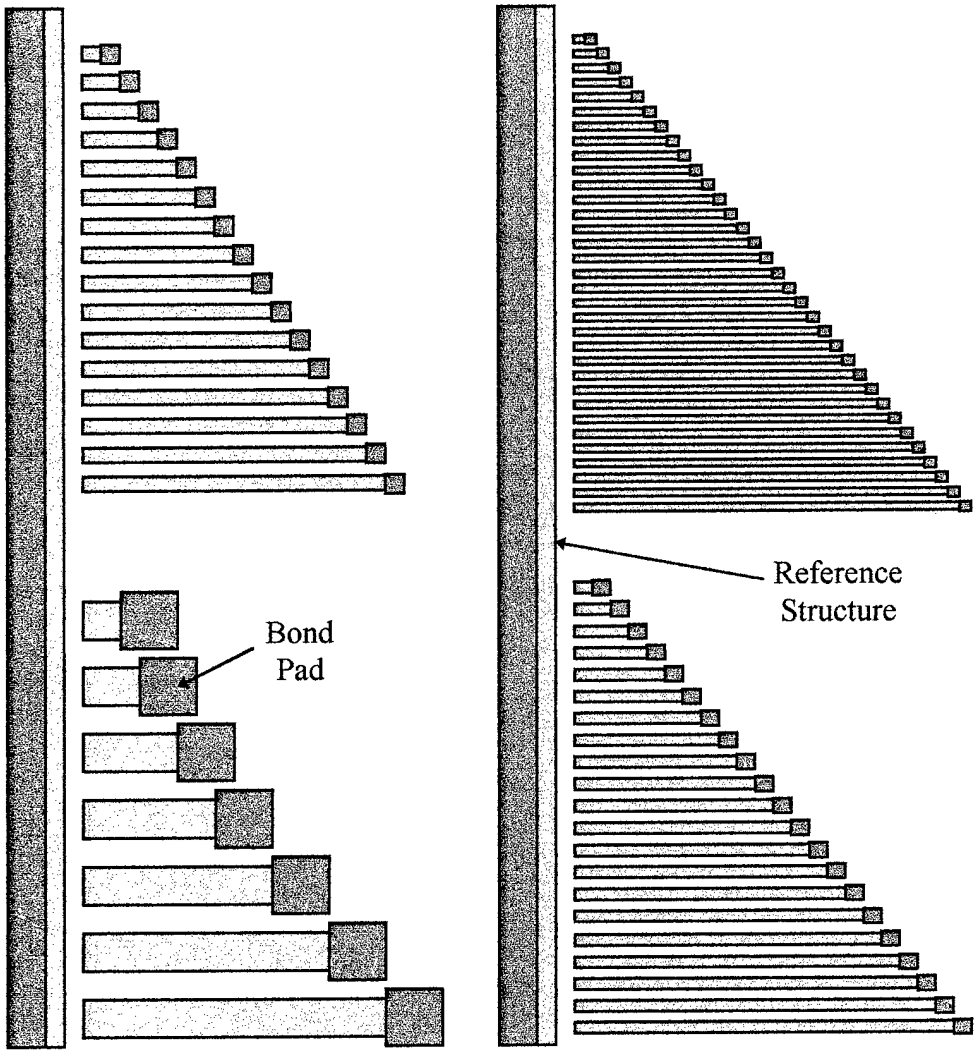

Figure 3: WYKO Tablet Layout

3.5 Wafer Fabrication Process

Before processing was begun, each wafer was scribed on the back with the lot number and a letter designation corresponding to a particular anneal condition. One test wafer was also processed with each experiment wafer. The test wafers did not contain any structures, and were designated by lot number and anneal temperature used. The lot

numbers used were "CS01" and "CS02" which stand for "Curl Study - run #01" and "Curl Study - run #02," respectively.

The wafer processing procedure described below was used to fabricate the wafers. See Figure 4 for an overall pictorial representation of the fabrication process.

KOH Etch - A pattern was created on the front (shiny) side of the wafer using photoresist as a mask. The unmasked portions of the wafer were etched to a depth of about 2.5μm to create "mesas." After etching, the photoresist was stripped off the wafer.

Boron Diffusion - Boron was diffused on the front side from a solid source. Diffusion temperature, duration, and environment were chosen based on experimental data and recommendations from the boron solid source manufacturer. Since many current micromechanical applications require structure thicknesses greater than 10μm, diffusion times are quite long. For this experiment, boron diffusion was done for 20 hours at 1150°C in a 4% oxygen environment to achieve the etch-stop concentration of $7x10^{19}cm^{-3}$ at a depth of about 11μm.

Dilution Oxidation - This step deposited an oxide on the wafer surface to more easily remove the boron-silicide coating (a remnant of boron diffusion) from the wafer front surface.

Oxide Etch - The oxide deposited in the previous step was removed along with the boron-silicide coating.

Plate Anneal - A high temperature treatment was conducted to help distribute the boron more uniformly through the thickness of interest. The term "anneal" is a

bit of a misnomer, but it is used in practice to refer to the post-diffusion high temperature treatment. As mentioned above, two wafers skipped this step. All other wafers were annealed for 90 minutes in a nitrogen and 6% oxygen ambient. Different wafers were subjected to different anneal temperatures, ranging from 900°C to 1175°C.

Reactive Ion Etch (RIE) - This process "digs trenches" straight down into the wafer to define structure edges. As in the KOH etch step, photoresist was used as a mask. All unmasked parts of the wafer were etched. Trench depth was about 25 μm.

Wafer Saw - The wafer was sawed into tablets.

Anodic Bond - The WYKO tablets were anodically bonded to glass substrate tablets. The bond points were the mesas created during the KOH etch step.

Ethylenediamine pyrazene catechol (EDP) Etch - The excess silicon was etched away from the back surface to release the cantilever structures on the WYKO tablets. Pure silicon etched away quickly. The etch rate slowed with increasing boron concentration up to a concentration of about $7x10^{19}$ atoms/cm^3 which provided a nearly complete etch stop.

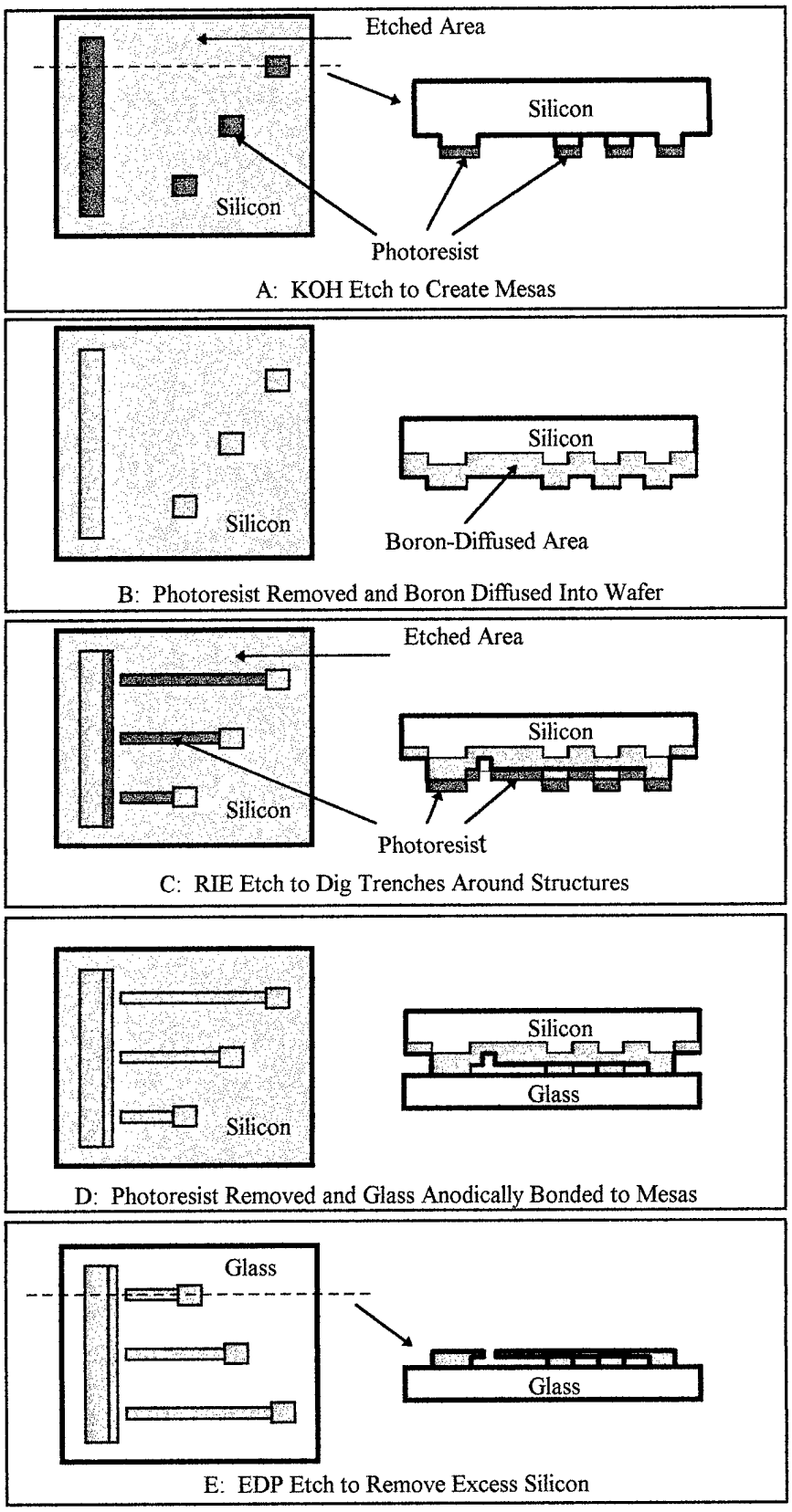

Figure 4: Pictorial Representation of Wafer Processing

CS01 wafer letter "A" was annealed at 1150°C, wafer "B" was annealed at 1100°C, wafer "C" was annealed at 1175°C, and wafer "D" did not undergo the anneal step. Since wafer CS01-D was not annealed it is called the CS01 control wafer.

Initial analysis of the CS01 WYKO tablets revealed that the cantilever structures from wafers A, B and C were all significantly curled up, while the CS01-D structures were all curled down. An RIE mask error was discovered which rendered all the CS01 tablets other than the WYKO tablets unusable. The bulk sections of the wafer had not been properly masked with photoresist prior to the RIE processing step. The RIE mask was repaired to correct the problem, and a second fabrication run, CS02, was done. The CS02 run also included a wider range of anneal temperatures to obtain continuous data from "curled down" beams to "curled up" beams.

CS02 wafer letter "A" was not annealed, wafer "B" was annealed at 900°C, wafer "C" was annealed at 950°C, wafer "D" was annealed at 1000°C, wafer "E" was annealed at 1050°C, wafer "F" was annealed at 1100°C, and wafer "G" was annealed at 1150°C.

After the "wafer saw" step, the various tablets from each wafer were separated into appropriate containers. Only the WYKO tablets completed the last two steps, "anodic bond" and "EDP etch". SIMS tablets were sent out for analysis. TEM specimens were made from both the plan-view and cross-section tablets.

3.6 Test Methods and Equipment

Several different tests were performed on the fabricated wafers to obtain meaningful results. Theories of operation for various types of test equipment used and sample preparation techniques are discussed below.

3.6.1 WYKO Tablet Cantilever Deflection

The WYKO surface profiler was used to measure deflections of the cantilever structures. Data acquired for the "W3" and "W5" tablets for each of the wafers are included in Appendix B.

"WYKO" is a trade name, as opposed to an acronym. The WYKO system is a non-contact optical profiler that can measure a range of surface heights up to 500μm. The vertical resolution of the particular instrument used was limited to about 0.08μm by its second floor location which experiences building vibration.

The WYKO uses a technique called vertical-scanning interferometry (VSI) to measure rough surfaces and steps. The following explanation of operation is taken directly from the WYKO Users Manual [20]: "In VSI, a white-light beam passes through a microscope objective to the sample surface. A beam splitter reflects half of the incident beam to the reference surface. The beams reflected from the sample and the reference surface recombine at the beam splitter to form interference fringes. During the measurement, a reference arm containing the interferometric objective moves vertically to scan the surface at varying heights. Fringe contrast reaches a peak as the sample becomes completely focused, then falls again. The system scans through focus, and the interference signal for each point is recorded. Finally, the vertical position corresponding

to the peak of the interference signal for each point on the surface is extracted, and a computer image of the surface height profile is displayed."

3.6.2 X-ray Diffraction

X-ray measurements were made with the Bede D^3 diffractometer using a silicon first crystal and copper Kα radiation, which gives a characteristic x-ray wavelength, λ, of 1.541Å. The X1 X-ray tablets from the CS01-1175°C test wafer and CS02-A, C, E, and F wafers were analyzed using the triple axis θ - 2θ scan technique to determine lattice constants in the wafers. Data acquired are contained in Appendix C.

For pure silicon with surface normal [001], the first Bragg reflection occurs from the (004) plane with Bragg angle, θ_B, of 34.571°. Using equations (4) and (5) from the Background Theory and Literature Review section and n=1, the interplanar spacing, d, is found to be 1.35788Å, and the lattice constant, α, computed as 5.43154Å.

3.6.3 Transmission Electron Microscopy (TEM)

The JEOL JEM-200CX TEM was used to examine dislocations and precipitates in test samples created under different anneal conditions. Selected photographs taken with the TEM are included in Appendix D.

Plan view TEM samples were prepared to look at the density of dislocations near the wafer surface and to look at the topology of the surface itself. Cross-section TEM samples were used to inspect dislocations throughout the wafer thickness.

The TEM used was capable of tilting the sample about two axes, thus allowing orientation of the sample along a particular crystallographic direction of interest. The

double-tilting capability of the TEM was used to view dislocations. The Kikuchi pattern of a single crystal can be observed when the microscope is in "SA Diffraction" mode. In general, higher index directions produce wider Kikuchi lines. The specimen is tilted until the transmitted beam is placed on one side of the Kikuchi line corresponding to the desired direction. At the correct location, another bright spot will light up on the opposite side of the Kikuchi line, producing a "2-beam" condition. Next, an objective aperture is inserted and centered around the transmitted beam. When the TEM is placed back into "MAG" (regular magnification) mode, the dislocations corresponding to the direction selected will appear as dark lines against a bright background. For more information on Kikuchi patterns and TEM theory and operation, see reference [21].

Plan-View Samples - Plan-view TEM specimens were made from the 2.25mm x 2.25mm specimens of the "P2" plan tablets. Each specimen was mechanically thinned from the back surface of the wafer using a South Bay Technologies Model 145 Lapping and Polishing Fixture. Bulk thinning was accomplished with 320 grit paper and final thinning with 600 grit paper. Polishing was then done with 3μm paper followed by 1μm paper to a mirror finish. Final specimens had an average thickness of about 45μm after mechanical thinning.

After each specimen was thinned and polished, a standard 3mm copper grid was cemented to it. Then the specimen was ion milled from the back side until a hole developed in it, so that the thinned area surrounding the hole could be used for TEM analysis. The final specimen had a normal direction of [001]. After inspecting the specimen surface under TEM, the top side of the specimen was milled to reveal

specimen surface at a depth of approximately 5μm, since dislocations were expected at this depth.

Cross-Section Samples - Cross-section TEM specimens were made from the 2.25mm x 3.00mm samples of the "C4" cross tablets. Four cross-section samples were bonded together to make a specimen "sandwich". The sandwich was then mechanically thinned from the 3.00mm edge to about half the original 2.25mm thickness using the same thinning and polishing method as described above for the plan-view TEM samples. The specimen was then turned over and the procedure repeated until a final polished thickness of about 45μm was accomplished. This procedure produced a viewing normal direction of [011]. After the specimen was thinned and polished, a standard 3mm copper grid was cemented to it. Then the specimen was ion milled from both sides until a hole developed in the center of the specimen, so that the thinned area surrounding the hole could be used for TEM analysis.

3.6.4 Secondary Ion Mass Spectroscopy (SIMS)

SIMS analysis was accomplished at Wright Laboratory, Wright-Patterson Air Force Base, Ohio, using a quadrupole-based SIMS with a mass-filtered 12kV oxygen beam at 70° incidence angle. SIMS depth profiling is a technique used to determine elemental concentrations of dopant and impurity atoms within a material as a function of depth. To generate a depth profile, a primary ion beam is scanned over the sample surface. Atoms are ejected from the surface, with some being positive or negative ions. These ions are collected, mass filtered, and ions with the desired mass are counted using

a mass spectrometer. The material surface is continuously eroded, and thus chemical information is determined as a function of depth.

The S2 SIMS tablets from two wafers were sent to Wright Laboratory at Wright-Patterson Air Force Base, Ohio, for SIMS analysis. SIMS depth profile data for boron content was acquired for the CS02-A wafer (control - no anneal) and the CS02-F wafer (1100°C anneal). Data received are contained in Appendix E.

Chapter 4: RESULTS AND DISCUSSIONS

High temperature treatment and its effects on curl and microstructure of heavily boron-doped silicon were investigated. The results of these investigations are included below, beginning with the direct optical measurement of curl of cantilever structures and followed by results of x-ray diffraction, TEM observations, and SIMS analysis.

4.1 Cantilever Structures

Data taken from the WYKO tablets are included in Appendix B. On most of the WYKO tablets, several beams were missing or broken after completing the EDP etch processing step. Beams that were missing or broken were reported as such in the data recorded in Appendix B.

The WYKO instrument was used to measure cantilever beam deflections. All measurements on the beams that were curled up were taken at the beam tip. These measurements were taken relative to the reference structures. For beams that were curled down, the tips of beams with sufficient length would contact the glass, causing the middle part of the beam to get pushed up. Therefore, for beams that were curled down far enough to touch the glass, a measurement was taken of the highest point on the beam. Since this point was often too far from the reference structure to include in the same measurement, measurements of highest points were taken relative to the glass. This measurement was then converted to a predicted tip deflection (as if the glass was not present) using equation (6), where v_t is the tip deflection, C is a constant, L is the beam

length, and h is the beam thickness. The derivation of equation (6) is included in Appendix A.

$$v_t = \frac{C L^2}{2 h} \qquad (6)$$

4.1.1 CS01 Results

The tip deflection data taken from the 150μm width beams of WYKO tablets number 5 from each wafer is shown graphically in Figure 5.

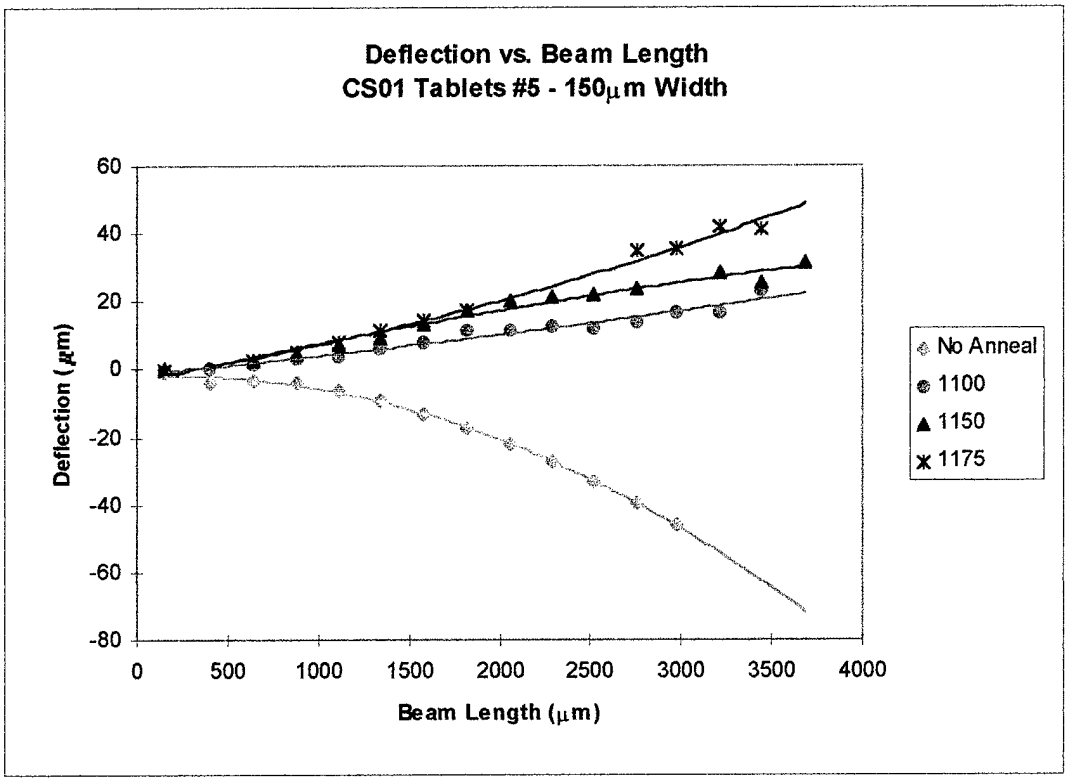

Figure 5: Comparison of Beam Tip Deflections for CS01 Wafers

Figure 5 clearly shows that all cantilever beams are curled down when no anneal is used (wafer CS01-D), and that all beams are curled up when annealed at temperatures of

1100°C and above (wafers CS01-A, B and C). Furthermore, Figure 5 shows that the upward curl becomes greater with increasing anneal temperature.

Unfortunately, none of the anneal temperatures used was low enough to allow the beams to remain curled down. Data from Figure 5 was used to predict the transition point from curled down cantilevers to curled up. First the data points for the 1100°C, 1150°C, and 1175°C wafers were plotted again and each data set was fit with a linear trendline. These data points, along with the trendline formulae are shown in Figure 6.

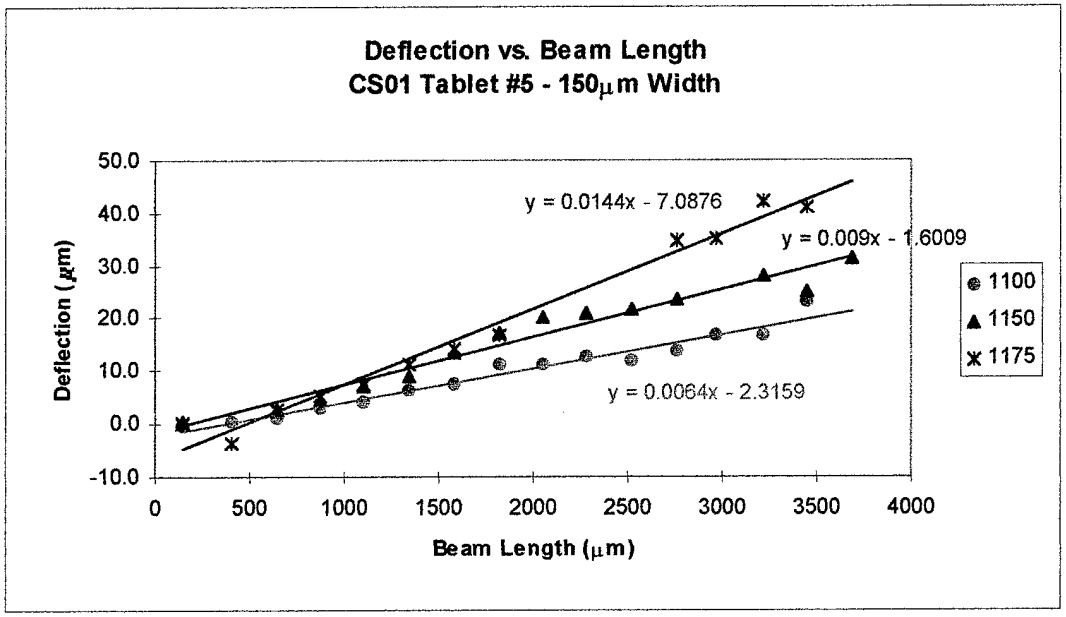

Figure 6: Linear Trendlines for Beam Tip Deflections for CS01 Wafers

Next, using the slopes calculated for the trendlines shown in Figure 6, another plot was created for anneal temperature vs. slope. This plot is shown in Figure 7. A linear trendline was fitted to this data, and the y-intercept (point of zero slope) was taken as the predicted curl reversal temperature. As seen in the trendline formula in Figure 7, the y-intercept was about 1050°C; this value is, therefore, a rough estimate of where curl reversal would be expected for a 90 minute anneal.

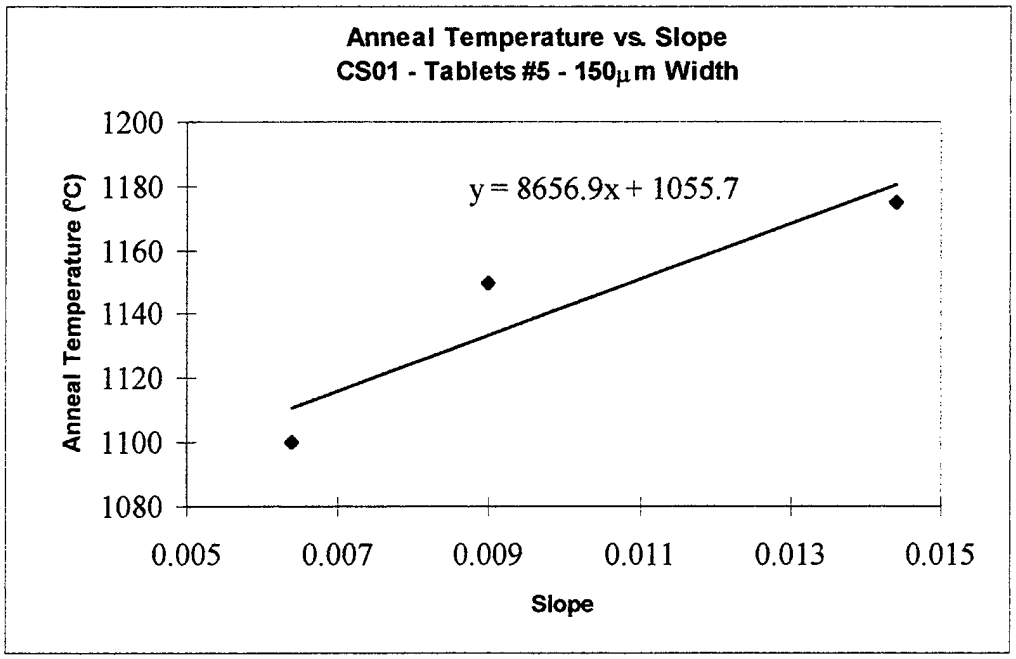

Figure 7: Prediction of Curl Reversal Anneal Temperature

4.1.2 CS02 Results

Based on data acquired from CS01, CS02 was processed to include several lower anneal temperatures. The tip deflection data taken from the 150μm width beams of WYKO tablets number 5 from each wafer is shown graphically in Figure 8. Wafer CS02-G (1150°C anneal) was not included because this wafer was destroyed during processing. Figure 8 clearly shows that all cantilever beams are curled down when no anneal is used (wafer CS02-A) or if the anneal temperatures are at or below 1000°C (wafers CS02-B, C and D), and that all beams are curled up for the 1100°C anneal temperature (wafer CS02-F). This data suggests that there is a transition from curled down to curled up somewhere between 1000°C and 1100°C.

Cantilever structures from the wafer annealed at 1050°C (CS02-E) exhibited interesting behavior. Narrow width cantilevers (30μm and 60μm) were primarily curled

up, while wider cantilevers (150μm and 400μm) were predominantly curled down. The reasons for this behavior are unknown. The wide cantilevers may be responding to curl stresses as plates instead of beams. This transitional behavior does support the prediction from CS01 data of a transition point near 1050°C.

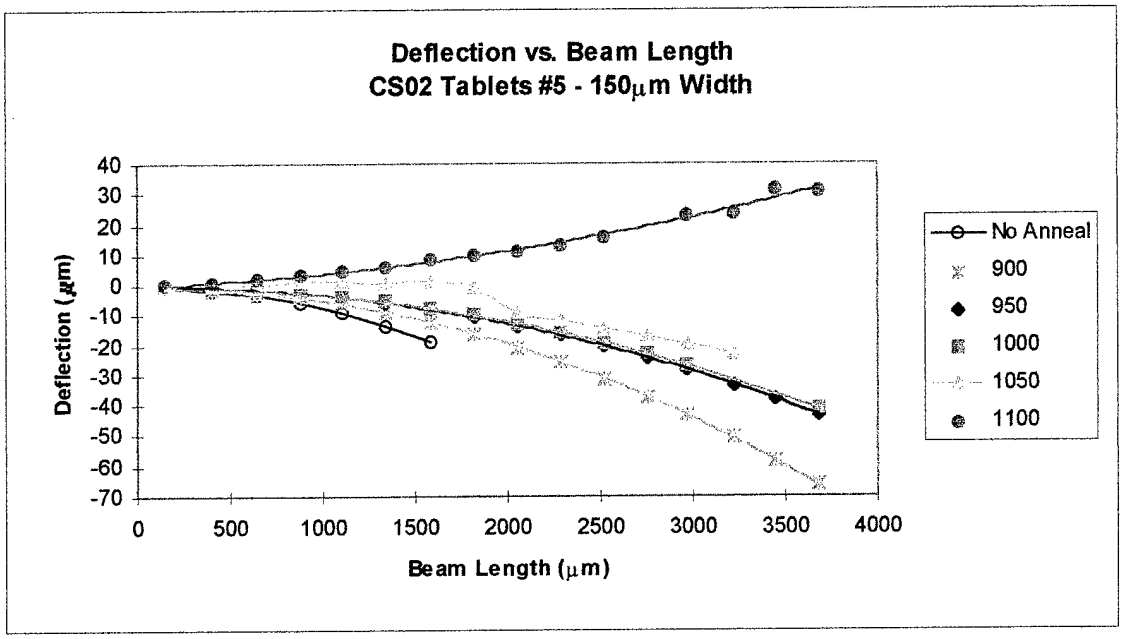

Figure 8: Comparison of Beam Tip Deflections for CS02 Wafers

4.1.3 Comparison of CS01 and CS02

A control wafer and a wafer with an 1100°C anneal were successfully fabricated in both processing runs. The cantilever beam tip deflection data was compared for these wafers to show run variations. All beams for both control wafers were curled down, all beams for the 1100°C wafers were curled up, and there was good agreement between the magnitudes of the deflections. Data for the 150μm width beams on tablets number 5 of the 1100°C annealed wafers are compared in Figure 9.

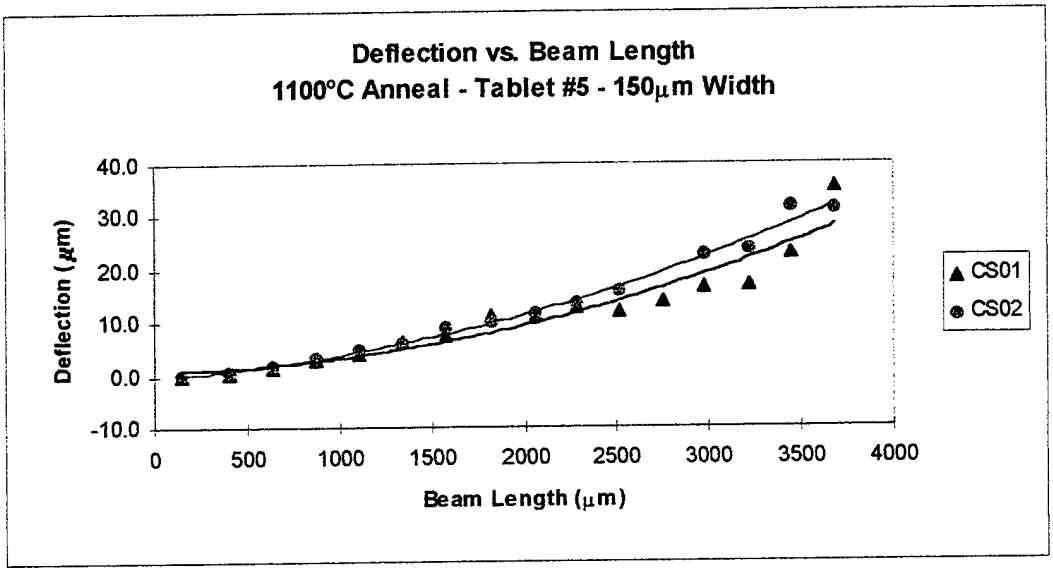

Figure 9: Comparison of Tip Deflections for CS01 and CS02 1100°C Annealed Wafers

Figure 10 shows a comparison of data for the 150μm width beams on tablets number 5 of the control wafers to the theoretical deflection expected using equation (3) from the Background Theory and Literature Review section.

In equation (3), the following values were used: $\alpha_T = 5.4274$Å, which corresponds to a top surface boron concentration of $7x10^{19}cm^{-3}$ (etch-stop concentration), $\alpha_B = 5.4240$Å, which corresponds to a bottom surface boron concentration of $2x10^{20}cm^{-3}$, $\alpha_{Si} = 5.4315$Å, and h = 11μm. The boron concentrations were converted to lattice constants using data compiled by Baribeau and Rolfe [13]. Note that the bottom surface of the cantilever beam was originally the front (diffused) surface of the wafer, and the top surface of the beam was formed from the EDP etch processing step (see Figure 1 in Background Theory and Literature Review section). Equation (3) gives an expected cantilever deflection of 28.45 y^2/m along the length y.

From Figure 10, it is clear that the theoretical solution is not accurate for the cantilever beams fabricated in this experiment. This is true because equation (3) holds for a completely strained lattice. The presence of dislocations would significantly reduce the expected deflection.

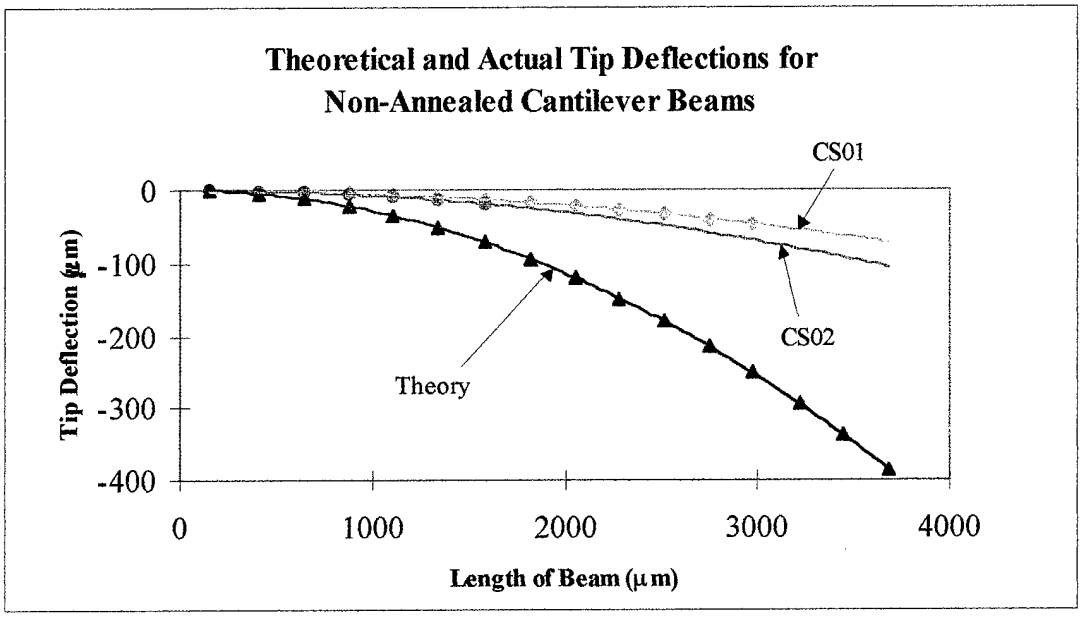

Figure 10: Comparison of Control Wafer Tip Deflections with Theory

4.2 X-ray Diffraction

Triple axis θ - 2θ scans were done on samples taken from the CS01-1175°C test wafer, and from the CS02-A, C, E, and F wafers (control, 950°C, 1050°C, and 1100°C, respectively). X-ray diffractometer data are included in Appendix C. It is known that the first narrow peak of the θ - 2θ scans corresponds to silicon for all the wafers tested. Therefore, all plots were normalized to each other by giving the silicon peak an amplitude of 1000 counts at an angle of zero. Figure 11 shows this normalized plot.

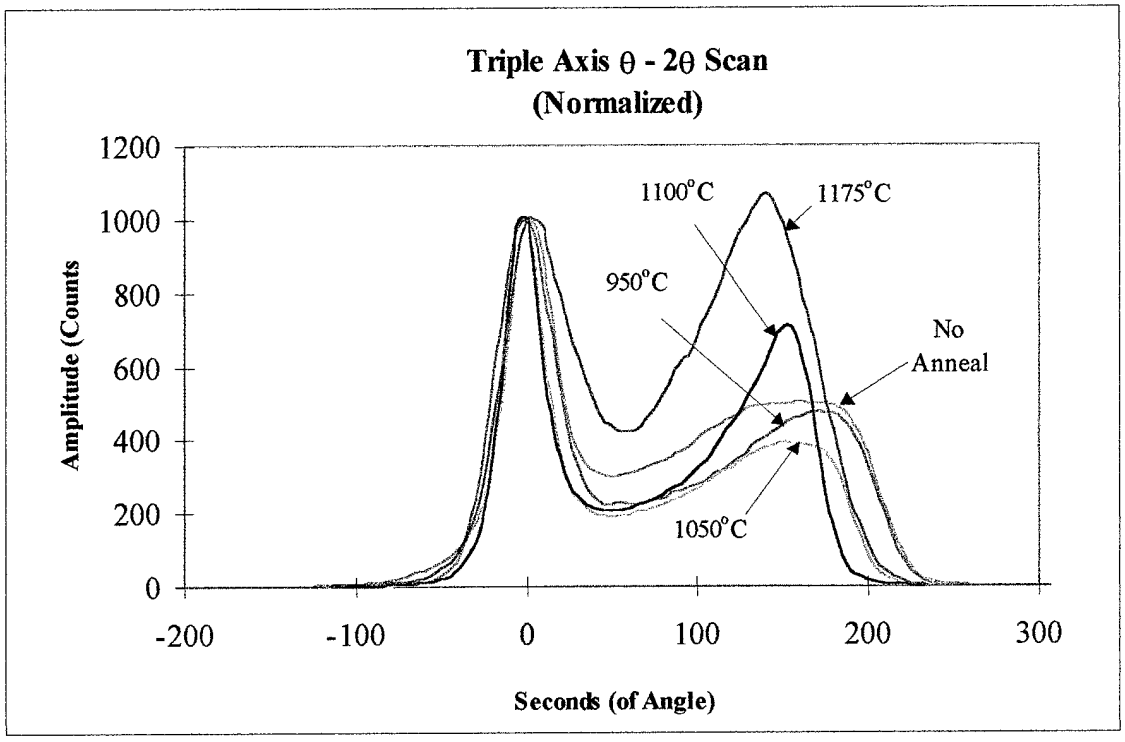

Figure 11: Normalized θ - 2θ Scan Plots

The second peaks showing other lattice constants in the wafers are all to the right of the silicon peak. This shows that the Bragg angles are larger and, therefore, the lattice constants smaller than that of pure silicon. This result was expected since the substitutional boron in the silicon lattice will decrease the lattice size. Previous SIMS work [7] has shown boron concentrations as high as $2x10^{20}cm^{-3}$ near the surface of as-diffused wafers. Using information recorded by Baribeau and Rolfe [13], boron concentrations from the $7x10^{19}cm^{-3}$ to $2x10^{20}cm^{-3}$ would give an expected range of lattice constants from 5.4240Å to 5.4274Å.

The second peaks are broad compared to the silicon peak, which indicates a range of lattice constants. The second peaks become more narrow with increasing anneal temperature and show increasing amplitude with increasing anneal temperature above 1100°C.

To determine the primary lattice constants present, a peak was considered to cover the range of angles corresponding to amplitudes at least 95% of the greatest amplitude in that particular peak. The angles were converted to lattice constants using equations (4) and (5) in the Background Theory and Literature Review section, with $\lambda = 1.541$Å and $\theta_B = 34.571 + \theta_d$, where θ_d is the angle difference between the silicon peak and the second peak of interest. For comparison, the lattice constant of pure silicon is 5.43154Å. These results are contained in Table 1.

Wafer Identification	95% Peak Angles (seconds)	Primary Lattice Constants (Å)	Difference From Silicon Lattice Constant (Å)
CS02 - None	130 to 185	5.42657 to **5.42448**	-0.00496 to -0.00706
CS02 - 950	155 to 185	5.42562 to **5.42448**	-0.00592 to -0.00706
CS02 - 1050	140 to 170	5.42619 to **5.42505**	-0.00534 to -0.00649
CS02 - 1100	150 to 155	5.42581 to **5.42562**	-0.00572 to -0.00592
CS01 - 1175	135 to 145	5.42638 to **5.42600**	-0.00515 to -0.00553

Table 1: Primary Lattice Constants

The range of primary lattice constants listed in Table 1 are all within the expected range of 5.4240Å to 5.4274Å. The boldface data in Table 1 show that the smallest primary lattice constant present in a wafer becomes larger with increasing anneal temperature. This result supports the theory presented by Cabuz et. al. [19], which suggests that the most highly boron-doped regions (which have the smallest lattice constants) experience a decrease in boron content during post-diffusion annealing, which increases their lattice constants.

4.3 TEM Observations

Several cross-section and plan-view TEM samples were made and inspected. For the cross-section samples, the distance from the wafer surface to the first and last dislocations, and the dislocation density were of interest. Visual inspection of photographs taken from each sample indicated that dislocation density remains roughly constant for all wafers. Measuring the distance of first dislocations from the wafer surface was fairly simple since all samples showed a clear dislocation-free zone near the surface. However, measuring the distance to the last dislocation was subjective, since small dislocations could still be found quite deep (i.e., >20μm) into the wafers. There was a slight trend of decreasing distance to first dislocations with increasing anneal temperature, as shown in Table 2. This motion is driven by the boron diffusion during the anneal process, and the mechanism may be dislocation climb. Representative photographs of cross-section TEM specimens are included in Appendix D.

Wafer Identification	Range of First Dislocation Depth (μm)	Average First Dislocation Depth (μm)
CS02 - No Anneal	3.7 to 6.2	4.93
CS02 - 950	3.5 to 5.0	4.00
CS02 - 1100	2.5 to 4.3	3.40
CS01 - 1175	2.5 to 4.3	3.65

Table 2: Cross-Section TEM Sample First Dislocation Depth

For the plan-view samples, dislocation density and precipitate density were of interest. As with the cross-section samples, visual inspection of photographs taken from each plan-view sample did not show any noticeable variation in dislocation density. Many precipitates were found, but there did not appear to be any change in precipitate density with different anneal processes. Close examination of precipitates revealed that

some dislocations nucleate at precipitate sites. TEM photographs are included in Appendix D.

4.4 SIMS Analysis

SIMS analysis was conducted on the CS02-A (control) wafer and the CS02-F (1100°C anneal) wafer. Data are included in Appendix E. The data provided by Wright Laboratory gives the amplitude ratio of boron to silicon signals versus sputter time. The B/Si signal amplitude ratio corresponds to boron concentration. Sputter time was converted to sputter depth using the sputter rate of 1.91 nm/sec provided by Wright Laboratory. Exact boron concentration information could not be determined from the data available, but concentration profiles of the two wafers were compared. The profile amplitudes were adjusted to reflect the assumption that total boron content remains constant during annealing. This comparison is shown in Figure 12.

Figure 12 indicates that the boron concentration profile for non-annealed wafers is fairly linear from 1μm to 11μm in depth. Since the expected etch-stop depth in this wafer was 11μm, this result shows that the boron distribution through the thickness of a non-annealed structure was reasonably linear. Figure 12 also reveals that the profile flattens out considerably after annealing at 1100°C. This result is expected since the boron gradient in a non-annealed wafer will cause further boron diffusion upon heating to a sufficiently high temperature.

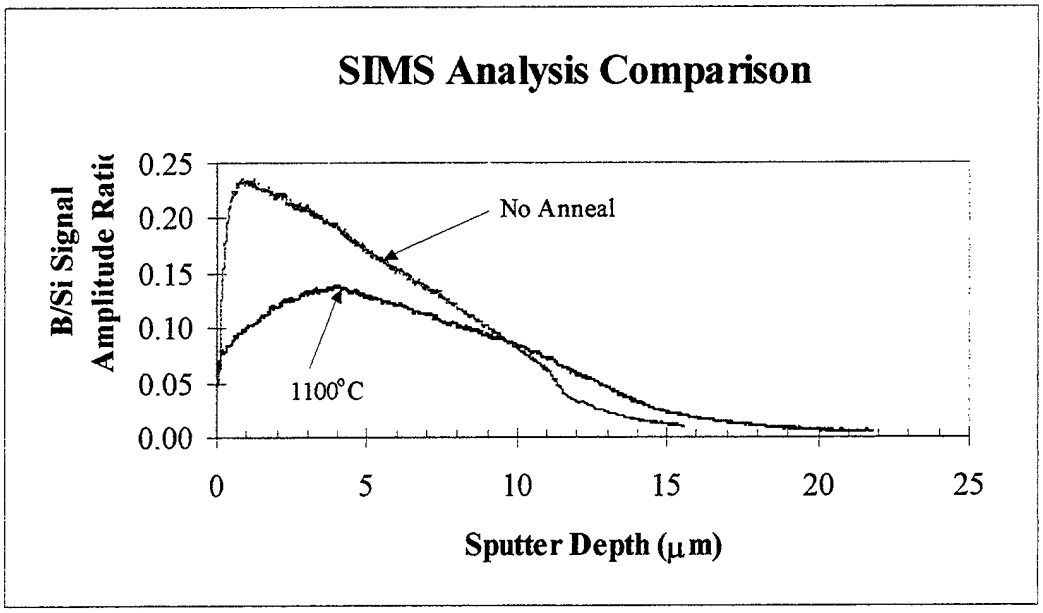

Figure 12: Comparison of Boron Profiles for CS02 Control and 1100°C Wafers

Chapter 5: CONCLUSIONS

Several conclusions have been reached from the data acquired in this work and review of previous work.

5.1 Cantilever Structures

Data from cantilever structure tip deflections has shown that curl is a strong function of anneal temperature. Downward curl decreases with increasing anneal temperature until some transition temperature at which the curl reverses; upward curl increases with further increase in anneal temperature. The transition temperature is difficult to predict exactly, but is between 1000°C and 1100°C, and most probably near 1050°C. Near the transition temperature, narrow and wide cantilevers tend to curl in opposite directions.

The optimum anneal temperature must not be too close to the actual transition point since structure curl may be unstable at the transition temperature. Further work must be done to pinpoint an optimum stable temperature.

The control wafers and 1100°C annealed wafers showed good agreement in tip deflections from CS01 to CS02.

The tip deflections of the control wafers were much smaller in magnitude than the theoretical deflections calculated from equation (3). This is primarily due to the presence of dislocations, which relax the lattice. The presence of boron-rich silicon precipitates also creates a deviation from the model. Also, since the etch-stop ($7x10^{19}cm^{-3}$) is reached inside the graded boron-silicon region, the lattice constant change through the thickness of actual cantilever beams will not be linear. Thus, the

assumptions of a completely strained (i.e., unrelaxed) lattice and linear change in lattice constant were not correct in the derivation of equation (3).

5.2 X-Ray Diffraction

Magnitudes of lattice constants obtained through triple axis θ - 2θ scans were in the range expected using data compiled by Baribeau and Rolfe [13] for lattice constant as a function of boron concentration in silicon. Amplitude of the second (contracted lattice) peaks increased with increasing anneal temperature above 1100°C, which is expected to occur with a flattening of the boron concentration profile, since a greater area would be obtaining the same lattice constant. Magnitude of the smallest lattice constant present in a wafer increased with increasing anneal temperature. This increase in lattice constant results from areas of highest boron concentration losing boron during the anneal process.

5.3 TEM Observations

A dislocation-free zone is present near the surface of all annealed and non-annealed wafers. The large spread in this data may be due to within-wafer variations during boron diffusion and subsequent annealing. The size of the dislocation-free zone appears to decrease slightly with increasing anneal temperature.

The decrease in the size of the dislocation-free zone may be due to diffusion of boron during annealing. During the anneal process, boron moves to cause a more uniform distribution through the wafer. The areas of high boron concentration (near the front surface of the wafer) lose boron, which should be accompanied by the removal of

dislocations. Thus, dislocations would be observed moving toward the surface of the boron-silicon layer, which is the front surface of the wafer.

Dislocation and precipitate density did not visually change with anneal temperature. Some precipitates served as dislocation nucleation sites. Boron-rich precipitates did not dissociate with high temperature anneals, in contrast to results reported by Wang et. al. [17] for rapid thermal anneals above 1100°C.

5.4 SIMS Analysis

The boron concentration profile for non-annealed wafers is fairly linear from 1μm to 11μm in depth. The profile becomes much more flat, indicating a more uniform boron distribution, to a depth of about 11μm after annealing at 1100°C. This results from boron diffusion that occurs during the anneal treatment.

If the boron diffusion takes place more quickly than the dislocations in the wafer can move, the areas of decreasing boron concentration would develop a compressive stress, and the areas of increasing boron concentration would develop a tensile stress.

5.5 Correlation Between Microstructural Observations and Curl Reversal

The data acquired in this work partially supports the theory presented by Cabuz et. al. [19] as discussed in the Background Theory and Literature Review section. For the theory to hold, the following must be observed after anneal at sufficiently high temperature: 1) the boron concentration profile should become more flat, 2) the smallest lattice constants should disappear, and 3) dislocations should not move.

This work has shown that the boron concentration profile does flatten, and that the smallest lattice constants do disappear after annealing. However, dislocations do not remain stationary.

Although dislocation motion does occur, this motion may not be great enough to fully relax the lattice. In this case, stresses may still remain which explain the curl reversal behavior found in annealed cantilevers.

Chapter 6: RECOMMENDATIONS FOR FUTURE WORK

There is still much useful work yet to be done in the investigations of microstructure and curling behavior of heavily boron-doped silicon. Repeatability of experiments done in this work should first be thoroughly tested. In particular, more fabrication runs should be done using the same environments to verify repeatability of the process used.

There are several areas where more extensive research could be done to continue the work presented in this thesis. The curl reversal anneal temperature should be investigated more thoroughly by focusing on anneal temperatures between 1000°C and 1100°C, particularly in the region around 1050°C. The apparent width dependence of curl direction seen in cantilever structures annealed at 1050°C should also be verified.

More extensive TEM analysis should be done. Actual dislocation and precipitate densities should be determined. Dislocation types should be determined for different anneal conditions, and studies done to describe dislocation motion during annealing.

Since temperature was the only variable in this experiment, other annealing variables should also be analyzed, such as time and environment.

A related issue is variation of properties at different locations on a single wafer. A study of this problem might begin by comparing cantilever beam deflections from different areas on a single wafer.

APPENDIX A: DERIVATION OF EQUATIONS

Derivation of Equation (3): Theoretical Curl in Non-Annealed Cantilever Structures

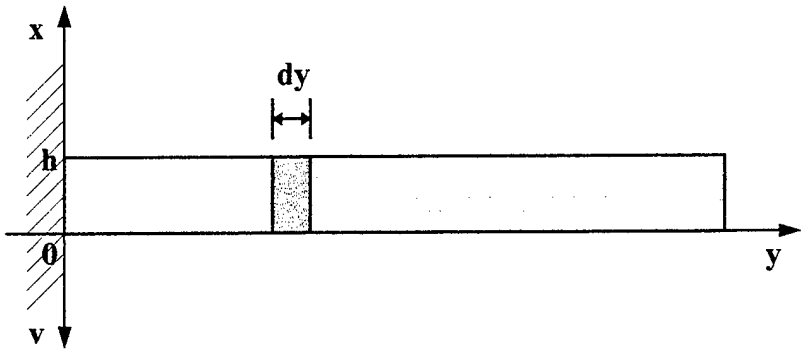

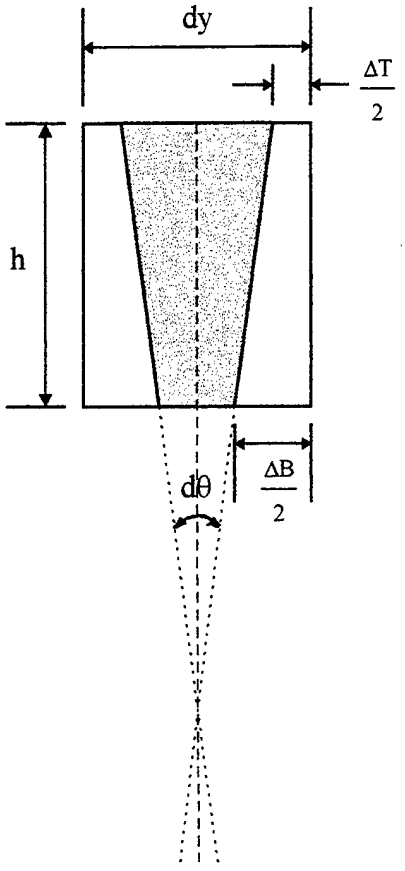

Definition of Terms

v = vertical deflection of beam (positive down)

h = height of beam

ΔT = shrinkage of top surface of beam

ΔB = shrinkage of bottom surface of beam

θ = angle of rotation of beam

α_{Si} = lattice constant of pure silicon

α_T = lattice constant of top surface of beam

α_B = lattice constant of bottom surface of beam

$$\Delta T = dy\left(1 - \frac{\alpha_T}{\alpha_{Si}}\right) \qquad \Delta B = dy\left(1 - \frac{\alpha_B}{\alpha_{Si}}\right)$$

$$\frac{dy}{\alpha_{Si}} = \frac{dy - \Delta T}{\alpha_T} = \frac{dy - \Delta B}{\alpha_B}$$

$$\tan\left(\frac{d\theta}{2}\right) = \frac{\frac{\Delta B - \Delta T}{2}}{h}$$

For small $d\theta$, $\tan(d\theta/2) \approx d\theta/2 \Rightarrow d\theta = \frac{\Delta B - \Delta T}{h} = \frac{dy}{h}\left[\frac{\alpha_T - \alpha_B}{\alpha_{Si}}\right]$

$$\boxed{\frac{d\theta}{dy} = \frac{\alpha_T - \alpha_B}{h\,\alpha_{Si}}} \qquad \text{For curl, } \frac{d\theta}{dy} = \frac{d^2v}{dy^2}$$

$$\frac{d^2v}{dy^2} = \frac{\alpha_T - \alpha_B}{h\,\alpha_{Si}} = \frac{d}{dy}\left(\frac{dv}{dy}\right)$$

$$\frac{dv}{dy} = \int \frac{\alpha_T - \alpha_B}{h\,\alpha_{Si}}\,dy = \frac{\alpha_T - \alpha_B}{h\,\alpha_{Si}}\,y + K1$$

$$v = \int\left(\frac{\alpha_T - \alpha_B}{h\,\alpha_{Si}}\,y + K1\right)dy = \frac{\alpha_T - \alpha_B}{2\,h\,\alpha_{Si}}\,y^2 + K1\,y + K2 \qquad (A)$$

Boundary Conditions:

At $y = 0$, $dv/dy = 0 \Rightarrow K1 = 0$

At $y = 0$, $v = 0 \Rightarrow K2 = 0$

$$\boxed{v = \frac{\alpha_T - \alpha_B}{2\,h\,\alpha_{Si}}\,y^2} \qquad (3)$$

Derivation of Equation (6): Predicted Tip Deflection of Beams Curled Down

Beginning with Equation (A) from above:

$$v = \frac{\alpha_T - \alpha_B}{2\,h\,\alpha_{Si}}\,y^2 + K1\,y + K2 \qquad (A)$$

To simplify the nomenclature, let $\frac{\alpha_T - \alpha_B}{\alpha_{Si}} = C$.

For beams that are curled down far enough for the tip to contact the glass (giving measured tip deflection of G, which is about 3.5μm), we have the following boundary conditions:

$$\text{At } y = 0,\ v = 0 \Rightarrow K2 = 0$$

$$\text{At } y = L,\ v = G \Rightarrow K1 = \frac{G}{L} - \frac{C\,L}{2\,h}, \text{ where L = length of the beam.}$$

This gives: $v = C\,\frac{y^2 - L\,y}{2\,h} + \frac{G\,y}{L}$

We can measure experimentally the highest beam deflection, v_h, and the length along the beam at which that deflection occurs, y_h. C can be found by substituting these values, and rearranging the above equation to give:

$$C = \frac{2\,h}{y_h^{\,2} - L\,y_h}\left(v_h - \frac{G\,y_h}{L}\right) \text{ which is a unitless constant.}$$

Now, the predicted tip deflection, v_t (as if the glass was not there) can be found by substituting C and y = L into Equation (3) from above, to give Equation (6):

$$\boxed{v_t = \frac{C\,L^2}{2\,h}} \qquad (6)$$

APPENDIX B: WYKO DATA

Wafer	CS01 - A

Tablet #	3

Width = 30μm

	Beam Length (μm)	Tip Deflection (μm)
1	28	-0.75
2	67	-0.98
3	108	-0.96
4	147	-0.93
5	188	-0.77
6	228	-0.88
7	258	-0.68
8	357	-4.25
9	457	0.06
10	557	1.02
11	657	1.70
12	759	1.79
13	857	3.66
14	958	3.92
15	1054	4.58
16	1153	6.07
17	1254	6.43
18	1356	8.36
19	1451	10.33
20	1556	11.76
21	1653	11.63
22	1762	16.75
23	1861	17.38
24	1955	16.67
25	2050	24.05
26	2153	20.88
27	2253	22.80
28	2352	25.82
29	2451	31.12
30	2550	29.67
31	2691	43.67
32	2892	38.84
33	3184	missing

Width = 60μm

	Beam Length (μm)	Tip Deflection (μm)
1	49	-1.07
2	70	-0.82
3	107	-0.96
4	188	-0.73
5	230	-0.75
6	360	-0.16
7	459	0.38
8	658	1.78
9	759	2.43
10	959	4.37
11	1056	5.55
12	1256	8.13
13	1356	10.74
14	1558	12.07
15	1697	missing
16	1987	16.74
17	2289	24.26
18	2588	32.07
19	2895	41.17
20	3197	48.22
21	3498	66.18

Width = 150μm

	Beam Length (μm)	Tip Deflection (μm)
1	148	-0.06
2	408	0.91
3	644	2.36
4	878	4.35
5	1106	6.81
6	1345	9.00
7	1581	12.06
8	1819	13.46
9	2056	15.06
10	2284	17.32
11	2520	19.95
12	2756	20.31
13	2973	22.08
14	3218	23.46
15	3449	22.15
16	3684	23.53

Width = 400μm

	Beam Length (μm)	Tip Deflection (μm)
1	393	1.27
2	872	4.20
3	1343	2.46
4	1823	5.65
5	2287	missing
6	2751	26.65
7	3211	51.49

Wafer	CS01 - B

Tablet #	3

Width = 30μm

	Beam Length (μm)	Tip Deflection (μm)
1	28	-1.23
2	67	-1.10
3	108	-1.09
4	147	-1.31
5	188	-1.00
6	228	-0.76
7	258	-0.71
8	357	broken
9	457	broken
10	557	0.63
11	657	0.92
12	759	1.27
13	857	1.89
14	958	4.09
15	1054	4.08
16	1153	5.12
17	1254	5.08
18	1356	5.11
19	1451	7.80
20	1556	8.07
21	1653	10.56
22	1762	8.99
23	1861	broken
24	1955	12.34
25	2050	15.31
26	2153	19.62
27	2253	21.03
28	2352	13.86
29	2451	16.42
30	2550	21.01
31	2691	19.78
32	2892	missing
33	3184	missing

Width = 60μm

	Beam Length (μm)	Tip Deflection (μm)
1	49	-0.80
2	70	-1.02
3	107	-0.85
4	188	-0.82
5	230	-0.61
6	360	broken
7	459	broken
8	658	0.80
9	759	1.50
10	959	3.31
11	1056	3.85
12	1256	5.44
13	1356	6.20
14	1558	broken
15	1697	broken
16	1987	broken
17	2289	broken
18	2588	broken
19	2895	broken
20	3197	broken
21	3498	broken

Width = 150μm

	Beam Length (μm)	Tip Deflection (μm)
1	148	-0.44
2	408	0.29
3	644	1.26
4	878	2.55
5	1106	3.16
6	1345	4.73
7	1581	6.60
8	1819	6.31
9	2056	6.04
10	2284	8.64
11	2520	10.40
12	2756	8.05
13	2973	broken
14	3218	7.65
15	3449	broken
16	3684	13.01

Width = 400μm

	Beam Length (μm)	Tip Deflection (μm)
1	393	0.77
2	872	1.06
3	1343	0.92
4	1823	broken
5	2287	broken
6	2751	broken
7	3211	20.85

Wafer	CS01 - C

Tablet #	3

Width= 30μm

	Beam Length (μm)	Tip Deflection (μm)
1	28	-1.00
2	67	-1.04
3	108	-0.99
4	147	-1.04
5	188	-0.89
6	228	-0.66
7	258	-0.37
8	357	-0.25
9	457	0.60
10	557	1.25
11	657	1.91
12	759	2.91
13	857	4.36
14	958	5.21
15	1054	6.35
16	1153	7.02
17	1254	9.69
18	1356	11.85
19	1451	12.39
20	1556	15.31
21	1653	16.20
22	1762	17.73
23	1861	21.56
24	1955	22.89
25	2050	24.65
26	2153	25.56
27	2253	28.58
28	2352	32.34
29	2451	32.59
30	2550	37.85
31	2691	44.78
32	2892	47.19
33	3184	46.57

Width= 60μm

	Beam Length (μm)	Tip Deflection (μm)
1	49	-1.22
2	70	-0.98
3	107	-0.93
4	188	-0.79
5	230	-0.60
6	360	0.07
7	459	-4.06
8	658	2.52
9	759	3.19
10	959	4.71
11	1056	7.22
12	1256	9.79
13	1356	12.55
14	1558	14.39
15	1697	16.76
16	1987	-3.65
17	2289	missing
18	2588	missing
19	2895	missing
20	3197	missing
21	3498	missing

Width= 150μm

	Beam Length (μm)	Tip Deflection (μm)
1	148	0.27
2	408	0.96
3	644	2.68
4	878	5.01
5	1106	7.81
6	1345	10.92
7	1581	13.87
8	1819	16.79
9	2056	19.11
10	2284	24.64
11	2520	25.74
12	2756	34.01
13	2973	38.45
14	3218	36.56
15	3449	38.38
16	3684	45.61

Width= 400μm

	Beam Length (μm)	Tip Deflection (μm)
1	393	1.55
2	872	3.94
3	1343	5.95
4	1823	9.54
5	2287	17.90
6	2751	33.07
7	3211	54.42

Wafer	CS01 - D

Tablet #	3

Width= 30μm

	Beam Length (μm)	Tip Deflection (μm)
1	28	-1.63
2	67	-1.92
3	108	-1.82
4	147	-1.93
5	188	-1.96
6	228	-2.13
7	258	-2.41
8	357	-4.64
9	457	-4.65
10	557	-4.78
11	657	-4.59
12	759	-4.54
13	857	-4.46
14	958	-4.27
15	1054	-4.14
16	1153	-4.02
17	1254	-3.66
18	1356	-3.79
19	1451	-3.78
20	1556	-3.83
21	1653	-3.68
22	1762	-3.76
23	1861	-3.63
24	1955	-3.50
25	2050	-3.55
26	2153	-3.71
27	2253	-3.49
28	2352	-3.10
29	2451	-3.53
30	2550	missing
31	2691	missing
32	2892	missing
33	3184	missing

Width= 60μm

	Beam Length (μm)	Tip Deflection (μm)
1	49	-1.68
2	70	-1.73
3	107	-1.77
4	188	-1.94
5	230	-1.93
6	360	-2.45
7	459	-2.76
8	658	-4.04
9	759	-3.98
10	959	-4.02
11	1056	-3.85
12	1256	-3.75
13	1356	-3.68
14	1558	-3.59
15	1697	-3.59
16	1987	-3.32
17	2289	-2.97
18	2588	missing
19	2895	-3.29
20	3197	missing
21	3498	missing

Width= 150μm

	Beam Length (μm)	Tip Deflection (μm)
1	148	-0.72
2	408	-2.15
3	644	-3.33
4	878	-3.15
5	1106	-3.00
6	1345	-2.82
7	1581	-2.77
8	1819	-2.62
9	2056	-2.59
10	2284	-2.12
11	2520	-2.41
12	2756	-2.32
13	2973	-1.54
14	3218	-1.55
15	3449	-1.28
16	3684	-1.36

Width= 400μm

	Beam Length (μm)	Tip Deflection (μm)
1	393	-0.65
2	872	-1.53
3	1343	-1.29
4	1823	-1.38
5	2287	missing
6	2751	-1.50
7	3211	-2.12

Wafer	CS01 - A

Tablet #	5

Width= 30μm

	Beam Length (μm)	Tip Deflection (μm)
1	28	-0.96
2	67	-1.03
3	108	-1.14
4	147	-1.16
5	188	-0.98
6	228	-0.79
7	258	-0.87
8	357	-0.42
9	457	broken
10	557	broken
11	657	1.19
12	759	2.42
13	857	2.74
14	958	broken
15	1054	broken
16	1153	broken
17	1254	broken
18	1356	broken
19	1451	broken
20	1556	broken
21	1653	broken
22	1762	broken
23	1861	broken
24	1955	broken
25	2050	broken
26	2153	broken
27	2253	broken
28	2352	3.92
29	2451	broken
30	2550	26.35
31	2691	25.28
32	2892	missing
33	3184	missing

Width= 60μm

	Beam Length (μm)	Tip Deflection (μm)
1	49	-1.29
2	70	-1.15
3	107	-1.20
4	188	-0.91
5	230	-0.80
6	360	-0.33
7	459	broken
8	658	1.77
9	759	2.54
10	959	4.61
11	1056	5.59
12	1256	7.44
13	1356	9.74
14	1558	10.94
15	1697	14.51
16	1987	22.47
17	2289	missing
18	2588	9.64
19	2895	missing
20	3197	missing
21	3498	41.28

Width= 150μm

	Beam Length (μm)	Tip Deflection (μm)
1	148	0.30
2	408	-3.01
3	644	2.69
4	878	4.42
5	1106	7.23
6	1345	9.15
7	1581	13.36
8	1819	17.26
9	2056	20.06
10	2284	21.08
11	2520	21.64
12	2756	23.57
13	2973	18.80
14	3218	28.11
15	3449	25.20
16	3684	31.54

Width= 400μm

	Beam Length (μm)	Tip Deflection (μm)
1	393	1.43
2	872	3.07
3	1343	3.25
4	1823	4.02
5	2287	6.23
6	2751	25.75
7	3211	broken

Wafer	**CS01 - B**

Tablet #	**5**

Width= 30μm

	Beam Length (μm)	Tip Deflection (μm)
1	28	-0.99
2	67	-1.15
3	108	-0.91
4	147	-0.90
5	188	-0.84
6	228	-1.02
7	258	-0.86
8	357	-0.55
9	457	-0.04
10	557	0.51
11	657	1.02
12	759	1.01
13	857	2.44
14	958	2.84
15	1054	4.98
16	1153	4.89
17	1254	7.58
18	1356	7.71
19	1451	broken
20	1556	8.33
21	1653	10.86
22	1762	12.86
23	1861	13.35
24	1955	17.49
25	2050	18.84
26	2153	21.20
27	2253	20.88
28	2352	22.69
29	2451	25.59
30	2550	23.35
31	2691	35.94
32	2892	31.64
33	3184	missing

Width= 60μm

	Beam Length (μm)	Tip Deflection (μm)
1	49	-1.09
2	70	-1.02
3	107	-0.87
4	188	-0.77
5	230	-0.64
6	360	-0.09
7	459	0.42
8	658	1.74
9	759	2.37
10	959	3.46
11	1056	4.44
12	1256	5.68
13	1356	6.87
14	1558	8.79
15	1697	11.84
16	1987	missing
17	2289	missing
18	2588	27.82
19	2895	missing
20	3197	missing
21	3498	missing

Width= 150μm

	Beam Length (μm)	Tip Deflection (μm)
1	148	-0.21
2	408	0.31
3	644	1.28
4	878	3.02
5	1106	4.00
6	1345	6.33
7	1581	7.61
8	1819	11.35
9	2056	11.25
10	2284	12.77
11	2520	12.12
12	2756	13.68
13	2973	16.66
14	3218	16.84
15	3449	23.12
16	3684	35.37

Width= 400μm

	Beam Length (μm)	Tip Deflection (μm)
1	393	0.61
2	872	1.88
3	1343	2.29
4	1823	3.90
5	2287	missing
6	2751	14.13
7	3211	31.20

Wafer	CS01 - C

Tablet #	5

Width= 30μm

	Beam Length (μm)	Tip Deflection (μm)
1	28	-0.93
2	67	-1.17
3	108	-1.21
4	147	-1.17
5	188	-0.71
6	228	-0.84
7	258	-0.69
8	357	broken
9	457	broken
10	557	1.24
11	657	1.73
12	759	3.00
13	857	3.65
14	958	5.83
15	1054	6.74
16	1153	8.15
17	1254	8.72
18	1356	11.30
19	1451	13.22
20	1556	15.70
21	1653	15.44
22	1762	18.52
23	1861	19.39
24	1955	20.54
25	2050	22.96
26	2153	25.24
27	2253	25.93
28	2352	26.55
29	2451	30.32
30	2550	broken
31	2691	broken
32	2892	44.32
33	3184	missing

Width= 60μm

	Beam Length (μm)	Tip Deflection (μm)
1	49	-1.03
2	70	-0.94
3	107	-1.07
4	188	-0.63
5	230	-0.39
6	360	-0.08
7	459	0.43
8	658	1.73
9	759	2.53
10	959	4.84
11	1056	5.23
12	1256	7.60
13	1356	10.03
14	1558	12.81
15	1697	15.05
16	1987	missing
17	2289	missing
18	2588	29.41
19	2895	missing
20	3197	missing
21	3498	missing

Width= 150μm

	Beam Length (μm)	Tip Deflection (μm)
1	148	-0.07
2	408	-3.70
3	644	2.62
4	878	5.15
5	1106	7.68
6	1345	11.30
7	1581	14.07
8	1819	17.01
9	2056	broken
10	2284	broken
11	2520	broken
12	2756	34.56
13	2973	35.24
14	3218	42.08
15	3449	41.04
16	3684	11.77

Width= 400μm

	Beam Length (μm)	Tip Deflection (μm)
1	393	1.62
2	872	3.91
3	1343	6.88
4	1823	8.75
5	2287	missing
6	2751	33.38
7	3211	59.93

Wafer	CS01 - D

Tablet #	5

Width= 30μm

	Beam Length (μm)	Tip Deflection (μm)
1	28	-1.44
2	67	-2.01
3	108	-1.87
4	147	-2.16
5	188	-2.17
6	228	-2.34
7	258	-2.34
8	357	-4.60
9	457	-5.03
10	557	-4.55
11	657	-4.35
12	759	-4.72
13	857	-4.24
14	958	-4.48
15	1054	-4.47
16	1153	-4.31
17	1254	-3.06
18	1356	-3.84
19	1451	-4.17
20	1556	-3.66
21	1653	-3.95
22	1762	-3.82
23	1861	-3.97
24	1955	-3.93
25	2050	-3.92
26	2153	-3.61
27	2253	-3.89
28	2352	missing
29	2451	missing
30	2550	missing
31	2691	missing
32	2892	missing
33	3184	missing

Width= 60μm

	Beam Length (μm)	Tip Deflection (μm)
1	49	-1.66
2	70	-1.80
3	107	-1.88
4	188	-1.82
5	230	-1.70
6	360	-2.46
7	459	-2.97
8	658	-4.02
9	759	-4.51
10	959	-3.90
11	1056	-3.57
12	1256	-3.66
13	1356	-4.03
14	1558	-3.71
15	1697	-3.78
16	1987	-3.74
17	2289	-3.36
18	2588	-3.66
19	2895	missing
20	3197	missing
21	3498	-3.59

Width= 150μm

	Beam Length (μm)	Tip Deflection (μm)
1	148	-1.00
2	408	-3.91
3	644	-3.42
4	878	-3.19
5	1106	-2.82
6	1345	-2.67
7	1581	-2.86
8	1819	-2.42
9	2056	-2.58
10	2284	-2.59
11	2520	-2.17
12	2756	-2.05
13	2973	-1.53
14	3218	-1.30
15	3449	-1.25
16	3684	-1.41

Width= 400μm

	Beam Length (μm)	Tip Deflection (μm)
1	393	-0.54
2	872	-1.57
3	1343	-1.28
4	1823	-1.83
5	2287	missing
6	2751	-2.42
7	3211	-2.10

Wafer	CS02 - A

Tablet #	3

Width= 30μm

	Beam Length (μm)	Tip Deflection (μm)
1	28	-1.26
2	67	-1.38
3	108	-1.21
4	147	-1.37
5	188	-1.52
6	228	-1.72
7	258	-1.83
8	357	-4.26
9	457	-2.81
10	557	-4.18
11	657	-4.32
12	759	missing
13	857	missing
14	958	-4.25
15	1054	-4.18
16	1153	missing
17	1254	missing
18	1356	missing
19	1451	missing
20	1556	missing
21	1653	missing
22	1762	missing
23	1861	missing
24	1955	missing
25	2050	missing
26	2153	missing
27	2253	missing
28	2352	missing
29	2451	missing
30	2550	missing
31	2691	missing
32	2892	missing
33	3184	missing

Width= 60μm

	Beam Length (μm)	Tip Deflection (μm)
1	49	-1.15
2	70	-1.11
3	107	-1.01
4	188	-1.43
5	230	-1.81
6	360	-2.10
7	459	-2.69
8	658	-4.10
9	759	-3.94
10	959	-4.01
11	1056	-3.92
12	1256	-3.74
13	1356	-3.57
14	1558	-3.53
15	1697	-3.59
16	1987	-3.53
17	2289	-3.51
18	2588	-3.54
19	2895	missing
20	3197	-3.48
21	3498	missing

Width= 150μm

	Beam Length (μm)	Tip Deflection (μm)
1	148	-0.56
2	408	-3.43
3	644	-3.52
4	878	-3.34
5	1106	-3.19
6	1345	-2.99
7	1581	-2.81
8	1819	-2.78
9	2056	-2.79
10	2284	-2.65
11	2520	-2.54
12	2756	-2.56
13	2973	-2.21
14	3218	-2.14
15	3449	-2.32
16	3684	-2.49

Width= 400μm

	Beam Length (μm)	Tip Deflection (μm)
1	393	-0.98
2	872	-2.34
3	1343	-1.01
4	1823	-2.17
5	2287	-2.23
6	2751	-2.46
7	3211	-2.68

Wafer	CS02 - C

Tablet #	3

Width= 30μm

	Beam Length (μm)	Tip Deflection (μm)
1	28	-0.91
2	67	-0.95
3	108	-1.01
4	147	-0.94
5	188	-1.13
6	228	-1.25
7	258	-1.30
8	357	-1.45
9	457	-1.79
10	557	-1.82
11	657	-2.76
12	759	-3.89
13	857	-3.97
14	958	-3.97
15	1054	-3.89
16	1153	-3.60
17	1254	-3.58
18	1356	-3.66
19	1451	-3.82
20	1556	-2.57
21	1653	-2.47
22	1762	-2.50
23	1861	-2.55
24	1955	-2.83
25	2050	-3.96
26	2153	missing
27	2253	missing
28	2352	missing
29	2451	missing
30	2550	missing
31	2691	missing
32	2892	missing
33	3184	missing

Width= 60μm

	Beam Length (μm)	Tip Deflection (μm)
1	49	-0.78
2	70	-0.88
3	107	-0.75
4	188	-1.00
5	230	-0.54
6	360	-0.77
7	459	-0.97
8	658	-1.72
9	759	-0.84
10	959	-1.98
11	1056	-2.29
12	1256	-2.26
13	1356	-3.56
14	1558	-3.51
15	1697	-3.46
16	1987	-3.41
17	2289	-1.67
18	2588	missing
19	2895	missing
20	3197	missing
21	3498	missing

Width= 150μm

	Beam Length (μm)	Tip Deflection (μm)
1	148	-0.27
2	408	-1.13
3	644	-2.12
4	878	-3.13
5	1106	-3.08
6	1345	-3.03
7	1581	-2.99
8	1819	-2.86
9	2056	-2.78
10	2284	-2.95
11	2520	-2.78
12	2756	-2.85
13	2973	-2.84
14	3218	-2.46
15	3449	-2.36
16	3684	-2.39

Width= 400μm

	Beam Length (μm)	Tip Deflection (μm)
1	393	-0.53
2	872	-2.41
3	1343	-2.56
4	1823	broke off
5	2287	missing
6	2751	-1.90
7	3211	-2.92

Wafer	CS02 - D

Tablet #	3

	Width= 30μm	
	Beam Length (μm)	Tip Deflection (μm)
1	28	-1.44
2	67	-1.53
3	108	-1.44
4	147	-1.64
5	188	-1.65
6	228	-1.71
7	258	-1.75
8	357	-4.73
9	457	-4.63
10	557	-0.33
11	657	-4.44
12	759	-4.31
13	857	-4.31
14	958	-4.33
15	1054	missing
16	1153	missing
17	1254	missing
18	1356	missing
19	1451	missing
20	1556	missing
21	1653	missing
22	1762	missing
23	1861	missing
24	1955	missing
25	2050	missing
26	2153	missing
27	2253	missing
28	2352	missing
29	2451	missing
30	2550	missing
31	2691	missing
32	2892	missing
33	3184	missing

	Width= 60μm	
	Beam Length (μm)	Tip Deflection (μm)
1	49	-1.39
2	70	-1.43
3	107	-1.36
4	188	-1.39
5	230	-1.42
6	360	-1.44
7	459	-1.63
8	658	-2.27
9	759	-2.46
10	959	-3.19
11	1056	-3.31
12	1256	-3.52
13	1356	-3.70
14	1558	-2.35
15	1697	-3.53
16	1987	-3.39
17	2289	-3.54
18	2588	missing
19	2895	missing
20	3197	-3.52
21	3498	missing

	Width= 150μm	
	Beam Length (μm)	Tip Deflection (μm)
1	148	-0.19
2	408	-0.61
3	644	-3.14
4	878	-3.08
5	1106	-2.88
6	1345	-2.91
7	1581	-2.72
8	1819	-2.81
9	2056	-2.80
10	2284	-2.84
11	2520	-2.44
12	2756	-2.63
13	2973	-2.63
14	3218	-2.35
15	3449	-2.05
16	3684	-2.01

	Width= 400μm	
	Beam Length (μm)	Tip Deflection (μm)
1	393	-0.13
2	872	-1.74
3	1343	-1.08
4	1823	-1.92
5	2287	missing
6	2751	-2.39
7	3211	-2.48

Wafer	CS02 - E

Tablet #	3

Width= 30μm

	Beam Length (μm)	Tip Deflection (μm)
1	28	-1.04
2	67	-1.31
3	108	-1.20
4	147	-1.17
5	188	-1.08
6	228	-1.14
7	258	-1.13
8	357	-1.18
9	457	-0.82
10	557	-0.39
11	657	-0.34
12	759	0.59
13	857	0.64
14	958	0.72
15	1054	3.51
16	1153	2.69
17	1254	4.28
18	1356	4.75
19	1451	4.52
20	1556	6.16
21	1653	5.54
22	1762	5.91
23	1861	7.73
24	1955	8.86
25	2050	8.98
26	2153	11.92
27	2253	11.74
28	2352	11.57
29	2451	16.08
30	2550	16.42
31	2691	missing
32	2892	missing
33	3184	missing

Width= 60μm

	Beam Length (μm)	Tip Deflection (μm)
1	49	-1.41
2	70	-1.60
3	107	-1.36
4	188	-1.19
5	230	-0.98
6	360	-1.22
7	459	-1.04
8	658	0.18
9	759	0.70
10	959	1.10
11	1056	3.28
12	1256	1.43
13	1356	2.24
14	1558	2.78
15	1697	missing
16	1987	missing
17	2289	missing
18	2588	missing
19	2895	missing
20	3197	1.26
21	3498	missing

Width= 150μm

	Beam Length (μm)	Tip Deflection (μm)
1	148	-0.04
2	408	0.20
3	644	0.81
4	878	1.20
5	1106	0.85
6	1345	1.16
7	1581	-0.94
8	1819	-2.64
9	2056	-2.46
10	2284	-2.15
11	2520	-2.46
12	2756	-2.38
13	2973	-2.48
14	3218	-2.27
15	3449	-2.34
16	3684	-2.30

Width= 400μm

	Beam Length (μm)	Tip Deflection (μm)
1	393	0.50
2	872	-0.89
3	1343	-2.03
4	1823	-1.17
5	2287	missing
6	2751	-2.93
7	3211	9.12

Wafer	CS02 - F

Tablet #	3

Width= 30μm

	Beam Length (μm)	Tip Deflection (μm)
1	28	-0.41
2	67	-0.60
3	108	-0.62
4	147	-0.63
5	188	-0.54
6	228	-0.64
7	258	-0.41
8	357	-0.18
9	457	broken
10	557	1.25
11	657	1.79
12	759	2.83
13	857	broken
14	958	3.13
15	1054	5.61
16	1153	6.42
17	1254	8.39
18	1356	10.16
19	1451	9.71
20	1556	12.42
21	1653	14.85
22	1762	15.40
23	1861	15.08
24	1955	broken
25	2050	missing
26	2153	missing
27	2253	missing
28	2352	missing
29	2451	missing
30	2550	missing
31	2691	missing
32	2892	missing
33	3184	missing

Width= 60μm

	Beam Length (μm)	Tip Deflection (μm)
1	49	-0.83
2	70	-0.93
3	107	-0.82
4	188	-0.78
5	230	-0.47
6	360	broken
7	459	0.60
8	658	1.42
9	759	1.91
10	959	4.14
11	1056	broken
12	1256	broken
13	1356	7.84
14	1558	broken
15	1697	broken
16	1987	broken
17	2289	21.47
18	2588	missing
19	2895	missing
20	3197	missing
21	3498	missing

Width= 150μm

	Beam Length (μm)	Tip Deflection (μm)
1	148	-0.08
2	408	0.78
3	644	1.84
4	878	3.74
5	1106	5.51
6	1345	7.32
7	1581	10.33
8	1819	10.05
9	2056	11.55
10	2284	13.36
11	2520	16.73
12	2756	18.13
13	2973	21.86
14	3218	27.72
15	3449	23.63
16	3684	34.47

Width= 400μm

	Beam Length (μm)	Tip Deflection (μm)
1	393	0.94
2	872	2.25
3	1343	1.65
4	1823	broken
5	2287	missing
6	2751	15.82
7	3211	38.86

Wafer	**CS02 - A**

Tablet #	**5**

	Width= 30μm	
	Beam Length (μm)	Tip Deflection (μm)
1	28	-1.10
2	67	-1.10
3	108	-1.30
4	147	-1.35
5	188	-1.61
6	228	-1.47
7	258	-1.89
8	357	-2.11
9	457	-2.86
10	557	-4.06
11	657	-4.35
12	759	-4.31
13	857	-4.14
14	958	-4.34
15	1054	-4.22
16	1153	-3.42
17	1254	-3.79
18	1356	-3.82
19	1451	-3.72
20	1556	-3.77
21	1653	-4.00
22	1762	-4.08
23	1861	-3.94
24	1955	-4.02
25	2050	-3.92
26	2153	-4.12
27	2253	-4.14
28	2352	-4.25
29	2451	-4.23
30	2550	-4.20
31	2691	-4.12
32	2892	missing
33	3184	-4.27

	Width= 60μm	
	Beam Length (μm)	Tip Deflection (μm)
1	49	-1.25
2	70	-1.18
3	107	-1.08
4	188	-1.22
5	230	-1.46
6	360	-1.87
7	459	-2.47
8	658	-3.79
9	759	-3.75
10	959	-3.91
11	1056	-3.82
12	1256	-3.69
13	1356	-3.03
14	1558	-3.08
15	1697	-3.51
16	1987	-3.60
17	2289	-3.51
18	2588	missing
19	2895	missing
20	3197	missing
21	3498	missing

	Width= 150μm	
	Beam Length (μm)	Tip Deflection (μm)
1	148	-0.60
2	408	-1.75
3	644	-3.24
4	878	-3.06
5	1106	-2.76
6	1345	-0.67
7	1581	-2.44
8	1819	-2.22
9	2056	-2.13
10	2284	-1.97
11	2520	-2.37
12	2756	-2.22
13	2973	-2.05
14	3218	-2.22
15	3449	-2.39
16	3684	-2.49

	Width= 400μm	
	Beam Length (μm)	Tip Deflection (μm)
1	393	-0.95
2	872	-5.18
3	1343	broke off
4	1823	broke off
5	2287	missing
6	2751	missing
7	3211	-13.89

Wafer	CS02 - C

Tablet #	5

Width= 30μm

	Beam Length (μm)	Tip Deflection (μm)
1	28	-0.85
2	67	-0.97
3	108	-0.88
4	147	-1.08
5	188	-1.31
6	228	-1.10
7	258	-1.14
8	357	-3.97
9	457	-4.03
10	557	-2.20
11	657	-4.34
12	759	-4.21
13	857	-4.02
14	958	-3.99
15	1054	-4.13
16	1153	-4.36
17	1254	-4.33
18	1356	-4.30
19	1451	-4.16
20	1556	-4.30
21	1653	-3.98
22	1762	-3.89
23	1861	-4.04
24	1955	-3.96
25	2050	-3.94
26	2153	missing
27	2253	missing
28	2352	missing
29	2451	missing
30	2550	missing
31	2691	missing
32	2892	missing
33	3184	missing

Width= 60μm

	Beam Length (μm)	Tip Deflection (μm)
1	49	-1.20
2	70	-1.12
3	107	-1.18
4	188	-1.15
5	230	-1.00
6	360	-1.35
7	459	-1.35
8	658	-2.63
9	759	-3.11
10	959	-3.53
11	1056	-3.38
12	1256	-3.32
13	1356	-3.51
14	1558	-3.65
15	1697	-3.59
16	1987	missing
17	2289	missing
18	2588	missing
19	2895	-3.58
20	3197	-3.58
21	3498	missing

Width= 150μm

	Beam Length (μm)	Tip Deflection (μm)
1	148	-0.38
2	408	-0.70
3	644	-2.00
4	878	-3.05
5	1106	-3.08
6	1345	-3.02
7	1581	-2.71
8	1819	-2.78
9	2056	-2.14
10	2284	-2.87
11	2520	-2.83
12	2756	-2.68
13	2973	-2.78
14	3218	-2.44
15	3449	-2.35
16	3684	-2.31

Width= 400μm

	Beam Length (μm)	Tip Deflection (μm)
1	393	-0.36
2	872	-2.15
3	1343	-2.61
4	1823	-2.26
5	2287	missing
6	2751	-2.69
7	3211	-2.80

Wafer	CS02 - D

Tablet #	5

Width= 30μm

	Beam Length (μm)	Tip Deflection (μm)
1	28	-1.66
2	67	-1.41
3	108	-1.77
4	147	-1.76
5	188	-1.69
6	228	-1.53
7	258	-1.55
8	357	-1.61
9	457	-2.31
10	557	-2.73
11	657	-2.77
12	759	-3.20
13	857	-4.27
14	958	-4.17
15	1054	-4.29
16	1153	-4.30
17	1254	-4.09
18	1356	-4.14
19	1451	-4.15
20	1556	-4.18
21	1653	-4.28
22	1762	-4.02
23	1861	-4.29
24	1955	-4.30
25	2050	-4.35
26	2153	-4.18
27	2253	-4.21
28	2352	-4.03
29	2451	-4.13
30	2550	-4.13
31	2691	missing
32	2892	missing
33	3184	missing

Width= 60μm

	Beam Length (μm)	Tip Deflection (μm)
1	49	-1.30
2	70	-1.38
3	107	-1.56
4	188	-1.40
5	230	-1.37
6	360	-1.32
7	459	-1.31
8	658	-2.11
9	759	-2.56
10	959	-3.71
11	1056	broke off
12	1256	-3.67
13	1356	-3.69
14	1558	-3.63
15	1697	-3.74
16	1987	missing
17	2289	missing
18	2588	-3.65
19	2895	missing
20	3197	-3.83
21	3498	missing

Width= 150μm

	Beam Length (μm)	Tip Deflection (μm)
1	148	-0.51
2	408	-1.27
3	644	-2.05
4	878	-3.39
5	1106	-3.41
6	1345	-3.30
7	1581	-2.99
8	1819	-3.32
9	2056	-3.22
10	2284	-3.14
11	2520	-3.13
12	2756	-2.84
13	2973	-2.75
14	3218	-2.74
15	3449	-2.43
16	3684	-2.67

Width= 400μm

	Beam Length (μm)	Tip Deflection (μm)
1	393	-0.49
2	872	-2.37
3	1343	-2.61
4	1823	-2.54
5	2287	broke off
6	2751	-2.82
7	3211	-2.91

Wafer	**CS02 - E**

Tablet #	**5**

Width= 30μm

	Beam Length (μm)	Tip Deflection (μm)
1	28	missing
2	67	missing
3	108	missing
4	147	missing
5	188	missing
6	228	missing
7	258	missing
8	357	missing
9	457	missing
10	557	missing
11	657	missing
12	759	missing
13	857	missing
14	958	missing
15	1054	missing
16	1153	missing
17	1254	missing
18	1356	missing
19	1451	missing
20	1556	missing
21	1653	missing
22	1762	missing
23	1861	missing
24	1955	missing
25	2050	missing
26	2153	missing
27	2253	missing
28	2352	missing
29	2451	missing
30	2550	missing
31	2691	missing
32	2892	missing
33	3184	missing

Width= 60μm

	Beam Length (μm)	Tip Deflection (μm)
1	49	-0.95
2	70	-0.96
3	107	-0.93
4	188	-1.11
5	230	-1.00
6	360	-0.77
7	459	-0.68
8	658	-0.70
9	759	0.05
10	959	0.01
11	1056	0.65
12	1256	1.34
13	1356	0.08
14	1558	1.14
15	1697	0.09
16	1987	-0.45
17	2289	missing
18	2588	missing
19	2895	missing
20	3197	missing
21	3498	missing

Width= 150μm

	Beam Length (μm)	Tip Deflection (μm)
1	148	-0.33
2	408	0.23
3	644	0.23
4	878	1.12
5	1106	1.06
6	1345	0.95
7	1581	1.31
8	1819	-0.36
9	2056	-1.40
10	2284	-2.66
11	2520	-2.46
12	2756	-2.52
13	2973	-2.17
14	3218	-2.30
15	3449	-2.23
16	3684	-2.24

Width= 400μm

	Beam Length (μm)	Tip Deflection (μm)
1	393	0.23
2	872	-0.67
3	1343	-2.35
4	1823	-1.83
5	2287	broke off
6	2751	-2.77
7	3211	-2.87

Wafer	CS02 - F

Tablet #	5

Width= 30μm

	Beam Length (μm)	Tip Deflection (μm)
1	28	-0.72
2	67	-0.68
3	108	-0.79
4	147	-0.75
5	188	-0.77
6	228	-0.68
7	258	-0.49
8	357	-0.40
9	457	0.24
10	557	0.87
11	657	1.36
12	759	2.14
13	857	3.09
14	958	3.90
15	1054	4.73
16	1153	6.68
17	1254	7.42
18	1356	8.38
19	1451	9.51
20	1556	12.34
21	1653	15.22
22	1762	15.74
23	1861	18.98
24	1955	20.99
25	2050	23.25
26	2153	23.47
27	2253	25.63
28	2352	29.72
29	2451	28.65
30	2550	35.12
31	2691	37.51
32	2892	missing
33	3184	missing

Width= 60μm

	Beam Length (μm)	Tip Deflection (μm)
1	49	-0.97
2	70	-1.14
3	107	-0.89
4	188	-0.76
5	230	-0.71
6	360	-0.08
7	459	0.26
8	658	1.52
9	759	2.19
10	959	3.68
11	1056	3.89
12	1256	6.82
13	1356	7.34
14	1558	10.47
15	1697	10.61
16	1987	missing
17	2289	missing
18	2588	missing
19	2895	missing
20	3197	missing
21	3498	missing

Width= 150μm

	Beam Length (μm)	Tip Deflection (μm)
1	148	-0.22
2	408	0.51
3	644	1.93
4	878	3.08
5	1106	4.70
6	1345	5.97
7	1581	8.87
8	1819	10.13
9	2056	11.44
10	2284	13.48
11	2520	15.93
12	2756	broken
13	2973	22.66
14	3218	23.65
15	3449	31.53
16	3684	31.12

Width= 400μm

	Beam Length (μm)	Tip Deflection (μm)
1	393	0.98
2	872	1.63
3	1343	1.47
4	1823	1.05
5	2287	broke off
6	2751	13.70
7	3211	32.32

	Tablets #5		150μm Beam Width			
		CS01-D		CS02-A		CS02-B
		C = 1.15E-4		C = 1.68E-4		C = 1.08E-4
	Beam Length (μm)	Highest Deflection (μm)	Predicted Tip Deflection (μm)	Highest Deflection (μm)	Predicted Tip Deflection (μm)	Highest Deflection (μm)	Predicted Tip Deflection (μm)
1	148	Actual	-1.00	Actual	-0.60	Actual	-0.69
2	408	Actual	-3.91	Actual	-1.75	Actual	-1.92
3	644	Actual	-3.42	Actual	-3.24	Actual	-3.17
4	878	12.85	-4.01	14.57	-5.89	14.47	-3.77
5	1106	13.44	-6.37	14.88	-9.35	14.95	-5.99
6	1345	13.98	-9.41	15.8	-13.82	15.12	-8.85
7	1581	14.96	-13.01	16.24	-19.10	15.83	-12.23
8	1819	15.54	-17.23	broken	broken	16.79	-16.19
9	2056	16.75	-22.00	broken	broken	17.43	-20.68
10	2284	18.1	-27.15	broken	broken	18.79	-25.52
11	2520	19.6	-33.05	broken	broken	19.82	-31.07
12	2756	20.26	-39.54	broken	broken	21.06	-37.16
13	2973	22.85	-46.00	broken	broken	22.28	-43.24
14	3218	broken	broken	broken	broken	24.3	-50.67
15	3449	broken	broken	broken	broken	25.98	-58.21
16	3684	broken	broken	broken	broken	28.12	-66.40

		CS02-C		CS02-D		CS02-E	
		C = 7.01E-5		C = 6.69E-5		C = 4.87E-5	
	Beam Length (μm)	Highest Deflection (μm)	Predicted Tip Deflection (μm)	Highest Deflection (μm)	Predicted Tip Deflection (μm)	Highest Deflection (μm)	Predicted Tip Deflection (μm)
1	148	Actual	-0.38	Actual	-0.51	Actual	-0.33
2	408	Actual	-0.70	Actual	-1.27	Actual	0.23
3	644	Actual	-2.00	Actual	-2.05	Actual	0.23
4	878	14.29	-2.46	Actual	-3.39	Actual	1.12
5	1106	14.51	-3.90	14.59	-3.72	Actual	1.06
6	1345	14.85	-5.76	14.93	-5.50	Actual	0.95
7	1581	15.05	-7.97	15.32	-7.61	Actual	1.31
8	1819	15.9	-10.55	15.68	-10.07	Actual	-0.36
9	2056	16.16	-13.47	16.08	-12.86	15.95	-9.36
10	2284	16.73	-16.63	16.85	-15.87	16.26	-11.56
11	2520	broken	-20.24	17.36	-19.32	16.67	-14.07
12	2756	broken	-24.22	18.54	-23.11	16.64	-16.83
13	2973	broken	-28.17	19.85	-26.89	17.24	-19.58
14	3218	20.16	-33.02	broken	broken	17.97	-22.95
15	3449	21.61	-37.93	broken	broken	broken	broken
16	3684	21.84	-43.26	22.54	-41.29	broken	broken

APPENDIX C: X-RAY DIFFRACTION θ - 2θ SCAN DATA

CS02-A, Control Sample, No Anneal

Position	Count	Position	Count	Position	Count	Position	Count
-600.02	0.5	-430.06	1	-260.1	1.17	-90.143	144.5
-595.02	0.67	-425.06	1.67	-255.1	2.33	-85.144	181.83
-590.02	0.17	-420.06	1.17	-250.1	1.67	-80.145	223.83
-585.02	0.5	-415.06	1.17	-245.11	2.17	-75.146	269.33
-580.02	0.33	-410.07	0.33	-240.11	1.67	-70.148	327.5
-575.02	0.67	-405.07	1	-235.11	2.33	-65.149	407.5
-570.03	0.33	-400.07	1.17	-230.11	2.83	-60.15	516.83
-565.03	0.67	-395.07	1.17	-225.11	3	-55.151	651
-560.03	0.83	-390.07	1.67	-220.11	4.33	-50.153	869.67
-555.03	1.17	-385.07	1.83	-215.11	3.83	-45.154	1195.83
-550.03	1.17	-380.07	0.67	-210.11	3.5	-40.155	1709.33
-545.03	0.5	-375.07	0.83	-205.12	3.83	-35.156	2470.17
-540.03	0.17	-370.07	1.17	-200.12	3.67	-30.157	3446.5
-535.03	0.5	-365.08	0.83	-195.12	5.17	-25.159	4422
-530.04	1.67	-360.08	0.5	-190.12	4	-20.16	4971
-525.04	0.83	-355.08	0.67	-185.12	2.33	-15.161	4912.83
-520.04	1	-350.08	1	-180.12	5.33	-10.162	4489.5
-515.04	0.5	-345.08	1.17	-175.12	5.5	-5.164	3601.83
-510.04	0.67	-340.08	1.33	-170.12	6.83	-0.165	2806.17
-505.04	1.17	-335.08	0.83	-165.13	9.5	4.834	2229.67
-500.04	0.5	-330.08	1	-160.13	7	9.833	1836.5
-495.04	0.83	-325.09	2.83	-155.13	8.17	14.832	1640.5
-490.05	0.5	-320.09	2.17	-150.13	10.67	19.83	1566.17
-485.05	0.83	-315.09	1.17	-145.13	12.33	24.829	1498.83
-480.05	0.83	-310.09	1.5	-140.13	14.17	29.828	1480.17
-475.05	0.33	-305.09	2.5	-135.13	15.5	34.827	1521.67
-470.05	0.83	-300.09	1.67	-130.13	21.5	39.825	1536
-465.05	0.5	-295.09	1.33	-125.13	25.17	44.824	1578.67
-460.05	0.67	-290.09	0.83	-120.14	32.33	49.823	1618.17
-455.05	1.17	-285.1	1.17	-115.14	36.33	54.822	1666.33
-450.06	0.67	-280.1	2	-110.14	48	59.821	1700.33
-445.06	1.33	-275.1	1.5	-105.14	66.33	64.819	1766.83
-440.06	0.5	-270.1	2.67	-100.14	82	69.818	1839.67
-435.06	1	-265.1	1.83	-95.142	105.67	74.817	1892.33

CS02-A, Control Sample, No Anneal

Position	Count	Position	Count	Position	Count	Position	Count
79.816	1984	209.784	140.67	339.752	2.33	469.72	0.5
84.814	2097.17	214.783	80.5	344.751	1.33	474.719	0.83
89.813	2152.33	219.781	54.5	349.75	1.67	479.718	0.33
94.812	2200	224.78	33.67	354.749	1.5	484.717	0.17
99.811	2294.17	229.779	23.67	359.747	1.17	489.716	0.67
104.81	2350.17	234.778	17.67	364.746	0.83	494.714	0.83
109.808	2418.5	239.777	10	369.745	1.17	499.713	1
114.807	2455.67	244.775	9.33	374.744	1.17	504.712	0.67
119.806	2444.67	249.774	8.5	379.742	1	509.711	0.33
124.805	2471.33	254.773	4.67	384.741	0.33	514.709	0.83
129.803	2491	259.772	5.67	389.74	1.17	519.708	1
134.802	2473.33	264.771	4	394.739	1.17	524.707	0.5
139.801	2506.17	269.769	5.17	399.738	0.5	529.706	1
144.8	2483.67	274.768	1.5	404.736	0.33	534.705	0.5
149.799	2486	279.767	2.83	409.735	0.5	539.703	0.83
154.797	2480.17	284.766	1.83	414.734	1	544.702	0.67
159.796	2457.83	289.764	2.33	419.733	1.33	549.701	0.33
164.795	2402.17	294.763	2.33	424.731	0.83	554.7	1.17
169.794	2297.67	299.762	1.33	429.73	0.5	559.698	0.67
174.792	2088	304.761	1.17	434.729	0.33	564.697	1
179.791	1797	309.76	1.33	439.728	0.83	569.696	1
184.79	1437.67	314.758	1.83	444.727	0.67	574.695	0.67
189.789	1050.5	319.757	1.5	449.725	0.83	579.694	0.67
194.788	717.5	324.756	1.17	454.724	0.5	584.692	0.17
199.786	449.5	329.755	1.5	459.723	0.83	589.691	0.5
204.785	271.33	334.753	1.5	464.722	0.83	594.69	0.67
						599.689	0.17

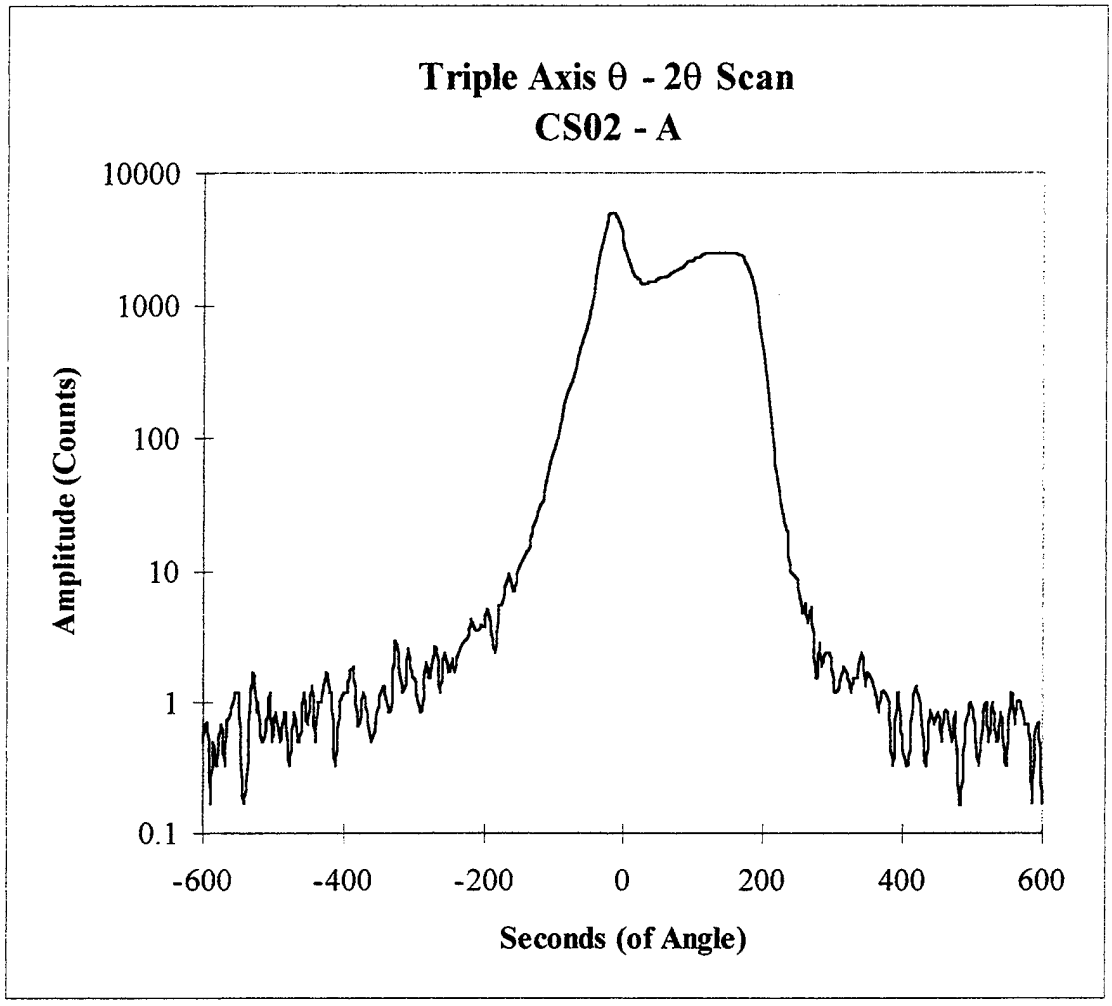
Triple Axis θ - 2θ Scan
CS02 - A
10000
1000
100
10
1
0.1
Amplitude (Counts)
-600
-400
-200
0
200
400
600
Seconds (of Angle)

CS02-C, 950°C Anneal Temperature

Position	Count	Position	Count	Position	Count	Position	Count
-600.02	0.67	-430.06	1.33	-260.1	1.17	-90.143	7.83
-595.02	0.5	-425.06	0.83	-255.1	0.83	-85.144	8.5
-590.02	0.5	-420.06	1	-250.1	0.83	-80.145	9
-585.02	0.17	-415.06	0.33	-245.11	1.33	-75.146	11.5
-580.02	0.33	-410.07	1.33	-240.11	1	-70.148	12.33
-575.02	0.5	-405.07	0.5	-235.11	1.83	-65.149	12.83
-570.03	0.5	-400.07	1	-230.11	1.5	-60.15	20.17
-565.03	0.5	-395.07	0.83	-225.11	0.5	-55.151	25.5
-560.03	0.83	-390.07	1.5	-220.11	1.17	-50.153	35.5
-555.03	0.83	-385.07	0.83	-215.11	1.5	-45.154	44.67
-550.03	0.17	-380.07	0.5	-210.11	0.83	-40.155	68.33
-545.03	0.83	-375.07	0.17	-205.12	0.83	-35.156	95.83
-540.03	0.33	-370.07	0.83	-200.12	1.5	-30.157	138.17
-535.03	1.17	-365.08	1.17	-195.12	1.5	-25.159	247.5
-530.04	0.83	-360.08	1	-190.12	2.17	-20.16	400.33
-525.04	0.67	-355.08	0.83	-185.12	2	-15.161	724.83
-520.04	0.67	-350.08	1	-180.12	3.33	-10.162	1199.83
-515.04	0.33	-345.08	0.5	-175.12	2.33	-5.164	1879.83
-510.04	0.83	-340.08	0	-170.12	1.33	-0.165	2735.83
-505.04	0.67	-335.08	0.33	-165.13	3.17	4.834	3650.33
-500.04	1.17	-330.08	1	-160.13	3.5	9.833	4458
-495.04	0.17	-325.09	0.83	-155.13	1.67	14.832	4951.5
-490.05	0.83	-320.09	1	-150.13	2.17	19.83	5087.5
-485.05	0.83	-315.09	0.83	-145.13	2.83	24.829	4858.5
-480.05	1	-310.09	0.33	-140.13	4.83	29.828	4177.83
-475.05	0.83	-305.09	1.17	-135.13	4.17	34.827	3486.17
-470.05	0.5	-300.09	0.67	-130.13	4.33	39.825	2718.5
-465.05	0.67	-295.09	0.67	-125.13	2.83	44.824	2118.17
-460.05	0.5	-290.09	0.83	-120.14	4.67	49.823	1647.5
-455.05	0.5	-285.1	1.33	-115.14	5.83	54.822	1370.17
-450.06	0.67	-280.1	1.33	-110.14	4.67	59.821	1237.33
-445.06	0.33	-275.1	1.17	-105.14	6.5	64.819	1139.83
-440.06	0.5	-270.1	1.17	-100.14	6.67	69.818	1138.5
-435.06	0.5	-265.1	1.17	-95.142	5.5	74.817	1150.67

CS02-C, 950°C Anneal Temperature

Position	Count	Position	Count	Position	Count	Position	Count
79.816	1136.83	209.784	2204.33	339.752	3.5	469.72	0.83
84.814	1124.83	214.783	1955.67	344.751	3.33	474.719	0.83
89.813	1159	219.781	1648	349.75	2.17	479.718	1.33
94.812	1212.33	224.78	1341.33	354.749	3	484.717	0.5
99.811	1206.17	229.779	987.17	359.747	3	489.716	1
104.81	1285.33	234.778	629.83	364.746	2.5	494.714	0.33
109.808	1329	239.777	383.67	369.745	3.5	499.713	0.33
114.807	1369.17	244.775	232.83	374.744	3.5	504.712	1
119.806	1420.5	249.774	126.83	379.742	3.33	509.711	0.5
124.805	1472.33	254.773	66.5	384.741	2.5	514.709	0.67
129.803	1564	259.772	37.33	389.74	1.83	519.708	0.67
134.802	1615.5	264.771	24.33	394.739	2	524.707	1.17
139.801	1726	269.769	19.17	399.738	3.17	529.706	0.5
144.8	1808.33	274.768	12.83	404.736	2	534.705	0.67
149.799	1891.33	279.767	10.67	409.735	1.5	539.703	0.5
154.797	2013.17	284.766	11	414.734	1.33	544.702	0.5
159.796	2062.83	289.764	7.33	419.733	1.17	549.701	0.5
164.795	2167.33	294.763	7.5	424.731	1.67	554.7	1
169.794	2249	299.762	5.83	429.73	1.83	559.698	0.5
174.792	2311.83	304.761	7	434.729	1.67	564.697	0.33
179.791	2340.17	309.76	5.83	439.728	1.17	569.696	0.83
184.79	2396.33	314.758	4.5	444.727	2.17	574.695	0.67
189.789	2427.5	319.757	3.5	449.725	1	579.694	0.83
194.788	2400.83	324.756	3.17	454.724	1.33	584.692	0.67
199.786	2398.83	329.755	3.67	459.723	1.17	589.691	0.67
204.785	2321.83	334.753	3.67	464.722	0.83	594.69	0.5
						599.689	0.67

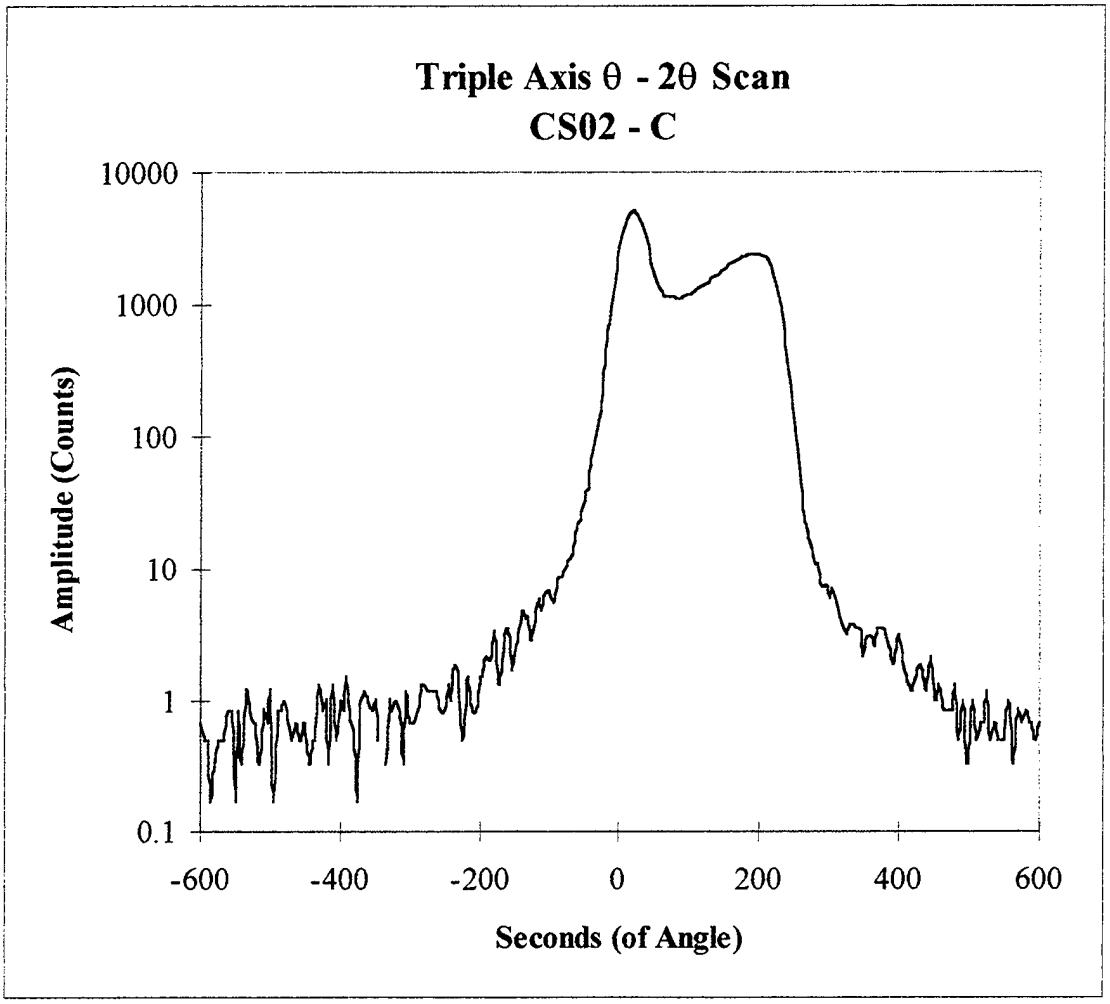
Triple Axis θ - 2θ Scan
CS02 - C
Amplitude (Counts)
10000
1000
100
10
1
0.1
-600
-400
-200
0
200
400
600
Seconds (of Angle)

CS02-E, 1050°C Anneal Temperature

Position	Count	Position	Count	Position	Count	Position	Count
-600.02	1	-430.06	0.67	-260.1	3	-90.143	27.83
-595.02	0.83	-425.06	0.83	-255.1	1.67	-85.144	38.17
-590.02	1.33	-420.06	1.67	-250.1	2.5	-80.145	40.5
-585.02	0.67	-415.06	0.83	-245.11	2.17	-75.146	52.33
-580.02	0.83	-410.07	0.5	-240.11	2.33	-70.148	68.83
-575.02	1.83	-405.07	1.33	-235.11	3.17	-65.149	91.67
-570.03	1.5	-400.07	1.33	-230.11	2.5	-60.15	125.5
-565.03	0.83	-395.07	1.33	-225.11	2.83	-55.151	179.17
-560.03	1	-390.07	1.33	-220.11	3.67	-50.153	261.83
-555.03	0.67	-385.07	1.67	-215.11	3	-45.154	368.17
-550.03	0.83	-380.07	1	-210.11	2	-40.155	589.17
-545.03	0.5	-375.07	1.67	-205.12	3.83	-35.156	933
-540.03	1	-370.07	1.33	-200.12	4.17	-30.157	1595.33
-535.03	1	-365.08	1.67	-195.12	4.5	-25.159	2672.33
-530.04	0.67	-360.08	1.33	-190.12	3.33	-20.16	4679.83
-525.04	0.67	-355.08	1.17	-185.12	4.33	-15.161	8010.33
-520.04	0.83	-350.08	0.83	-180.12	4.67	-10.162	12741.3
-515.04	0.5	-345.08	1.17	-175.12	4.17	-5.164	18018.3
-510.04	1.33	-340.08	1.67	-170.12	6	-0.165	21509.7
-505.04	0.83	-335.08	1.83	-165.13	5.33	4.834	21589
-500.04	0.17	-330.08	1.17	-160.13	6.17	9.833	18752.8
-495.04	1.17	-325.09	2.5	-155.13	8.17	14.832	14277.3
-490.05	0.83	-320.09	1.33	-150.13	7.67	19.83	10514.8
-485.05	1.17	-315.09	1.5	-145.13	7.33	24.829	7774.5
-480.05	1.67	-310.09	1.5	-140.13	9.17	29.828	6095
-475.05	1	-305.09	1.17	-135.13	8.17	34.827	5145
-470.05	0.67	-300.09	2.17	-130.13	10.83	39.825	4648.17
-465.05	1.5	-295.09	2.5	-125.13	12.5	44.824	4311
-460.05	1.33	-290.09	2	-120.14	11.33	49.823	4206.83
-455.05	0.83	-285.1	1	-115.14	15.5	54.822	4123.5
-450.06	1.33	-280.1	1.67	-110.14	14.17	59.821	4164
-445.06	1.17	-275.1	1.17	-105.14	19.33	64.819	4269.33
-440.06	0.67	-270.1	1.83	-100.14	21.33	69.818	4407.67
-435.06	1.5	-265.1	1.5	-95.142	26.33	74.817	4498.5

CS02-E, 1050°C Anneal Temperature

Position	Count	Position	Count	Position	Count	Position	Count
79.816	4727.67	209.784	1069.17	339.752	2	469.72	0.5
84.814	4800.17	214.783	565.33	344.751	3.5	474.719	1
89.813	5092.83	219.781	306	349.75	2	479.718	1
94.812	5305	224.78	167	354.749	2	484.717	
99.811	5562.5	229.779	102.17	359.747	2.17	489.716	0.33
104.81	5791	234.778	60.67	364.746	1.5	494.714	0.67
109.808	6073.5	239.777	46	369.745	1.17	499.713	0.5
114.807	6471.83	244.775	29.83	374.744	1.83	504.712	0.17
119.806	6777.67	249.774	23.67	379.742	1.33	509.711	1
124.805	7035.5	254.773	18.5	384.741	1	514.709	1
129.803	7392.17	259.772	14.67	389.74	1.67	519.708	1
134.802	7757.67	264.771	13.17	394.739	2.17	524.707	0.5
139.801	8000.5	269.769	9.67	399.738	1.33	529.706	0.17
144.8	8257.67	274.768	7.83	404.736	0.5	534.705	0.17
149.799	8370	279.767	7.5	409.735	1	539.703	0.33
154.797	8532.17	284.766	6	414.734	1	544.702	0.67
159.796	8496	289.764	6.17	419.733	1.5	549.701	0.67
164.795	8441	294.763	4.5	424.731	0.67	554.7	0.83
169.794	8377.67	299.762	5.17	429.73	0.83	559.698	0.83
174.792	8262.33	304.761	4.67	434.729	1.33	564.697	0.83
179.791	7924.17	309.76	3.17	439.728	0.83	569.696	0.83
184.79	7163.17	314.758	3.5	444.727	0.67	574.695	0.83
189.789	6053.67	319.757	2	449.725	0.83	579.694	1.67
194.788	4557.83	324.756	3.67	454.724	0.33	584.692	0.5
199.786	3090	329.755	3	459.723	0.67	589.691	0.5
204.785	1897.17	334.753	1.67	464.722	0.67	594.69	1.17
						599.689	0.33

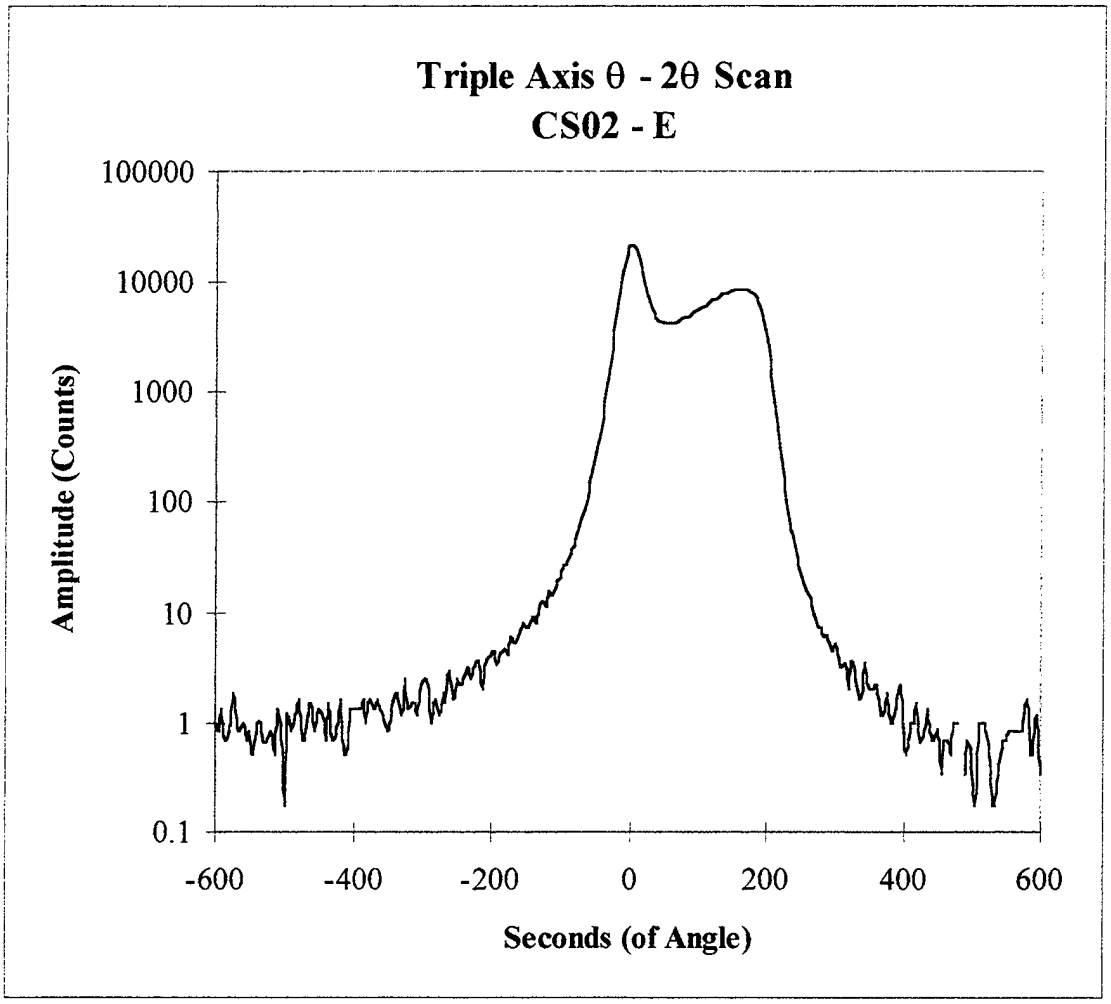
Triple Axis θ - 2θ Scan
CS02 - E
Amplitude (Counts)
100000
10000
1000
100
10
1
0.1
-600
-400
-200
0
200
400
600
Seconds (of Angle)

CS02-F, 1100°C Anneal Temperature

Position	Count	Position	Count	Position	Count	Position	Count
-600.02	0.5	-430.06	1.5	-260.1	2.33	-90.143	29.17
-595.02	0.5	-425.06	0.67	-255.1	1.83	-85.144	28.33
-590.02	0.33	-420.06	1.17	-250.1	3.17	-80.145	40.5
-585.02	0.67	-415.06	1	-245.11	2.33	-75.146	50.5
-580.02	0.17	-410.07	1.33	-240.11	3.5	-70.148	60.5
-575.02	0.5	-405.07	1	-235.11	3.67	-65.149	76.5
-570.03	1	-400.07	1.33	-230.11	2.17	-60.15	94.67
-565.03	0.83	-395.07	1	-225.11	3.5	-55.151	134.33
-560.03	1	-390.07	1.17	-220.11	3.17	-50.153	204.83
-555.03	0.67	-385.07	1.33	-215.11	4.33	-45.154	319
-550.03	0.67	-380.07	1.33	-210.11	3.17	-40.155	473.67
-545.03	1	-375.07	1	-205.12	2.83	-35.156	762
-540.03	0.83	-370.07	0.83	-200.12	5	-30.157	1231.5
-535.03	0.83	-365.08	1.67	-195.12	3.67	-25.159	1970.67
-530.04	1	-360.08	0.83	-190.12	4.5	-20.16	3256.33
-525.04	0.5	-355.08	2.17	-185.12	4.17	-15.161	5496.5
-520.04	0.83	-350.08	1.5	-180.12	5.33	-10.162	8804.83
-515.04	1	-345.08	1	-175.12	5.5	-5.164	12916.2
-510.04	0.67	-340.08	1	-170.12	5	-0.165	16038.8
-505.04	0.5	-335.08	1.67	-165.13	6.33	4.834	16224
-500.04	0.67	-330.08	1.83	-160.13	4.67	9.833	13519.5
-495.04	0.67	-325.09	1	-155.13	7.67	14.832	9915.83
-490.05	1.33	-320.09	0.67	-150.13	7.5	19.83	7157.17
-485.05	0.33	-315.09	1.5	-145.13	6.83	24.829	5602
-480.05	1.17	-310.09	0.67	-140.13	8.67	29.828	4579.83
-475.05	0.83	-305.09	1.67	-135.13	9.83	34.827	3988.5
-470.05	0.5	-300.09	2.67	-130.13	9.33	39.825	3610.33
-465.05	0.67	-295.09	1.83	-125.13	12.33	44.824	3396.5
-460.05	1	-290.09	2.17	-120.14	11	49.823	3371.5
-455.05	0.67	-285.1	1.5	-115.14	13.83	54.822	3356.67
-450.06	1	-280.1	1.5	-110.14	15	59.821	3334.83
-445.06	1.17	-275.1	3	-105.14	18.17	64.819	3458.5
-440.06	0.33	-270.1	2.33	-100.14	17	69.818	3587.5
-435.06	1	-265.1	2.83	-95.142	22.5	74.817	3703.67

CS02-F, 1100°C Anneal Temperature

Position	Count	Position	Count	Position	Count	Position	Count
79.816	3834	209.784	143.5	339.752	2.5	469.72	0.83
84.814	4053.17	214.783	92	344.751	1.17	474.719	1.33
89.813	4281.33	219.781	68.17	349.75	1.5	479.718	1.17
94.812	4506.83	224.78	51.33	354.749	1	484.717	0.83
99.811	4886.5	229.779	33.33	359.747	0.33	489.716	0.67
104.81	5219.33	234.778	22.17	364.746	1.5	494.714	1.17
109.808	5561.17	239.777	21.5	369.745	0.83	499.713	1.33
114.807	6106.5	244.775	17	374.744	2.5	504.712	1.17
119.806	6632.5	249.774	12.83	379.742	1.33	509.711	0.33
124.805	7207.33	254.773	9.83	384.741	0.83	514.709	0.33
129.803	7795.17	259.772	7.5	389.74	1.83	519.708	0.5
134.802	8434.17	264.771	6.33	394.739	0.67	524.707	0.33
139.801	9173.83	269.769	4.67	399.738	0.67	529.706	1
144.8	9868.67	274.768	5.5	404.736	1.5	534.705	1
149.799	10728.5	279.767	4.5	409.735	1.33	539.703	0.33
154.797	11441.3	284.766	3.33	414.734	1.17	544.702	0.67
159.796	11410	289.764	4.5	419.733	0.17	549.701	1
164.795	10674.3	294.763	3.67	424.731	0.83	554.7	0.83
169.794	9007.83	299.762	4.17	429.73	0.67	559.698	0.83
174.792	6617.17	304.761	3.5	434.729	0.67	564.697	1
179.791	4292.33	309.76	2.5	439.728	1.67	569.696	1
184.79	2432.17	314.758	3.33	444.727	0.83	574.695	0.67
189.789	1339.83	319.757	2.83	449.725	1.17	579.694	1.17
194.788	741.17	324.756	1.67	454.724	0.17	584.692	1.33
199.786	412.5	329.755	2.67	459.723	0.67	589.691	0.83
204.785	235.67	334.753	2	464.722	1.17	594.69	0.5
						599.689	0.67

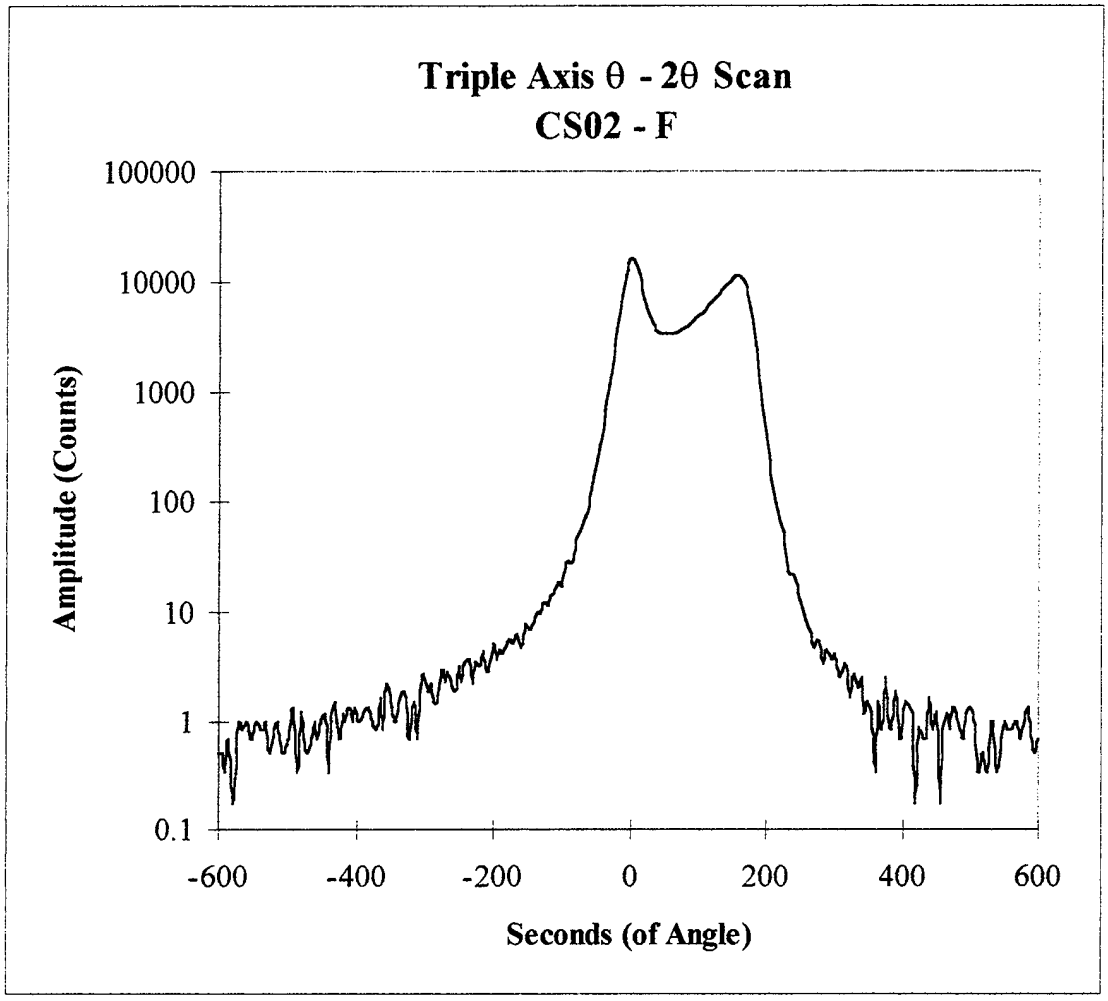
Triple Axis θ - 2θ Scan
CS02 - F
Amplitude (Counts)
100000
10000
1000
100
10
1
0.1
-600
-400
-200
0
200
400
600
Seconds (of Angle)

CS01, 1175°C Anneal Temperature Test Wafer

Position	Count	Position	Count	Position	Count	Position	Count
-600.02	0.5	-430.06	1	-260.1	0.5	-90.143	16.67
-595.02	0.83	-425.06	1.17	-255.1	0.5	-85.144	18.33
-590.02	0.17	-420.06	0.83	-250.1	1	-80.145	26.33
-585.02	0.33	-415.06	0.83	-245.11	0.83	-75.146	33.83
-580.02	0.17	-410.07	0.5	-240.11	0.83	-70.148	46.33
-575.02	0.33	-405.07	0.33	-235.11	0.5	-65.149	60.5
-570.03	1	-400.07	0.33	-230.11	0.67	-60.15	91.83
-565.03	0.5	-395.07	0.67	-225.11	0.5	-55.151	125.33
-560.03	0.83	-390.07		-220.11	1	-50.153	183.33
-555.03	0.83	-385.07	0.17	-215.11	0.5	-45.154	273.17
-550.03	0.33	-380.07	1	-210.11	0.67	-40.155	385.5
-545.03	0.17	-375.07	0.83	-205.12	0.17	-35.156	572.83
-540.03	0.83	-370.07	1	-200.12	1.83	-30.157	838.17
-535.03	0.33	-365.08	0.33	-195.12	2	-25.159	1141.5
-530.04	0.67	-360.08	0.33	-190.12	0.83	-20.16	1471.33
-525.04	0.5	-355.08		-185.12	1.33	-15.161	1781.67
-520.04	0.83	-350.08	0.67	-180.12	1.17	-10.162	1985.33
-515.04	0.17	-345.08	0.67	-175.12	2.33	-5.164	1982.17
-510.04	0.5	-340.08	0.17	-170.12	1.67	-0.165	1947.5
-505.04	0.67	-335.08	0.67	-165.13	1.17	4.834	1700.83
-500.04	0.67	-330.08	0.5	-160.13	1.33	9.833	1577.83
-495.04	1	-325.09	0.33	-155.13	1.5	14.832	1388.33
-490.05	0.5	-320.09	0.17	-150.13	1.33	19.83	1238.83
-485.05	0.5	-315.09	0.67	-145.13	1.83	24.829	1111.83
-480.05	1	-310.09	0.67	-140.13	3	29.828	1000.5
-475.05	0.5	-305.09	0.67	-135.13	3.33	34.827	900
-470.05	0.33	-300.09	0.67	-130.13	4.5	39.825	874.5
-465.05	1	-295.09	1	-125.13	3.83	44.824	840.33
-460.05	1	-290.09	0.83	-120.14	5.67	49.823	845.83
-455.05	0.67	-285.1	0.67	-115.14	6.5	54.822	856.5
-450.06	0.5	-280.1	0.83	-110.14	7.83	59.821	907
-445.06	0.33	-275.1	0.67	-105.14	11.5	64.819	966.83
-440.06	0.83	-270.1	0.33	-100.14	11.83	69.818	1044.17
-435.06	0.33	-265.1	0.5	-95.142	13.33	74.817	1121.83

CS01, 1175°C Anneal Temperature Test Wafer

Position	Count	Position	Count	Position	Count	Position	Count
79.816	1213.83	209.784	27.5	339.752	0.83	469.72	0.67
84.814	1254.5	214.783	14.67	344.751	0.17	474.719	0.5
89.813	1351.5	219.781	10	349.75	1	479.718	0.17
94.812	1466.67	224.78	5.33	354.749	0.33	484.717	0.83
99.811	1552.33	229.779	4.33	359.747	0.33	489.716	0.33
104.81	1658	234.778	2.83	364.746	0.17	494.714	0.17
109.808	1821.83	239.777	2.83	369.745	0.33	499.713	0.33
114.807	1914.33	244.775	2.17	374.744	1.17	504.712	1.17
119.806	1978.33	249.774	1.33	379.742	1.17	509.711	0.67
124.805	2076.83	254.773	2	384.741	0.83	514.709	0.33
129.803	2128.67	259.772	2.33	389.74	0.83	519.708	0.33
134.802	2076.67	264.771	1	394.739	1	524.707	0.17
139.801	1964.5	269.769	1.33	399.738	0.67	529.706	0.5
144.8	1808.5	274.768	0.83	404.736	0.67	534.705	0.17
149.799	1655.67	279.767	0.5	409.735	0.17	539.703	0.33
154.797	1429.5	284.766	0.83	414.734	1	544.702	0.5
159.796	1268.83	289.764	1.17	419.733	0.17	549.701	0.33
164.795	1033.17	294.763	0.83	424.731	0.17	554.7	0.67
169.794	845.5	299.762	1.17	429.73	1.5	559.698	0.17
174.792	637.67	304.761	0.5	434.729	0.33	564.697	0.5
179.791	468	309.76	0.33	439.728	0.33	569.696	0.5
184.79	337.5	314.758	0.67	444.727	0.83	574.695	0.5
189.789	231.33	319.757	0.5	449.725	0.83	579.694	0.67
194.788	137.67	324.756	0.67	454.724	0.5	584.692	0.67
199.786	84.67	329.755	0.67	459.723	0.5	589.691	0.33
204.785	49	334.753	1	464.722	0.83	594.69	1
						599.689	1.33

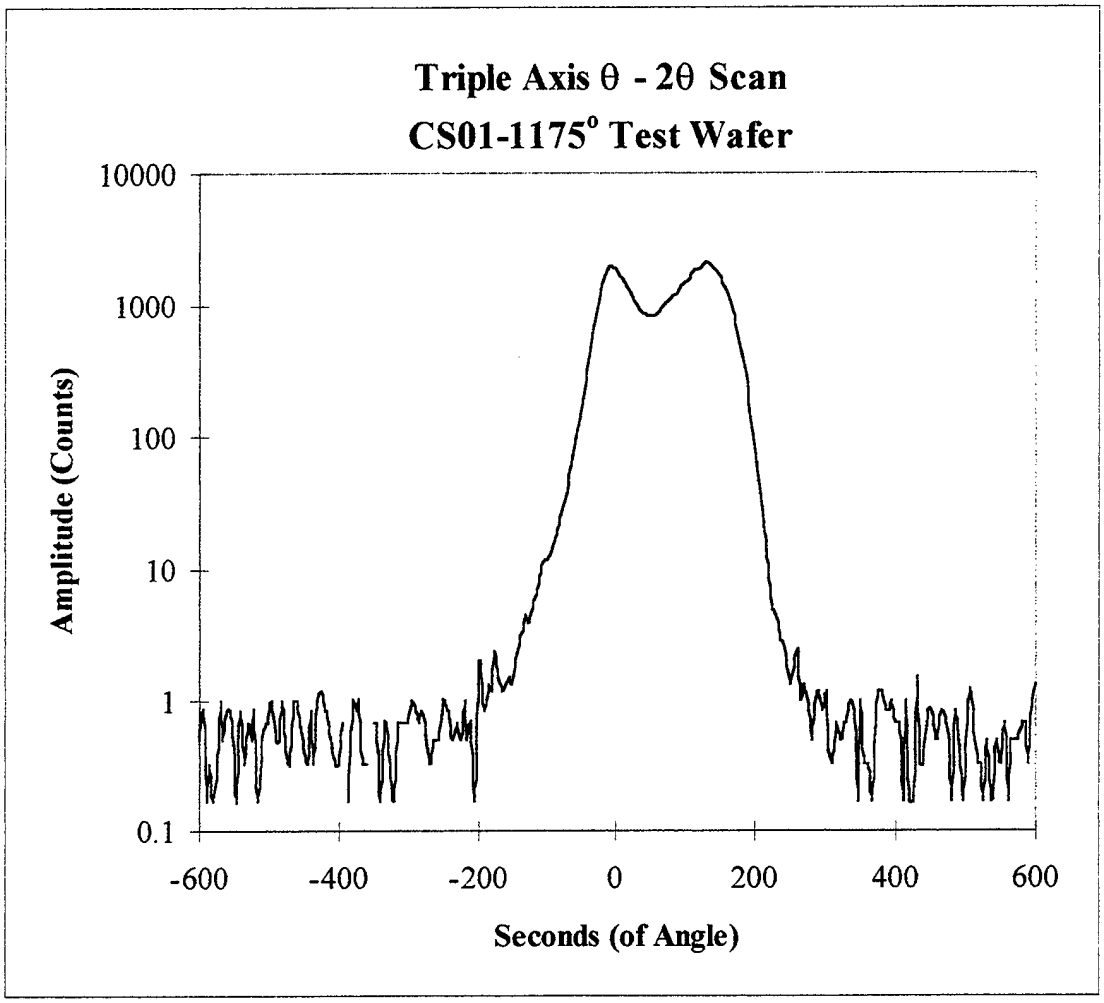
Triple Axis θ - 2θ Scan
CS01-1175° Test Wafer
10000
1000
100
10
1
0.1
Amplitude (Counts)
-600
-400
-200
0
200
400
600
Seconds (of Angle)

APPENDIX D: TEM PHOTOGRAPHS

Cross-Section TEM Photographs

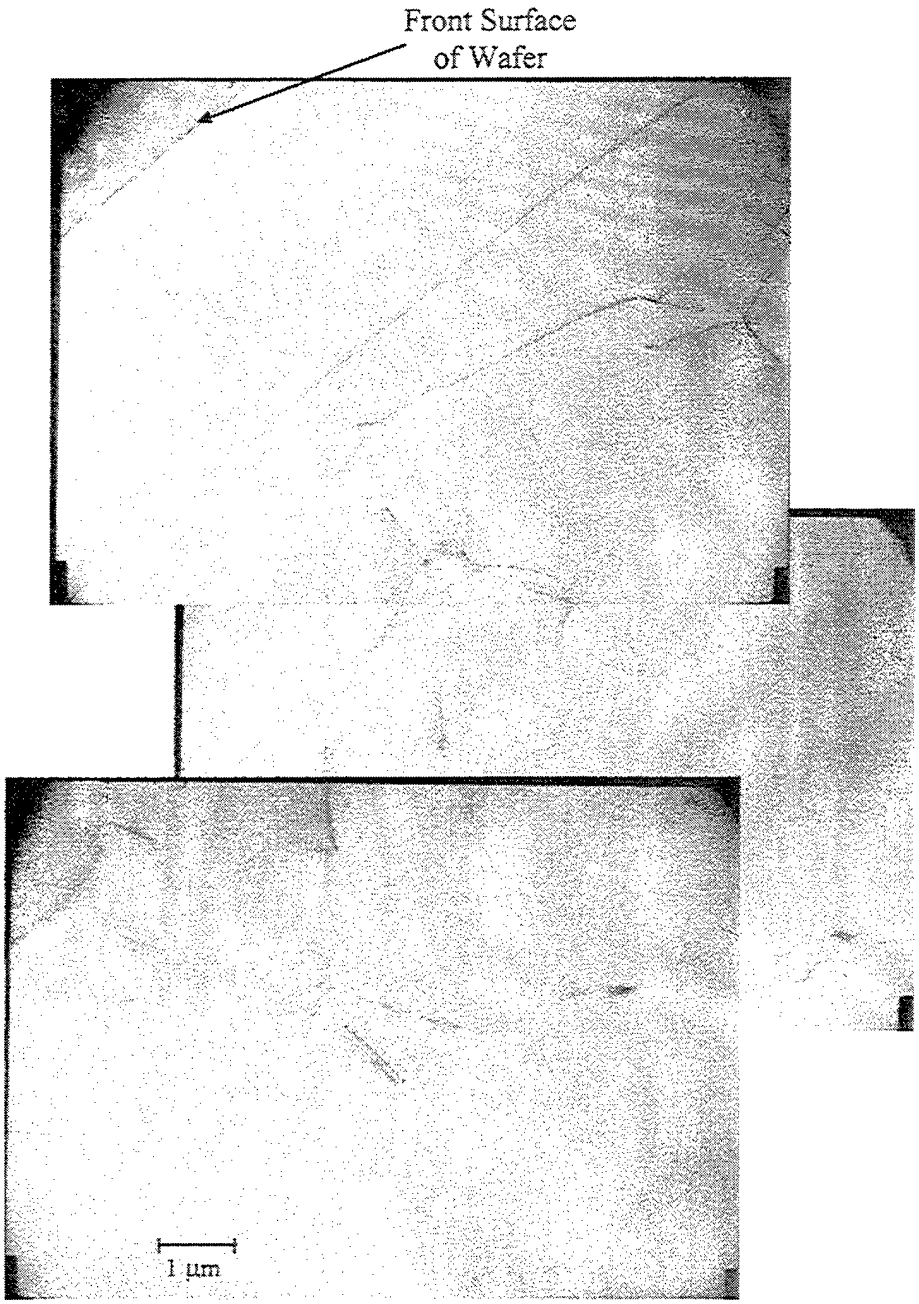

Figure 13: CS02-A Cross-Section Sample Dislocations

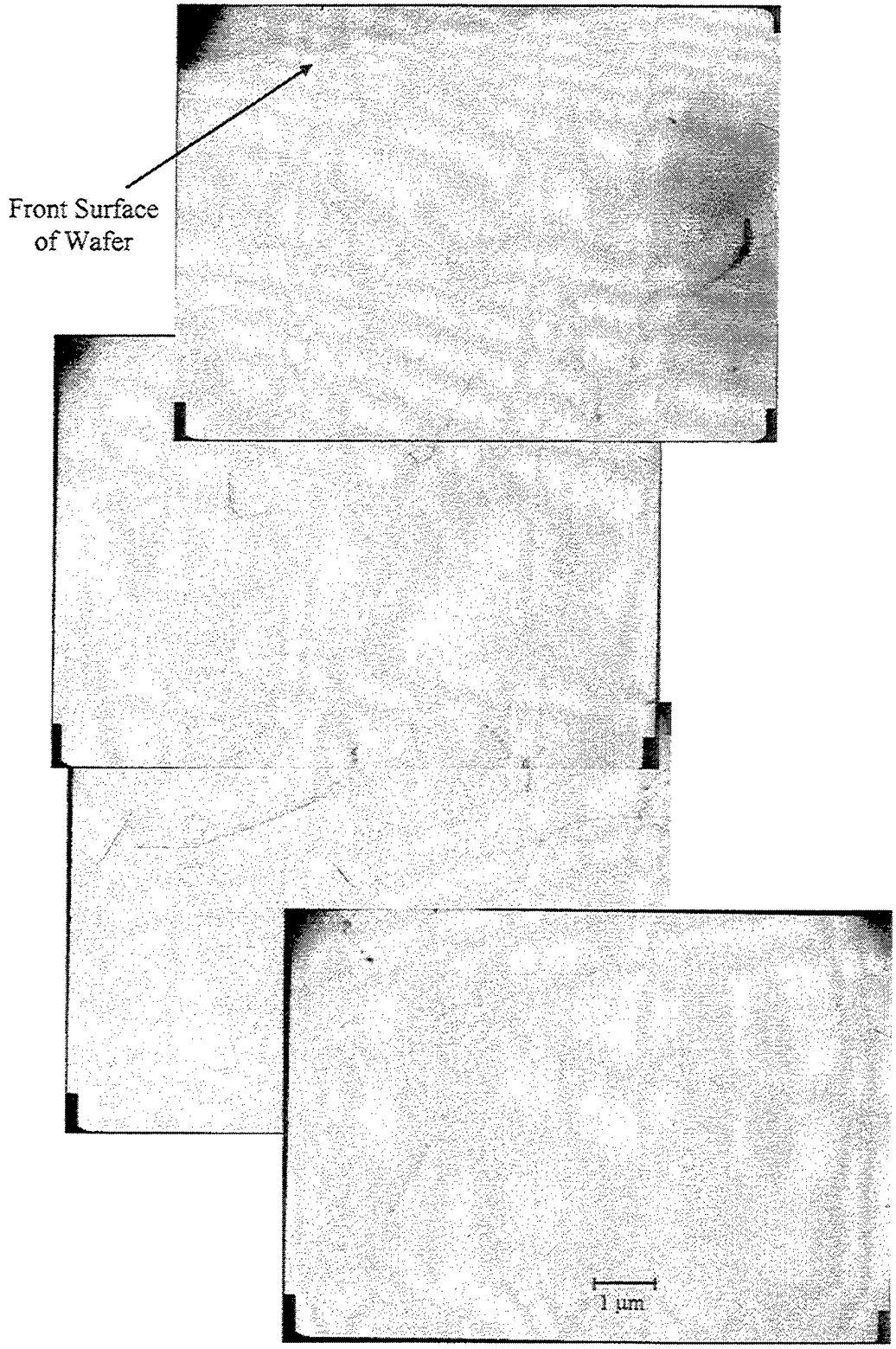

Figure 14: CS02-F Cross-Section Sample Dislocations

Plan-View TEM Photographs

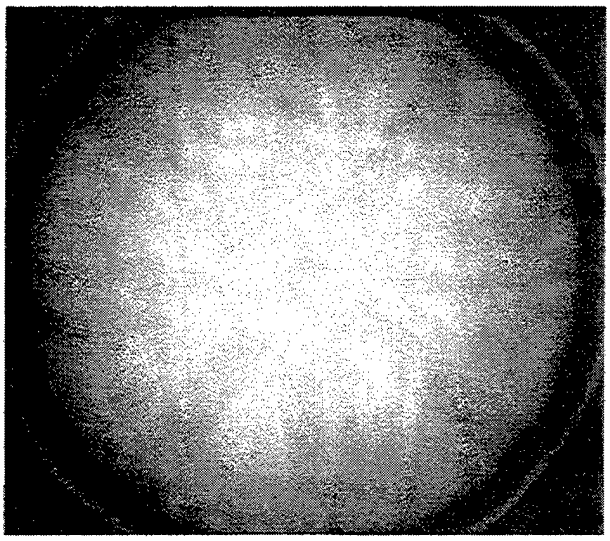

Figure 15: CS02-A Plan-View Sample Kikuchi Pattern

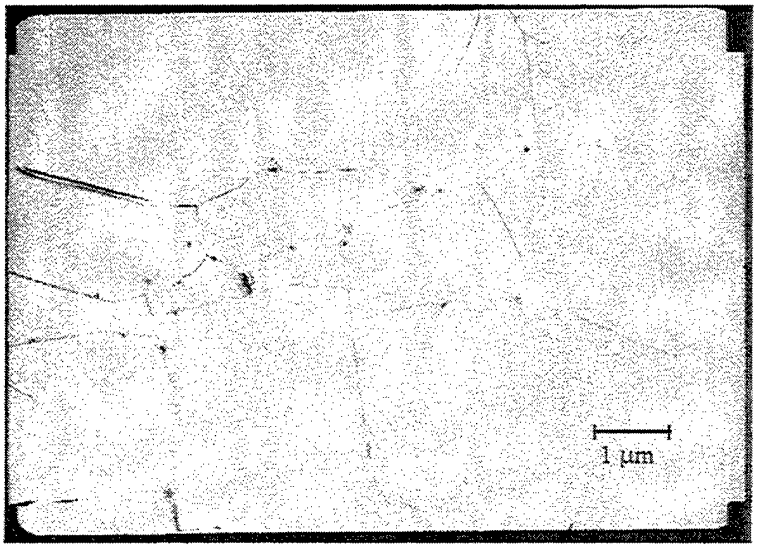

Figure 16: CS02-A Plan-View Sample Dislocations and Precipitates

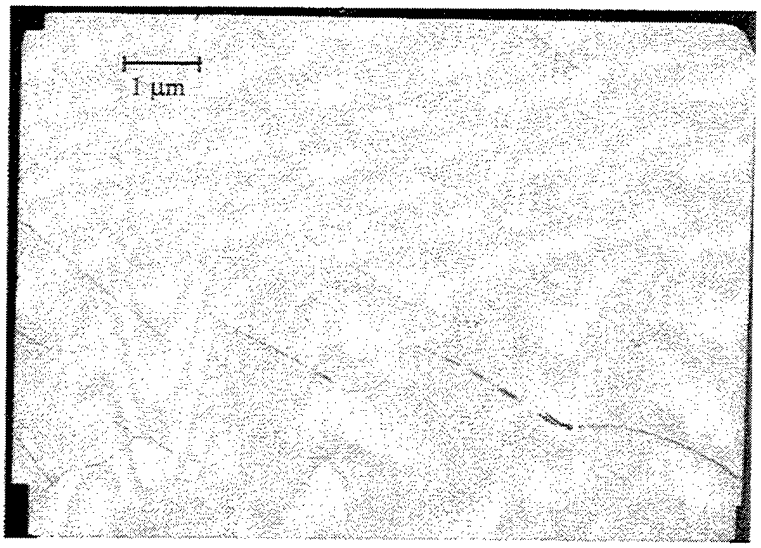

Figure 17: Plan-View Sample Precipitate-Free Region
(CS01-1175°C Test Wafer)

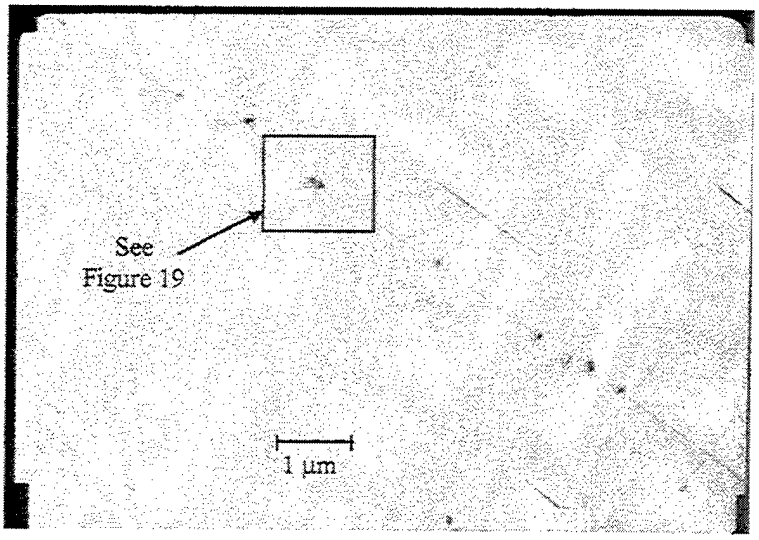

Figure 18: Plan-View Sample Dislocations and Precipitates
(CS01-1175°C Test Wafer)

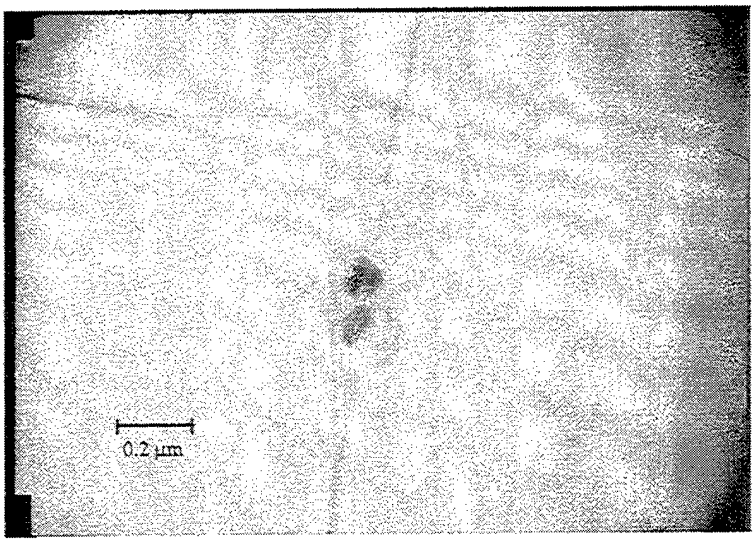

Figure 19: Plan-View Sample Precipitates -- Boxed Region of Figure 18
(CS01-1175°C Test Wafer)

APPENDIX E: SIMS DATA

CS02 - A: No Anneal

Sputter Time (seconds)	Si Signal Amplitude	B Signal Amplitude	B/Si Amplitude Ratio
22.47	222,447	12,274	0.0551772
37.26	219,183	12,839	0.0585766
52.04	211,433	13,383	0.0632966
66.83	182,997	19,931	0.1089144
81.62	221,001	26,201	0.1185560
96.41	218,245	28,221	0.1293088
111.20	219,259	32,633	0.1488331
125.99	218,567	34,405	0.1574117
140.78	212,463	36,378	0.1712204
155.57	214,493	38,559	0.1797681
170.35	213,561	40,230	0.1883771
185.14	217,037	41,511	0.1912623
199.93	214,183	42,726	0.1994836
214.72	214,443	43,738	0.2039610
229.51	214,621	45,454	0.2117873
244.30	217,155	46,113	0.2123506
259.09	213,673	46,810	0.2190731
273.88	216,009	48,206	0.2231666
288.66	215,147	48,259	0.2243071
303.45	218,071	48,219	0.2211161
318.24	219,321	49,170	0.2241919
333.03	219,197	48,989	0.2234930
347.82	218,125	50,623	0.2320825
362.61	217,805	50,409	0.2314410
377.40	221,587	50,674	0.2286867
392.18	217,439	50,566	0.2325526
406.97	218,187	50,458	0.2312603
421.76	220,619	50,945	0.2309185
436.55	218,561	51,322	0.2348177
451.34	220,369	50,883	0.2308991
466.13	219,763	51,183	0.2329009
480.92	221,981	50,927	0.2294205
495.71	222,259	51,964	0.2337993
510.49	219,249	50,963	0.2324435
525.42	223,705	51,659	0.2309247
540.21	218,909	51,221	0.2339831
554.99	222,897	51,121	0.2293481
569.78	222,099	51,670	0.2326440
584.57	222,605	51,040	0.2292851
599.36	224,073	51,982	0.2319869
614.15	221,149	51,624	0.2334354
628.94	224,267	51,615	0.2301498
643.73	223,105	50,766	0.2275431
658.52	220,879	51,912	0.2350246
673.30	225,189	51,103	0.2269338
688.09	225,199	51,488	0.2286333
702.88	226,367	51,540	0.2276834
717.67	222,587	51,384	0.2308491
732.46	222,657	50,538	0.2269769
747.25	226,251	51,041	0.2255946
762.05	226,049	51,068	0.2259156
776.84	225,589	50,986	0.2260128
791.63	225,449	50,719	0.2249688
806.42	227,401	50,978	0.2241767
821.21	223,507	50,725	0.2269504
836.00	225,981	51,259	0.2268288
850.79	226,225	50,808	0.2245906
865.58	223,867	50,423	0.2252364
880.36	224,391	50,651	0.2257265
895.15	223,625	51,178	0.2288563
909.94	225,621	50,385	0.2233170
924.73	230,047	51,211	0.2226110
939.52	227,589	50,046	0.2198964
954.31	224,269	50,539	0.2253499
969.10	226,389	50,196	0.2217246
983.88	223,977	49,336	0.2202726
998.67	226,119	49,435	0.2186238
1013.46	227,073	49,508	0.2180268
1028.42	227,787	49,601	0.2177517
1043.21	225,781	50,289	0.2227335
1058.00	224,159	49,866	0.2224582
1072.79	225,159	49,240	0.2186899
1087.58	224,903	49,514	0.2201571
1102.36	225,231	49,605	0.2202406
1117.15	221,141	49,234	0.2226362
1131.94	223,473	49,877	0.2231903
1146.73	227,813	49,532	0.2174239
1161.52	224,011	50,071	0.2235203
1176.31	223,867	48,901	0.2184377
1191.10	224,203	49,308	0.2199257
1205.89	226,831	48,993	0.2159890
1220.67	227,543	48,166	0.2116787

CS02 - A: No Anneal (continued)

Sputter Time (seconds)	Si Signal Amplitude	B Signal Amplitude	B/Si Amplitude Ratio
1235.46	227,857	48,742	0.2139149
1250.25	227,745	48,056	0.2110079
1265.04	224,449	48,051	0.2140843
1279.83	226,303	48,970	0.2163913
1294.62	228,157	47,774	0.2093909
1309.41	225,761	48,397	0.2143727
1324.20	226,887	48,036	0.2117177
1338.98	228,023	47,622	0.2088474
1353.77	227,765	47,235	0.2073848
1368.56	227,199	48,086	0.2116471
1383.35	225,705	47,738	0.2115062
1398.14	225,993	47,582	0.2105463
1412.93	227,505	47,465	0.2086328
1427.72	224,303	47,770	0.2129709
1442.51	229,507	47,191	0.2056190
1457.29	228,819	47,130	0.2059707
1472.08	229,373	48,004	0.2092836
1486.87	225,915	47,457	0.2100657
1501.68	227,307	47,882	0.2106490
1516.69	227,743	47,132	0.2069526
1531.48	227,067	46,780	0.2060185
1546.27	225,283	47,161	0.2093411
1561.06	223,735	47,402	0.2118667
1575.85	226,281	46,736	0.2065397
1590.63	225,883	47,316	0.2094713
1605.42	225,849	47,122	0.2086438
1620.21	225,629	46,440	0.2058246
1635.00	228,455	46,236	0.2023856
1649.79	226,791	46,277	0.2040513
1664.58	227,431	46,747	0.2055437
1679.37	227,129	46,947	0.2066975
1694.16	230,513	46,350	0.2010733
1708.94	229,617	46,152	0.2009956
1723.73	227,405	46,442	0.2042259
1738.52	228,627	46,375	0.2028413
1753.31	228,399	46,002	0.2014107
1768.10	227,453	46,190	0.2030749
1782.89	227,585	45,881	0.2015994
1797.68	228,247	46,215	0.2024780
1812.46	229,171	45,683	0.1993402
1827.25	224,277	45,464	0.2027136
1842.04	228,803	45,295	0.1979651
1856.83	228,763	44,617	0.1950359
1871.62	228,953	44,865	0.1959573
1886.41	229,049	45,138	0.1970670
1901.20	229,661	44,979	0.1958495
1915.99	229,667	45,575	0.1984395
1930.77	228,497	45,062	0.1972105
1945.56	228,203	44,547	0.1952078
1960.35	230,465	44,609	0.1935608
1975.14	228,597	44,763	0.1958162
1989.93	229,439	44,346	0.1932801
2004.72	227,929	44,399	0.1947931
2019.79	230,859	44,458	0.1925764
2034.58	228,829	44,371	0.1939046
2049.37	228,315	43,938	0.1924447
2064.15	229,535	44,352	0.1932254
2078.94	226,605	44,075	0.1945015
2093.73	231,389	43,739	0.1890280
2108.52	229,005	43,358	0.1893321
2123.31	227,477	43,746	0.1923096
2138.10	228,295	43,755	0.1916599
2152.89	231,231	43,376	0.1875873
2167.68	232,569	43,262	0.1860179
2182.46	231,149	42,850	0.1853783
2197.25	231,011	42,543	0.1841601
2212.04	228,047	43,091	0.1889567
2226.83	231,121	42,713	0.1848080
2241.64	232,259	42,341	0.1823008
2256.43	229,139	42,751	0.1865723
2271.22	231,891	42,130	0.1816802
2286.00	230,515	41,838	0.1814980
2300.79	227,367	41,959	0.1845431
2315.58	231,453	41,375	0.1787620
2330.37	232,091	41,429	0.1785033
2345.16	227,695	41,692	0.1831046
2359.95	230,961	41,461	0.1795152
2374.74	230,553	40,930	0.1775297
2389.53	229,525	41,484	0.1807385
2404.31	229,835	40,768	0.1773794
2419.10	231,453	40,402	0.1745581
2433.89	225,859	40,411	0.1789214
2448.68	231,533	41,289	0.1783288
2463.47	230,293	40,599	0.1762928
2478.26	232,635	40,572	0.1744020
2493.05	231,457	40,645	0.1756050

CS02 - A: No Anneal (continued)

Sputter Time (seconds)	Si Signal Amplitude	B Signal Amplitude	B/Si Amplitude Ratio
2507.84	229,797	40,461	0.1760728
2522.96	232,347	40,177	0.1729181
2537.75	227,713	40,382	0.1773373
2552.54	231,335	39,293	0.1698532
2567.33	230,305	40,025	0.1737913
2582.12	230,135	40,130	0.1743759
2596.91	229,785	39,222	0.1706900
2611.69	231,919	39,395	0.1698653
2626.48	233,917	39,460	0.1686923
2641.27	231,537	39,505	0.1706207
2656.06	231,057	38,700	0.1674911
2670.85	231,383	38,964	0.1683961
2685.64	231,291	39,370	0.1702185
2700.43	237,083	38,788	0.1636052
2715.22	229,107	38,825	0.1694623
2730.00	231,191	38,196	0.1652140
2744.79	231,391	38,362	0.1657886
2759.58	231,451	38,643	0.1669598
2774.37	232,549	37,909	0.1630151
2789.16	233,845	38,361	0.1640446
2803.95	233,017	38,203	0.1639494
2818.74	233,495	38,075	0.1630656
2833.53	230,869	37,927	0.1642793
2848.31	236,235	38,035	0.1610049
2863.10	232,229	37,586	0.1618489
2877.89	232,455	37,302	0.1604698
2892.68	231,007	37,818	0.1637093
2907.47	232,409	37,457	0.1611685
2922.26	235,483	37,326	0.1585083
2937.05	231,751	36,841	0.1589680
2951.84	231,605	37,002	0.1597634
2966.62	233,645	36,684	0.1570074
2981.43	229,947	36,940	0.1606457
2996.22	229,873	37,077	0.1612934
3011.01	231,971	36,495	0.1573257
3026.19	231,829	36,381	0.1569303
3040.98	232,415	35,686	0.1535443
3055.77	231,143	36,289	0.1569981
3070.56	231,635	36,060	0.1556760
3085.35	231,035	35,343	0.1529768
3100.14	233,095	35,634	0.1528733
3114.93	230,735	35,932	0.1557284
3129.71	235,443	35,206	0.1495309

Sputter Time (seconds)	Si Signal Amplitude	B Signal Amplitude	B/Si Amplitude Ratio
3144.50	232,185	35,624	0.1534294
3159.29	231,787	35,704	0.1540380
3174.08	233,045	35,498	0.1523225
3188.87	232,103	34,860	0.1501919
3203.66	226,611	34,922	0.1541055
3218.45	230,313	35,444	0.1538949
3233.24	232,795	35,174	0.1510943
3248.02	231,921	35,005	0.1509350
3262.81	234,189	34,508	0.1473511
3277.60	231,111	34,716	0.1502135
3292.39	230,615	34,417	0.1492401
3307.18	232,293	34,640	0.1491220
3321.97	230,081	34,511	0.1499950
3336.76	235,787	34,088	0.1445712
3351.55	233,775	33,876	0.1449086
3366.33	233,535	34,407	0.1473312
3381.12	233,455	33,882	0.1451329
3395.91	236,331	33,956	0.1436798
3410.70	232,443	33,627	0.1446677
3425.49	231,789	33,390	0.1440534
3440.28	233,435	32,953	0.1411656
3455.07	233,661	33,345	0.1427067
3469.86	238,499	33,120	0.1388685
3484.64	235,556	33,516	0.1422846
3499.43	234,859	33,303	0.1418000
3514.22	233,479	32,955	0.1411476
3529.46	235,285	33,401	0.1419598
3544.25	231,357	33,187	0.1434450
3559.04	235,871	33,188	0.1407040
3573.83	234,891	32,532	0.1384983
3588.62	231,263	32,453	0.1403294
3603.41	237,307	32,792	0.1381839
3618.20	236,621	32,073	0.1355459
3632.98	230,993	32,168	0.1392596
3647.77	236,641	32,558	0.1375839
3662.56	234,051	31,985	0.1366583
3677.35	233,901	32,404	0.1385372
3692.14	234,973	31,698	0.1349006
3706.93	232,867	31,677	0.1360304
3721.74	235,503	31,431	0.1334633
3736.53	233,243	31,542	0.1352324
3751.32	232,281	30,801	0.1326023
3766.10	234,243	30,852	0.1317094

CS02 - A: No Anneal (continued)

Sputter Time (seconds)	Si Signal Amplitude	B Signal Amplitude	B/Si Amplitude Ratio
3780.89	232,357	31,201	0.1342804
3795.68	233,865	30,795	0.1316785
3810.47	233,403	31,291	0.1340643
3825.26	233,703	30,666	0.1312178
3840.05	230,797	31,068	0.1346118
3854.84	235,583	30,542	0.1296443
3869.63	231,548	30,922	0.1335447
3884.41	235,799	30,191	0.1280370
3899.20	236,007	30,066	0.1273945
3913.99	231,989	30,768	0.1326270
3928.78	236,119	30,103	0.1274908
3943.57	235,199	30,086	0.1279172
3958.36	235,139	29,769	0.1266017
3973.15	232,645	29,659	0.1274861
3987.94	232,365	29,337	0.1262540
4002.72	234,121	29,328	0.1252686
4018.02	236,745	28,780	0.1215654
4032.81	232,645	29,074	0.1249715
4047.60	236,419	29,644	0.1253876
4062.39	234,463	28,809	0.1228723
4077.17	234,063	28,583	0.1221167
4091.96	233,259	28,588	0.1225590
4106.75	234,683	28,807	0.1227486
4121.54	237,579	28,723	0.1208987
4136.33	232,239	28,535	0.1228691
4151.12	236,407	28,648	0.1211808
4165.91	232,939	28,485	0.1222852
4180.70	234,791	27,640	0.1177217
4195.48	235,396	28,008	0.1189825
4210.27	234,575	27,548	0.1174379
4225.06	234,935	27,314	0.1162619
4239.85	235,259	27,557	0.1171347
4254.64	233,589	27,425	0.1174071
4269.43	233,923	27,450	0.1173463
4284.22	234,191	27,416	0.1170668
4299.01	237,069	27,381	0.1154980
4313.80	235,453	26,963	0.1145154
4328.58	233,017	26,839	0.1151804
4343.37	235,555	26,858	0.1140201
4358.16	237,491	27,375	0.1152675
4372.95	236,705	26,352	0.1113285
4387.74	236,871	26,347	0.1112293
4402.53	235,755	26,352	0.1117771
4417.32	236,861	26,016	0.1098366
4432.11	237,173	26,198	0.1104595
4446.90	235,865	26,167	0.1109406
4461.70	235,189	26,019	0.1106302
4476.49	237,149	25,969	0.1095050
4491.28	236,211	25,608	0.1084116
4506.07	236,477	25,439	0.1075749
4521.42	237,235	25,484	0.1074209
4536.21	242,235	25,488	0.1052201
4551.00	237,985	25,476	0.1070488
4565.79	237,177	25,163	0.1060938
4580.58	239,425	25,237	0.1054067
4595.36	236,963	24,958	0.1053245
4610.15	234,878	25,006	0.1064638
4624.94	237,153	24,381	0.1028071
4639.73	236,795	24,264	0.1024684
4654.52	236,889	23,714	0.1001060
4669.31	237,904	23,893	0.1004313
4684.10	238,625	24,174	0.1013054
4698.89	232,719	23,717	0.1019126
4713.68	236,355	23,987	0.1014872
4728.46	234,231	23,576	0.1006528
4743.25	237,165	23,842	0.1005292
4758.04	236,569	23,480	0.0992522
4772.83	233,295	23,169	0.0993120
4787.62	235,255	23,322	0.0991350
4802.41	239,614	22,831	0.0952824
4817.20	235,611	22,528	0.0956152
4831.99	238,807	22,875	0.0957886
4846.78	233,767	23,035	0.0985383
4861.56	238,725	22,610	0.0947115
4876.35	236,215	22,422	0.0949220
4891.14	239,185	22,126	0.0925058
4905.93	236,437	21,789	0.0921556
4920.72	234,285	22,269	0.0950509
4935.51	236,625	21,602	0.0912921
4950.30	236,457	21,872	0.0924988
4965.09	235,910	21,709	0.0920224
4979.88	236,983	21,597	0.0911331
4994.66	235,925	21,535	0.0912790
5009.45	237,579	21,419	0.0901553
5024.86	236,815	21,162	0.0893609
5039.65	237,553	20,769	0.0874289

CS02 - A: No Anneal (continued)

Sputter Time (seconds)	Si Signal Amplitude	B Signal Amplitude	B/Si Amplitude Ratio
5054.44	237,225	20,585	0.0867742
5069.23	239,569	20,922	0.0873318
5084.02	234,429	20,463	0.0872887
5098.81	237,051	20,593	0.0868716
5113.59	237,329	20,882	0.0879876
5128.38	234,227	20,022	0.0854812
5143.17	234,466	20,328	0.0866991
5157.96	233,551	20,065	0.0859127
5172.75	232,413	19,916	0.0856923
5187.54	234,563	19,419	0.0827880
5202.35	236,311	19,278	0.0815789
5217.14	235,671	19,421	0.0824073
5231.92	236,363	19,240	0.0814002
5246.71	234,417	18,819	0.0802800
5261.50	233,975	18,639	0.0796624
5276.29	233,063	18,825	0.0807722
5291.08	231,939	18,539	0.0799305
5305.87	233,340	18,380	0.0787692
5320.66	232,169	18,297	0.0788090
5335.45	232,343	18,366	0.0790469
5350.23	233,475	18,033	0.0772374
5365.02	233,417	17,747	0.0760313
5379.81	229,961	18,025	0.0783829
5394.60	233,473	17,590	0.0753406
5409.39	234,707	17,408	0.0741691
5424.18	232,817	17,377	0.0746380
5438.97	232,127	17,331	0.0746617
5453.76	231,985	16,783	0.0723452
5468.55	226,409	16,883	0.0745686
5483.33	230,091	17,055	0.0741228
5498.12	229,449	16,736	0.0729400
5512.91	230,399	16,529	0.0717408
5528.38	229,749	16,794	0.0730972
5543.17	229,225	16,034	0.0699487
5557.95	227,997	16,219	0.0711369
5572.74	230,571	15,902	0.0689679
5587.53	228,949	15,782	0.0689324
5602.32	231,695	15,567	0.0671875
5617.11	230,113	15,650	0.0680101
5631.90	231,141	15,525	0.0671668
5646.69	226,041	15,365	0.0679744
5661.48	228,001	15,098	0.0662190
5676.27	231,461	14,589	0.0630301

Sputter Time (seconds)	Si Signal Amplitude	B Signal Amplitude	B/Si Amplitude Ratio
5691.05	230,807	14,523	0.0629227
5705.84	228,330	14,947	0.0654623
5720.63	228,255	14,665	0.0642483
5735.42	227,959	14,314	0.0627920
5750.21	227,041	14,404	0.0634423
5765.00	229,243	13,917	0.0607085
5779.79	229,023	14,239	0.0621728
5794.58	228,121	13,553	0.0594115
5809.37	226,395	13,788	0.0609024
5824.15	226,463	13,672	0.0603719
5838.94	228,763	13,048	0.0570372
5853.73	226,885	12,830	0.0565485
5868.52	229,007	12,321	0.0538018
5883.31	228,667	12,251	0.0535757
5898.10	229,131	11,782	0.0514204
5912.89	227,433	11,830	0.0520153
5927.68	226,877	11,309	0.0498464
5942.48	229,311	10,985	0.0479044
5957.27	226,737	10,831	0.0477690
5972.06	227,737	10,253	0.0450212
5986.85	225,915	10,660	0.0471859
6001.64	226,863	10,149	0.0447363
6017.16	231,525	9,936	0.0429155
6031.95	232,397	9,571	0.0411838
6046.73	228,369	9,008	0.0394449
6061.52	227,827	11,022	0.0483788
6076.31	228,725	15,517	0.0678413
6091.10	227,483	15,637	0.0687392
6105.89	229,299	15,053	0.0656479
6120.68	227,705	14,916	0.0655058
6135.47	229,355	14,870	0.0648340
6150.26	230,441	13,414	0.0582101
6165.04	228,486	8,188	0.0358359
6179.83	225,481	8,304	0.0368279
6194.62	229,701	8,166	0.0355506
6209.41	230,313	7,919	0.0343836
6224.20	227,313	7,741	0.0340544
6238.99	231,333	7,870	0.0340202
6253.78	230,251	7,565	0.0328554
6268.57	226,257	7,479	0.0330553
6283.36	231,077	7,390	0.0319807
6298.15	227,539	7,446	0.0327241
6312.93	231,273	7,370	0.0318671

CS02 - A: No Anneal (continued)

Sputter Time (seconds)	Si Signal Amplitude	B Signal Amplitude	B/Si Amplitude Ratio
6327.72	225,733	7,511	0.0332738
6342.51	230,981	7,553	0.0326997
6357.30	229,191	7,576	0.0330554
6372.09	227,031	7,322	0.0322511
6386.88	228,435	7,327	0.0320748
6401.67	228,855	7,347	0.0321033
6416.46	228,833	7,232	0.0316038
6431.25	227,833	7,036	0.0308823
6446.03	228,147	6,897	0.0302305
6460.82	230,161	6,906	0.0300051
6475.61	226,773	6,774	0.0298713
6490.40	230,225	6,882	0.0298925
6505.19	230,141	6,629	0.0288041
6520.76	229,433	6,583	0.0286925
6535.55	226,923	6,618	0.0291641
6550.34	228,655	6,529	0.0285539
6565.13	230,817	6,289	0.0272467
6579.92	229,709	6,299	0.0274217
6594.71	228,232	6,358	0.0278576
6609.50	231,207	5,978	0.0258556
6624.29	228,003	5,972	0.0261926
6639.07	228,209	6,028	0.0264144
6653.86	229,021	5,848	0.0255348
6668.65	227,045	5,715	0.0251712
6683.46	230,297	5,933	0.0257624
6698.25	228,301	5,832	0.0255452
6713.04	227,725	5,635	0.0247448
6727.83	227,583	5,883	0.0258499
6742.62	227,771	5,685	0.0249593
6757.40	226,833	5,496	0.0242293
6772.19	223,827	5,352	0.0239113
6786.98	226,693	5,453	0.0240546
6801.77	230,579	5,532	0.0239918
6816.56	229,236	5,167	0.0225401
6831.35	226,004	5,360	0.0237164
6846.14	227,229	5,167	0.0227392
6860.93	228,023	5,156	0.0226118
6875.72	224,993	5,087	0.0226096
6890.51	222,463	5,043	0.0226689
6905.29	225,731	5,039	0.0223230
6920.08	226,587	4,895	0.0216032
6934.87	228,885	4,872	0.0212858
6949.66	224,341	4,832	0.0215386

Sputter Time (seconds)	Si Signal Amplitude	B Signal Amplitude	B/Si Amplitude Ratio
6964.45	226,107	4,768	0.0210874
6979.24	226,757	4,749	0.0209431
6994.03	228,271	4,553	0.0199456
7008.82	224,933	4,492	0.0199704
7024.45	224,705	4,389	0.0195323
7039.24	225,755	4,360	0.0193130
7054.03	226,395	4,380	0.0193467
7068.82	228,841	4,601	0.0201057
7083.61	226,167	4,396	0.0194370
7098.39	225,327	4,319	0.0191677
7113.18	223,705	4,270	0.0190876
7127.97	228,353	4,307	0.0188611
7142.76	224,929	4,197	0.0186592
7157.55	224,389	3,996	0.0178084
7172.34	228,995	4,074	0.0177908
7187.13	225,313	4,061	0.0180238
7201.92	224,403	4,052	0.0180568
7216.71	227,557	3,902	0.0171474
7231.49	225,031	3,962	0.0176065
7246.28	226,061	3,856	0.0170573
7261.07	223,913	3,873	0.0172969
7275.86	226,870	3,955	0.0174329
7290.65	226,713	3,805	0.0167833
7305.44	227,767	3,731	0.0163808
7320.23	225,208	3,676	0.0163227
7335.02	224,693	3,651	0.0162488
7349.81	222,409	3,595	0.0161639
7364.60	223,977	3,589	0.0160240
7379.39	221,457	3,430	0.0154883
7394.17	222,903	3,434	0.0154058
7408.96	224,029	3,541	0.0158060
7423.77	225,115	3,513	0.0156054
7438.56	225,455	3,467	0.0153778
7453.35	224,633	3,373	0.0150156
7468.14	225,095	3,424	0.0152114
7482.93	224,207	3,335	0.0148746
7497.72	218,768	3,356	0.0153405
7512.51	226,121	3,398	0.0150274
7528.20	226,647	3,327	0.0146792
7542.98	224,379	3,211	0.0143106
7557.77	220,171	3,201	0.0145387
7572.56	223,113	3,277	0.0146876
7587.35	224,595	3,052	0.0135889

CS02 - A: No Anneal (continued)

Sputter Time (seconds)	Si Signal Amplitude	B Signal Amplitude	B/Si Amplitude Ratio
7602.14	222,023	3,212	0.0144670
7616.93	218,787	3,117	0.0142467
7631.72	221,743	3,026	0.0136464
7646.51	224,271	3,150	0.0140455
7661.30	222,395	3,058	0.0137503
7676.09	220,427	3,069	0.0139230
7690.87	222,003	2,998	0.0135043
7705.66	220,575	2,869	0.0130069
7720.45	222,021	2,994	0.0134852
7735.24	222,153	2,929	0.0131846
7750.03	220,663	2,798	0.0126800
7764.82	217,823	2,995	0.0137497
7779.61	220,431	2,874	0.0130381
7794.40	221,283	2,786	0.0125902
7809.19	221,057	2,729	0.0123452
7823.97	220,701	2,749	0.0124558
7838.76	223,765	2,675	0.0119545
7853.55	221,097	2,726	0.0123294
7868.34	223,103	2,808	0.0125861
7883.13	219,771	2,767	0.0125904

Sputter Time (seconds)	Si Signal Amplitude	B Signal Amplitude	B/Si Amplitude Ratio
7897.92	220,663	2,629	0.0119141
7912.71	221,017	2,601	0.0117683
7927.50	220,955	2,648	0.0119843
7942.29	218,747	2,486	0.0113647
7957.08	219,259	2,512	0.0114568
7971.86	218,711	2,687	0.0122856
7986.65	222,173	2,496	0.0112345
8001.44	222,481	2,452	0.0110212
8017.18	221,021	2,411	0.0109085
8031.97	219,775	2,452	0.0111569
8046.76	218,481	2,596	0.0118820
8061.55	219,863	2,496	0.0113525
8076.34	220,655	2,293	0.0103918
8091.13	217,463	2,496	0.0114778
8105.92	221,511	2,418	0.0109159
8120.71	221,541	2,389	0.0107836
8135.50	222,285	2,078	0.0093484
8150.28	223,549	2,172	0.0097160
8165.09	222,507	2,454	0.0110289

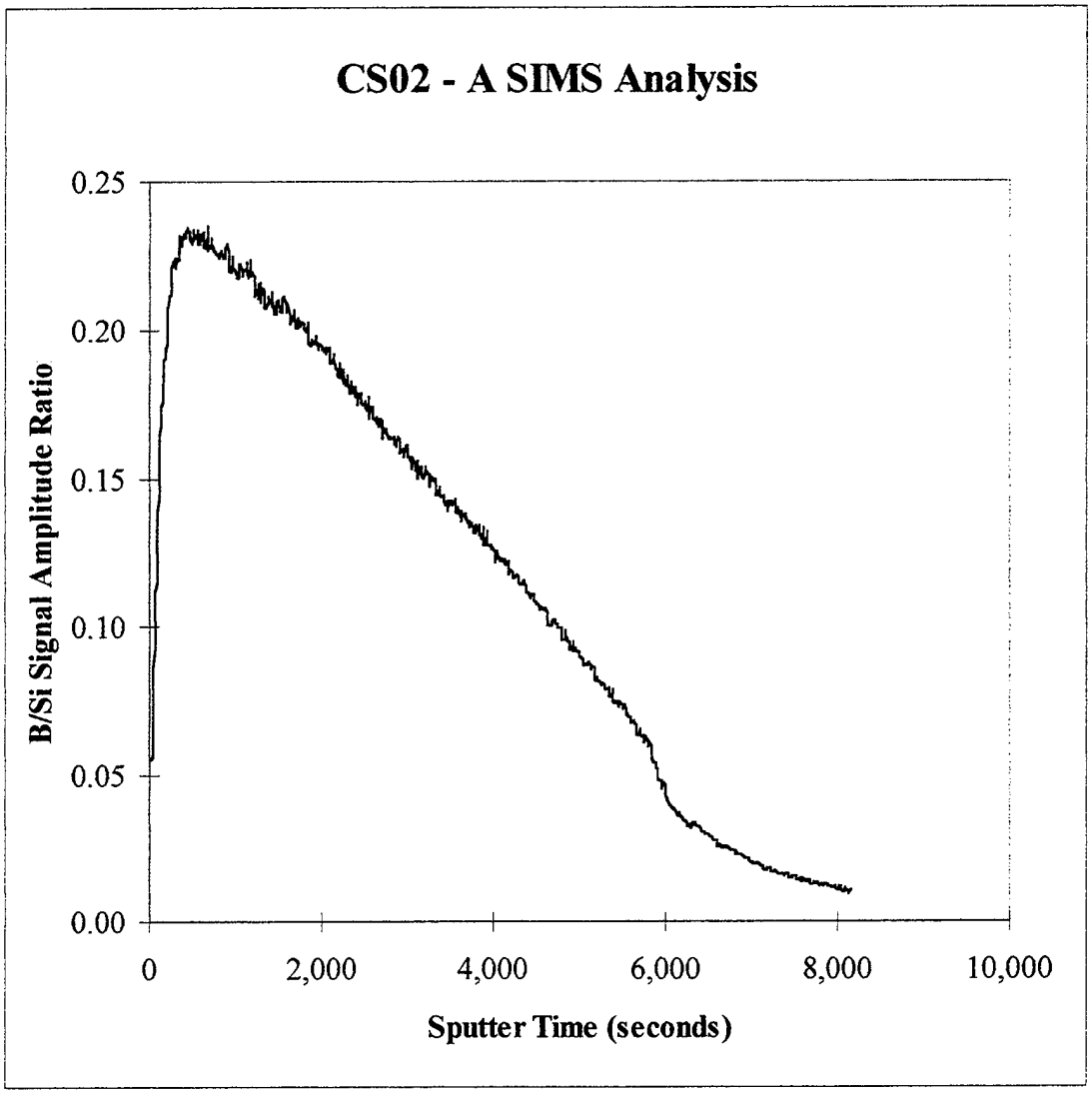
CS02 - A SIMS Analysis
B/Si Signal Amplitude Ratio
0.25
0.20
0.15
0.10
0.05
0.00
0
2,000
4,000
6,000
8,000
10,000
Sputter Time (seconds)

CS02 - F: 1100°C Anneal Temperature

Sputter Time (seconds)	Si Signal Amplitude	B Signal Amplitude	B/Si Amplitude Ratio
7.46	229,053	6,282	0.0274260
22.46	400,827	14,763	0.0368314
37.25	448,005	17,825	0.0397875
52.04	459,143	19,358	0.0421612
66.83	468,551	20,613	0.0439931
81.62	475,075	21,405	0.0450560
96.4	475,043	21,579	0.0454254
111.19	472,105	22,047	0.0466994
125.98	502,971	22,921	0.0455712
140.77	505,353	23,544	0.0465892
155.56	505,781	23,594	0.0466486
170.34	505,781	23,817	0.0470896
185.13	499,671	24,271	0.0485740
199.92	492,843	24,182	0.0490663
214.71	502,093	24,629	0.0490527
229.5	498,981	24,902	0.0499057
244.28	500,417	24,948	0.0498544
259.07	497,977	25,204	0.0506128
273.86	496,475	25,633	0.0516300
288.65	496,233	25,721	0.0518325
303.44	501,435	26,560	0.0529680
318.23	497,801	26,797	0.0538307
333.01	497,111	27,233	0.0547825
347.8	500,413	27,081	0.0541173
362.59	494,985	27,296	0.0551451
377.38	497,319	27,439	0.0551738
392.17	504,725	27,605	0.0546932
406.95	504,431	28,033	0.0555735
421.74	506,631	28,342	0.0559421
436.53	504,307	28,394	0.0563030
451.32	504,949	29,032	0.0574949
466.11	511,999	29,787	0.0581778
480.89	507,825	29,285	0.0576675
495.68	508,967	29,661	0.0582769
510.47	512,463	29,116	0.0568158
525.39	509,615	29,566	0.0580163
540.18	511,865	30,047	0.0587010
554.97	510,273	30,207	0.0591977
569.76	508,543	30,502	0.0599792
584.54	509,931	30,458	0.0597297
599.33	513,889	30,725	0.0597892

Sputter Time (seconds)	Si Signal Amplitude	B Signal Amplitude	B/Si Amplitude Ratio
614.12	514,325	30,778	0.0598415
628.91	513,735	30,929	0.0602042
643.7	517,475	30,837	0.0595913
658.49	516,095	30,890	0.0598533
673.27	520,801	31,603	0.0606815
688.06	518,659	31,884	0.0614739
702.85	522,569	32,314	0.0618368
717.64	524,215	33,040	0.0630276
732.43	520,181	32,234	0.0619669
747.21	529,193	33,451	0.0632113
762.02	531,991	33,624	0.0632041
776.81	530,469	33,967	0.0640320
791.6	529,515	34,332	0.0648367
806.38	528,075	34,637	0.0655911
821.17	536,787	34,785	0.0648022
835.96	539,223	35,536	0.0659022
850.75	542,347	35,704	0.0658324
865.54	546,905	36,017	0.0658560
880.32	544,371	36,011	0.0661516
895.11	543,769	37,051	0.0681374
909.9	548,033	36,682	0.0669339
924.69	548,355	38,109	0.0694970
939.48	545,575	38,143	0.0699134
954.26	551,075	38,378	0.0696421
969.05	549,393	38,639	0.0703303
983.84	560,584	38,678	0.0689959
998.63	569,013	40,060	0.0704026
1013.42	569,689	39,919	0.0700716
1028.37	576,775	40,246	0.0697776
1043.16	576,377	40,014	0.0694233
1057.95	570,755	40,103	0.0702631
1072.73	578,933	40,159	0.0693673
1087.52	574,111	40,342	0.0702686
1102.31	573,095	40,716	0.0710458
1117.1	573,631	41,341	0.0720690
1131.89	579,869	41,701	0.0719145
1146.68	581,103	41,248	0.0709823
1161.46	574,963	42,505	0.0739265
1176.25	576,039	42,004	0.0729187
1191.04	582,747	42,740	0.0733423
1205.83	579,489	42,922	0.0740687

CS02 - F: 1100°C Anneal Temperature (continued)

Sputter Time (seconds)	Si Signal Amplitude	B Signal Amplitude	B/Si Amplitude Ratio
1220.62	582,147	43,286	0.0743558
1235.4	582,511	42,930	0.0736982
1250.19	587,531	43,050	0.0732727
1264.98	586,489	42,906	0.0731574
1279.77	591,257	44,142	0.0746579
1294.56	591,729	44,378	0.0749972
1309.34	594,355	43,969	0.0739777
1324.13	598,757	43,694	0.0729745
1338.92	600,009	44,182	0.0736356
1353.71	599,157	44,691	0.0745898
1368.5	602,287	44,822	0.0744197
1383.29	604,465	44,447	0.0735311
1398.07	605,685	45,015	0.0743208
1412.86	608,039	45,261	0.0744377
1427.65	605,461	45,427	0.0750288
1442.44	600,117	45,609	0.0760002
1457.22	602,453	46,171	0.0766383
1472.01	597,137	46,429	0.0777527
1486.8	593,193	45,221	0.0762332
1501.61	599,623	46,140	0.0769483
1516.62	600,579	45,748	0.0761732
1531.4	599,087	46,816	0.0781456
1546.19	605,101	46,641	0.0770797
1560.98	602,137	46,713	0.0775787
1575.77	600,685	47,024	0.0782840
1590.56	602,179	45,987	0.0763677
1605.34	600,095	46,781	0.0779560
1620.13	602,304	46,565	0.0773115
1634.92	606,531	47,215	0.0778443
1649.71	606,177	47,041	0.0776027
1664.5	604,739	47,438	0.0784438
1679.28	602,069	46,676	0.0775260
1694.07	598,607	47,418	0.0792139
1708.86	604,775	47,569	0.0786557
1723.65	596,103	47,714	0.0800432
1738.44	596,687	47,235	0.0791621
1753.22	604,579	46,884	0.0775482
1768.01	597,549	46,952	0.0785743
1782.8	607,699	47,023	0.0773788
1797.59	606,855	47,486	0.0782493
1812.38	596,933	47,156	0.0789971
1827.17	599,375	47,143	0.0786536
1841.95	601,045	47,585	0.0791704

Sputter Time (seconds)	Si Signal Amplitude	B Signal Amplitude	B/Si Amplitude Ratio
1856.74	600,309	47,692	0.0794458
1871.53	599,511	47,352	0.0789844
1886.32	603,985	47,858	0.0792371
1901.11	603,845	47,674	0.0789507
1915.89	602,589	47,506	0.0788365
1930.68	598,028	47,928	0.0801434
1945.47	597,623	48,042	0.0803885
1960.26	597,865	47,935	0.0801770
1975.05	600,437	47,637	0.0793372
1989.83	598,063	48,322	0.0807975
2004.62	599,849	47,736	0.0795800
2019.69	600,783	48,030	0.0799457
2034.47	597,457	47,519	0.0795354
2049.26	596,537	48,363	0.0810729
2064.05	590,909	48,347	0.0818180
2078.84	592,739	48,016	0.0810070
2093.63	598,651	48,620	0.0812159
2108.41	596,429	48,875	0.0819460
2123.2	600,633	48,279	0.0803802
2137.99	592,707	47,929	0.0808646
2152.78	594,665	47,618	0.0800753
2167.57	596,951	47,470	0.0795208
2182.36	603,413	48,009	0.0795624
2197.14	594,701	47,168	0.0793138
2211.93	598,599	48,093	0.0803426
2226.72	591,303	47,645	0.0805763
2241.53	588,389	47,118	0.0800797
2256.31	597,003	47,225	0.0791035
2271.1	594,781	47,058	0.0791182
2285.89	597,307	46,778	0.0783148
2300.68	597,523	47,050	0.0787417
2315.47	598,253	46,394	0.0775491
2330.26	602,523	46,965	0.0779472
2345.04	602,443	46,810	0.0777003
2359.83	605,311	47,020	0.0776791
2374.62	599,233	46,186	0.0770752
2389.41	599,547	46,871	0.0781774
2404.2	602,459	47,194	0.0783356
2418.98	596,961	47,285	0.0792095
2433.77	597,781	46,294	0.0774431
2448.56	596,159	46,778	0.0784656
2463.35	600,414	46,260	0.0770468
2478.14	596,155	46,540	0.0780669

CS02 - F: 1100°C Anneal Temperature (continued)

Sputter Time (seconds)	Si Signal Amplitude	B Signal Amplitude	B/Si Amplitude Ratio
2492.93	596,931	45,441	0.0761244
2507.71	595,043	46,193	0.0776297
2522.83	597,699	45,591	0.0762775
2537.62	598,741	45,386	0.0758024
2552.41	601,081	45,792	0.0761827
2567.2	598,499	46,016	0.0768857
2581.99	597,871	45,202	0.0756049
2596.77	595,489	45,232	0.0759577
2611.56	596,729	45,305	0.0759222
2626.35	598,233	45,138	0.0754522
2641.14	593,449	45,488	0.0766502
2655.93	595,151	44,252	0.0743542
2670.72	594,679	45,435	0.0764026
2685.5	592,205	44,832	0.0757035
2700.29	591,702	44,405	0.0750462
2715.08	597,697	44,481	0.0744207
2729.87	593,283	44,400	0.0748378
2744.66	595,731	44,439	0.0745957
2759.44	589,929	44,091	0.0747395
2774.23	586,411	43,579	0.0743148
2789.02	586,113	43,941	0.0749702
2803.81	586,415	43,625	0.0743927
2818.6	588,605	43,690	0.0742263
2833.39	586,719	43,413	0.0739928
2848.17	582,109	43,244	0.0742885
2862.96	582,077	42,950	0.0737875
2877.75	587,685	42,867	0.0729421
2892.54	587,427	42,759	0.0727903
2907.33	591,025	42,444	0.0718142
2922.11	590,099	43,246	0.0732860
2936.9	583,945	42,917	0.0734949
2951.69	587,479	42,946	0.0731022
2966.48	589,505	43,131	0.0731648
2981.28	594,167	42,883	0.0721733
2996.07	592,125	42,958	0.0725489
3010.86	584,143	42,592	0.0729137
3026.04	588,463	42,053	0.0714624
3040.83	589,371	42,080	0.0713982
3055.61	586,143	42,196	0.0719893
3070.4	589,963	42,329	0.0717486
3085.19	593,731	42,851	0.0721724
3099.98	589,331	42,512	0.0721360
3114.77	592,649	41,983	0.0708396
3129.55	589,045	42,460	0.0720828
3144.34	589,785	41,826	0.0709174
3159.13	591,677	41,829	0.0706957
3173.92	592,429	42,272	0.0713537
3188.71	587,997	41,516	0.0706058
3203.5	586,134	42,130	0.0718778
3218.28	586,862	42,159	0.0718380
3233.07	583,789	41,113	0.0704244
3247.86	587,015	41,536	0.0707580
3262.65	589,943	40,847	0.0692389
3277.44	589,299	41,217	0.0699424
3292.22	585,547	41,426	0.0707475
3307.01	587,295	41,136	0.0700432
3321.8	582,245	40,650	0.0698160
3336.59	591,825	41,020	0.0693110
3351.38	589,569	40,712	0.0690538
3366.17	586,945	40,058	0.0682483
3380.95	586,215	40,072	0.0683572
3395.74	586,983	40,044	0.0682200
3410.53	589,473	40,582	0.0688445
3425.32	583,641	40,276	0.0690082
3440.11	589,431	39,851	0.0676093
3454.89	588,789	39,479	0.0670512
3469.68	583,467	39,150	0.0670989
3484.47	583,439	39,421	0.0675666
3499.26	585,985	39,689	0.0677304
3514.05	585,111	39,474	0.0674641
3529.28	587,575	39,321	0.0669208
3544.07	582,007	39,380	0.0676624
3558.85	587,995	39,351	0.0669240
3573.64	584,527	39,004	0.0667275
3588.43	582,045	38,963	0.0669416
3603.22	587,229	39,143	0.0666571
3618.01	576,727	38,683	0.0670733
3632.8	587,135	38,779	0.0660478
3647.58	581,323	38,274	0.0658395
3662.37	579,585	38,687	0.0667495
3677.16	585,901	39,232	0.0669601
3691.95	588,175	38,753	0.0658869
3706.74	590,623	39,166	0.0663130
3721.54	587,157	38,459	0.0655004
3736.33	586,713	38,240	0.0651767
3751.12	579,599	38,473	0.0663787

CS02 - F: 1100°C Anneal Temperature (continued)

Sputter Time (seconds)	Si Signal Amplitude	B Signal Amplitude	B/Si Amplitude Ratio
3765.91	583,841	38,245	0.0655058
3780.7	588,713	38,125	0.0647599
3795.48	589,455	37,590	0.0637708
3810.27	580,405	37,821	0.0651631
3825.06	587,359	37,227	0.0633803
3839.85	580,511	37,984	0.0654320
3854.64	582,016	37,263	0.0640240
3869.42	582,133	36,813	0.0632381
3884.21	583,045	36,732	0.0630003
3899	583,993	36,580	0.0626377
3913.79	582,621	36,492	0.0626342
3928.58	581,773	36,409	0.0625828
3943.37	587,595	36,431	0.0620002
3958.15	582,309	35,879	0.0616151
3972.94	578,627	36,279	0.0626984
3987.73	583,197	35,864	0.0614955
4002.52	584,039	35,581	0.0609223
4017.8	575,185	35,147	0.0611056
4032.59	583,461	35,174	0.0602851
4047.38	584,571	35,827	0.0612877
4062.17	582,109	35,441	0.0608838
4076.96	577,201	35,419	0.0613634
4091.74	583,384	35,281	0.0604765
4106.53	576,611	35,966	0.0623748
4121.32	579,267	35,432	0.0611670
4136.11	580,635	35,370	0.0609161
4150.9	579,850	35,337	0.0609416
4165.69	576,041	35,052	0.0608498
4180.47	580,679	35,442	0.0610354
4195.26	585,443	35,167	0.0600690
4210.05	581,819	34,586	0.0594446
4224.84	585,167	34,253	0.0585354
4239.63	582,195	34,870	0.0598940
4254.42	585,835	34,820	0.0594365
4269.2	585,375	34,308	0.0586086
4283.99	586,635	34,901	0.0594936
4298.78	579,621	34,260	0.0591076
4313.57	586,029	33,937	0.0579101
4328.36	590,509	33,982	0.0575470
4343.14	586,716	35,145	0.0599012
4357.93	587,966	34,152	0.0580850
4371.9	470,054	27,373	0.0582337
4385.86	583,311	34,116	0.0584868
4400.65	580,799	33,510	0.0576964
4415.44	585,293	34,358	0.0587022
4430.23	579,713	33,867	0.0584203
4445.02	582,909	33,392	0.0572851
4459.82	581,715	33,623	0.0577998
4474.61	584,181	33,580	0.0574822
4489.4	578,381	33,440	0.0578166
4504.19	581,847	33,748	0.0580015
4519.53	578,947	33,099	0.0571710
4534.32	582,517	33,026	0.0566953
4549.11	580,743	33,453	0.0576038
4563.89	581,993	32,744	0.0562618
4578.68	586,927	32,486	0.0553493
4593.47	582,899	32,728	0.0561469
4608.26	575,639	32,454	0.0563791
4623.05	577,119	32,993	0.0571685
4637.83	579,327	32,529	0.0561496
4652.62	583,587	32,095	0.0549961
4667.41	585,701	32,178	0.0549393
4682.2	580,937	32,035	0.0551437
4696.99	577,981	31,995	0.0553565
4711.78	581,455	32,087	0.0551840
4726.56	586,561	32,072	0.0546780
4741.35	586,177	31,400	0.0535674
4756.14	583,919	31,907	0.0546429
4770.93	584,963	31,383	0.0536495
4785.72	573,317	31,310	0.0546120
4800.51	581,159	31,128	0.0535619
4815.29	584,493	30,965	0.0529775
4830.08	579,389	31,116	0.0537049
4844.87	578,277	31,095	0.0537718
4859.66	581,443	31,462	0.0541102
4874.45	580,889	30,812	0.0530428
4889.24	578,561	31,726	0.0548361
4904.02	578,041	30,635	0.0529980
4918.81	581,973	30,722	0.0527894
4933.6	577,187	30,918	0.0535667
4948.39	574,109	30,325	0.0528210
4963.18	579,827	30,943	0.0533659
4977.96	580,099	30,634	0.0528082
4992.75	577,973	30,219	0.0522844
5007.54	581,277	30,256	0.0520509
5022.94	585,929	29,931	0.0510830

CS02 - F: 1100°C Anneal Temperature (continued)

Sputter Time (seconds)	Si Signal Amplitude	B Signal Amplitude	B/Si Amplitude Ratio
5037.73	580,439	29,806	0.0513508
5052.51	574,029	29,552	0.0514817
5067.3	580,713	29,670	0.0510924
5082.09	578,719	29,319	0.0506619
5096.88	577,127	29,026	0.0502940
5111.67	577,003	29,438	0.0510188
5126.45	577,715	29,279	0.0506807
5141.24	573,035	29,049	0.0506932
5156.03	576,092	29,457	0.0511325
5170.82	577,081	29,320	0.0508074
5185.61	578,003	29,179	0.0504824
5200.41	577,055	28,811	0.0499277
5215.2	579,853	29,158	0.0502852
5229.99	576,279	28,754	0.0498960
5244.78	578,472	28,463	0.0492038
5259.57	575,163	28,104	0.0488627
5274.36	578,903	28,260	0.0488165
5289.14	574,139	28,393	0.0494532
5303.93	577,583	28,199	0.0488224
5318.72	573,165	28,165	0.0491394
5333.51	578,351	28,155	0.0486815
5348.3	574,617	27,760	0.0483104
5363.09	574,733	27,541	0.0479196
5377.87	576,288	27,373	0.0474988
5392.66	574,359	27,808	0.0484157
5407.45	572,353	27,244	0.0476000
5422.24	574,599	27,336	0.0475740
5437.03	577,857	27,430	0.0474685
5451.81	579,141	26,886	0.0464239
5466.6	576,683	26,895	0.0466374
5481.39	581,241	26,956	0.0463766
5496.18	578,565	26,833	0.0463785
5510.97	572,293	25,806	0.0450923
5526.42	572,067	26,568	0.0464421
5541.21	573,895	26,332	0.0458830
5556	570,681	26,394	0.0462500
5570.79	574,721	26,473	0.0460624
5585.57	569,689	26,016	0.0456670
5600.36	576,539	25,781	0.0447168
5615.15	568,579	26,259	0.0461836
5629.94	571,081	25,781	0.0451442
5644.73	571,639	25,774	0.0450879
5659.51	571,193	25,476	0.0446014

Sputter Time (seconds)	Si Signal Amplitude	B Signal Amplitude	B/Si Amplitude Ratio
5674.3	581,865	24,969	0.0429120
5689.09	581,627	25,187	0.0433044
5703.88	577,665	24,957	0.0432032
5718.67	579,077	24,929	0.0430495
5733.46	580,223	24,971	0.0430369
5748.24	579,237	25,159	0.0434347
5763.03	580,057	24,572	0.0423614
5777.82	575,159	24,801	0.0431203
5792.61	575,773	24,560	0.0426557
5807.4	572,361	24,560	0.0429100
5822.19	579,405	24,542	0.0423572
5836.97	580,365	24,217	0.0417272
5851.76	577,025	24,471	0.0424089
5866.55	575,559	23,934	0.0415839
5881.34	576,549	23,907	0.0414657
5896.13	576,699	23,479	0.0407127
5910.92	584,997	23,956	0.0409506
5925.7	589,373	23,231	0.0394165
5940.51	581,431	23,225	0.0399446
5955.3	587,181	22,995	0.0391617
5970.09	588,385	22,950	0.0390051
5984.88	583,199	22,841	0.0391650
5999.66	587,451	22,668	0.0385870
6014.45	586,159	22,757	0.0388239
6029.96	587,409	22,267	0.0379071
6044.75	585,943	22,096	0.0377102
6059.54	588,212	22,254	0.0378333
6074.33	581,393	22,027	0.0378866
6089.11	580,273	21,951	0.0378287
6103.9	586,809	21,957	0.0374176
6118.69	587,539	21,720	0.0369678
6133.48	588,961	21,547	0.0365848
6148.27	577,563	21,695	0.0375630
6163.06	582,929	21,234	0.0364264
6177.84	591,557	20,526	0.0346983
6192.63	586,465	21,140	0.0360465
6207.42	587,131	20,803	0.0354316
6222.21	581,579	20,715	0.0356185
6237	576,483	20,672	0.0358588
6251.78	581,175	20,324	0.0349705
6266.57	588,517	19,948	0.0338954
6281.36	586,851	19,736	0.0336303
6296.15	587,895	19,706	0.0335196

CS02 - F: 1100°C Anneal Temperature (continued)

Sputter Time (seconds)	Si Signal Amplitude	B Signal Amplitude	B/Si Amplitude Ratio
6310.94	590,299	20,058	0.0339794
6325.73	579,927	19,691	0.0339543
6340.52	583,359	19,784	0.0339139
6355.3	582,643	19,620	0.0336741
6370.09	584,998	19,396	0.0331557
6384.88	577,771	19,445	0.0336552
6399.67	580,005	18,928	0.0326342
6414.46	579,239	19,208	0.0331608
6429.24	582,035	19,216	0.0330152
6444.03	586,049	18,834	0.0321372
6458.82	578,557	18,488	0.0319554
6473.61	585,385	18,505	0.0316117
6488.4	582,755	18,469	0.0316926
6503.19	577,963	18,338	0.0317287
6518.75	577,803	17,896	0.0309725
6533.54	582,399	18,017	0.0309358
6548.33	580,257	18,107	0.0312051
6563.11	577,751	17,810	0.0308264
6577.9	576,091	17,442	0.0302765
6592.69	576,747	17,418	0.0302004
6607.48	578,155	17,209	0.0297654
6622.27	575,011	17,221	0.0299490
6637.06	575,337	17,031	0.0296018
6651.84	574,439	16,720	0.0291067
6666.63	573,644	16,666	0.0290529
6681.44	577,299	16,393	0.0283960
6696.23	584,241	16,098	0.0275537
6711.02	574,757	16,425	0.0285773
6725.81	578,587	15,944	0.0275568
6740.59	572,624	15,974	0.0278961
6755.38	576,873	16,084	0.0278814
6770.17	574,397	15,753	0.0274253
6784.96	573,455	15,682	0.0273465
6799.75	570,953	15,583	0.0272930
6814.54	577,641	15,654	0.0270999
6829.32	573,517	15,177	0.0264630
6844.11	581,131	15,289	0.0263090
6858.9	577,703	14,945	0.0258697
6873.69	582,151	14,989	0.0257476
6888.48	572,013	14,820	0.0259085
6903.27	577,261	14,321	0.0248085
6918.05	569,971	14,694	0.0257803
6932.84	571,547	14,162	0.0247784

Sputter Time (seconds)	Si Signal Amplitude	B Signal Amplitude	B/Si Amplitude Ratio
6947.63	567,033	13,699	0.0241591
6962.42	561,465	14,091	0.0250968
6977.21	572,635	13,965	0.0243873
6992	573,187	13,640	0.0237968
7006.78	573,571	13,563	0.0236466
7022.4	575,235	13,214	0.0229715
7037.19	571,967	13,483	0.0235730
7051.98	572,425	13,202	0.0230633
7066.77	570,067	13,475	0.0236376
7081.55	570,427	13,144	0.0230424
7096.34	568,417	12,610	0.0221844
7111.13	565,923	12,182	0.0215259
7125.92	563,400	12,452	0.0221015
7140.71	567,635	12,251	0.0215825
7155.5	569,553	12,210	0.0214379
7170.28	570,449	12,086	0.0211868
7185.07	563,843	12,034	0.0213428
7199.86	562,003	11,587	0.0206173
7214.65	564,315	11,866	0.0210273
7229.44	563,907	11,438	0.0202835
7244.23	564,798	11,674	0.0206693
7259.01	565,785	11,222	0.0198344
7273.8	568,173	11,542	0.0203142
7288.59	566,661	11,408	0.0201320
7303.38	566,777	10,976	0.0193656
7318.17	563,367	10,855	0.0192681
7332.95	564,827	10,433	0.0184711
7347.74	565,469	10,570	0.0186924
7362.53	562,587	10,419	0.0185198
7377.32	564,581	10,678	0.0189131
7392.11	566,057	10,206	0.0180300
7406.9	560,405	10,561	0.0188453
7421.7	560,959	10,071	0.0179532
7436.49	561,431	9,930	0.0176869
7451.28	559,303	10,077	0.0180171
7466.07	562,323	9,707	0.0172623
7480.86	565,815	9,514	0.0168147
7495.65	560,965	9,850	0.0175590
7510.43	558,066	9,630	0.0172560
7526.11	561,999	9,517	0.0169342
7540.9	559,407	9,166	0.0163852
7555.68	562,465	9,061	0.0161094
7570.47	558,275	9,134	0.0163611

CS02 - F: 1100°C Anneal Temperature (continued)

Sputter Time (seconds)	Si Signal Amplitude	B Signal Amplitude	B/Si Amplitude Ratio
7585.26	557,688	8,974	0.0160914
7600.05	563,603	8,967	0.0159101
7614.84	559,547	9,230	0.0164955
7629.63	561,219	8,656	0.0154236
7644.41	557,075	8,655	0.0155365
7659.2	556,119	8,461	0.0152144
7673.99	560,051	8,285	0.0147933
7688.78	564,569	8,425	0.0149229
7703.57	559,803	8,267	0.0147677
7718.36	559,711	8,245	0.0147308
7733.15	562,249	8,207	0.0145967
7747.93	555,527	7,869	0.0141649
7762.72	553,037	8,082	0.0146139
7777.51	551,059	7,814	0.0141800
7792.3	552,630	8,016	0.0145052
7807.09	556,271	7,954	0.0142988
7821.87	557,327	7,593	0.0136240
7836.66	555,923	7,737	0.0139174
7851.45	558,875	7,730	0.0138314
7866.24	549,047	7,327	0.0133449
7881.03	553,727	7,470	0.0134904
7895.82	553,867	7,276	0.0131367
7910.6	546,361	7,049	0.0129017
7925.39	547,205	7,341	0.0134154
7940.18	547,257	7,266	0.0132771
7954.97	548,687	7,000	0.0127577
7969.76	550,379	7,041	0.0127930
7984.55	551,765	7,135	0.0129312
7999.33	546,179	6,856	0.0125527
8014.12	547,127	6,852	0.0125236
8029.85	545,055	6,904	0.0126666
8044.64	546,933	6,950	0.0127072
8059.43	544,847	6,642	0.0121906
8074.22	544,761	6,789	0.0124623
8089.01	540,465	6,712	0.0124189
8103.79	546,742	6,584	0.0120422
8118.58	542,565	6,495	0.0119709
8133.37	540,389	6,463	0.0119599
8148.16	543,625	6,270	0.0115337
8162.97	539,263	6,335	0.0117475
8177.75	541,907	6,260	0.0115518
8192.54	541,577	6,188	0.0114259
8207.33	542,039	6,340	0.0116966

Sputter Time (seconds)	Si Signal Amplitude	B Signal Amplitude	B/Si Amplitude Ratio
8222.12	540,003	6,094	0.0112851
8236.91	534,343	6,047	0.0113167
8251.7	536,513	5,978	0.0111423
8266.48	536,203	5,989	0.0111693
8281.27	539,911	5,691	0.0105406
8296.06	538,300	5,863	0.0108917
8310.85	541,417	5,734	0.0105907
8325.64	537,751	5,811	0.0108061
8340.43	537,867	5,719	0.0106327
8355.22	542,159	5,652	0.0104250
8370	539,903	5,686	0.0105315
8384.79	541,261	5,557	0.0102668
8399.58	537,532	5,465	0.0101668
8414.37	532,343	5,557	0.0104388
8429.16	539,379	5,334	0.0098892
8443.95	536,067	5,375	0.0100267
8458.73	533,161	5,171	0.0096988
8473.52	531,735	5,381	0.0101197
8488.31	531,423	5,339	0.0100466
8503.1	532,067	5,090	0.0095665
8518.88	519,770	5,054	0.0097235
8533.67	514,957	5,098	0.0098999
8548.46	511,569	5,090	0.0099498
8563.25	519,549	5,177	0.0099644
8578.03	521,809	5,213	0.0099902
8592.82	517,345	4,969	0.0096048
8607.61	521,535	4,875	0.0093474
8622.4	518,757	4,866	0.0093801
8637.19	511,262	4,905	0.0095939
8651.97	524,215	4,918	0.0093816
8666.76	519,721	4,756	0.0091511
8681.55	518,333	4,625	0.0089228
8696.34	516,611	4,692	0.0090823
8711.13	508,559	4,576	0.0089980
8725.92	508,265	4,439	0.0087336
8740.71	505,083	4,438	0.0087867
8755.49	509,337	4,242	0.0083285
8770.28	512,953	4,285	0.0083536
8785.07	509,502	4,318	0.0084749
8799.86	506,309	4,260	0.0084138
8814.65	511,801	4,333	0.0084662
8829.44	518,467	4,254	0.0082050
8844.22	508,385	4,268	0.0083952

CS02 - F: 1100°C Anneal Temperature (continued)

Sputter Time (seconds)	Si Signal Amplitude	B Signal Amplitude	B/Si Amplitude Ratio
8859.01	507,979	4,243	0.0083527
8873.8	512,381	4,369	0.0085269
8888.59	504,323	4,346	0.0086175
8903.4	504,773	4,348	0.0086138
8918.19	512,475	4,119	0.0080375
8932.98	511,293	4,104	0.0080267
8947.76	508,979	4,236	0.0083225
8962.55	512,315	4,102	0.0080068
8977.34	505,023	4,132	0.0081818
8992.13	502,453	3,975	0.0079112
9006.92	505,419	3,990	0.0078944
9022.76	498,727	3,810	0.0076395
9037.54	500,761	3,846	0.0076803
9052.33	512,171	3,940	0.0076927
9067.12	507,047	3,772	0.0074392
9081.91	509,939	3,811	0.0074734
9096.7	511,029	3,804	0.0074438
9111.49	502,361	4,003	0.0079684
9126.27	514,385	3,738	0.0072669
9141.06	508,845	3,798	0.0074640
9155.85	505,931	3,827	0.0075643
9170.64	500,707	3,553	0.0070960
9185.43	490,139	3,496	0.0071327
9200.22	484,557	3,408	0.0070332
9215.01	494,321	3,448	0.0069752
9229.79	496,287	3,632	0.0073183
9244.58	488,711	3,584	0.0073336
9259.37	483,053	3,557	0.0073636
9274.16	485,519	3,434	0.0070728
9288.95	482,629	3,330	0.0068997
9303.74	488,409	3,436	0.0070351
9318.52	487,329	3,284	0.0067388
9333.31	482,195	3,307	0.0068582
9348.1	489,341	3,265	0.0066722
9362.89	479,211	3,289	0.0068634
9377.68	482,579	3,183	0.0065958
9392.47	483,185	3,322	0.0068752
9407.26	484,527	3,125	0.0064496
9422.04	477,959	3,181	0.0066554
9436.83	475,671	3,090	0.0064961
9451.62	477,793	3,024	0.0063291
9466.41	476,987	3,054	0.0064027
9481.2	472,517	2,966	0.0062770
9495.99	480,148	2,914	0.0060690
9510.77	475,661	2,985	0.0062755
9526.68	481,607	2,903	0.0060277
9541.47	474,055	3,007	0.0063431
9556.26	478,991	2,894	0.0060419
9571.05	484,697	3,055	0.0063029
9585.84	513,821	2,928	0.0056985
9600.63	510,681	2,926	0.0057296
9615.41	512,491	2,836	0.0055338
9630.2	508,839	2,830	0.0055617
9645.01	509,729	2,875	0.0056403
9659.8	512,097	2,888	0.0056396
9674.59	508,157	2,649	0.0052130
9689.38	517,075	2,839	0.0054905
9704.17	512,879	2,765	0.0053911
9718.95	513,141	2,780	0.0054176
9733.74	510,561	2,610	0.0051120
9748.53	498,707	2,730	0.0054742
9763.32	512,667	2,632	0.0051339
9778.11	506,197	2,640	0.0052154
9792.9	507,549	2,577	0.0050773
9807.68	504,619	2,636	0.0052237
9822.47	506,049	2,879	0.0056892
9837.26	496,205	2,606	0.0052519
9852.05	496,835	2,468	0.0049674
9866.84	502,029	2,511	0.0050017
9881.63	502,143	2,482	0.0049428
9896.42	502,221	2,409	0.0047967
9911.2	499,437	2,509	0.0050237
9925.99	498,233	2,461	0.0049395
9940.78	500,761	2,475	0.0049425
9955.57	504,511	2,546	0.0050465
9970.36	508,521	2,405	0.0047294
9985.15	503,793	2,360	0.0046845
9999.93	499,111	2,334	0.0046763
10014.72	490,019	2,605	0.0053161
10030.66	494,525	2,337	0.0047257
10045.45	493,701	2,345	0.0047498
10060.24	486,639	2,435	0.0050037
10075.03	493,909	2,320	0.0046972
10089.82	492,093	2,253	0.0045784
10104.61	499,676	2,146	0.0042948
10119.4	501,649	2,291	0.0045669

CS02 - F: 1100°C Anneal Temperature (continued)

Sputter Time (seconds)	Si Signal Amplitude	B Signal Amplitude	B/Si Amplitude Ratio
10134.18	496,217	2,331	0.0046975
10148.97	494,973	2,466	0.0049821
10163.76	496,165	2,095	0.0042224
10178.55	491,610	2,365	0.0048107
10193.34	495,221	2,291	0.0046262
10208.13	503,783	2,238	0.0044424
10222.92	485,743	2,277	0.0046877
10237.7	489,627	2,167	0.0044258
10252.49	491,053	2,259	0.0046003
10267.28	495,351	2,299	0.0046412
10282.07	492,017	2,044	0.0041543
10296.86	502,065	2,390	0.0047603
10311.65	488,937	2,173	0.0044443
10326.43	492,985	2,059	0.0041766
10341.22	491,033	2,078	0.0042319
10356.01	490,858	2,055	0.0041865
10370.8	496,029	2,073	0.0041792
10385.61	500,559	1,991	0.0039776
10400.4	489,109	2,100	0.0042935
10415.19	486,565	1,924	0.0039543
10429.97	490,077	2,073	0.0042299
10444.76	494,949	2,012	0.0040651
10459.55	501,433	1,904	0.0037971
10474.34	495,751	2,028	0.0040908
10489.13	488,344	1,907	0.0039050
10503.92	500,886	1,934	0.0038612
10519.92	497,309	1,897	0.0038145
10534.71	499,481	1,876	0.0037559
10549.49	494,981	1,873	0.0037840
10564.28	497,995	1,924	0.0038635
10579.07	501,333	2,091	0.0041709
10593.86	497,705	1,884	0.0037854
10608.65	487,077	1,788	0.0036709
10623.44	493,736	1,799	0.0036436
10638.22	491,533	1,814	0.0036905
10653.01	489,343	1,777	0.0036314
10667.8	487,427	1,812	0.0037175
10682.59	490,045	1,844	0.0037629
10697.38	483,167	1,713	0.0035454
10712.17	485,195	1,873	0.0038603
10726.96	492,849	1,845	0.0037435
10741.74	487,381	1,785	0.0036624
10756.53	486,907	1,766	0.0036270
10771.32	490,017	1,771	0.0036142

Sputter Time (seconds)	Si Signal Amplitude	B Signal Amplitude	B/Si Amplitude Ratio
10786.11	487,675	1,601	0.0032829
10800.9	493,201	1,667	0.0033800
10815.69	486,603	1,725	0.0035450
10830.48	493,851	1,842	0.0037299
10845.26	493,171	1,808	0.0036661
10860.05	490,743	1,663	0.0033887
10874.84	486,935	1,733	0.0035590
10889.63	482,207	1,826	0.0037868
10904.42	483,361	1,614	0.0033391
10919.21	490,365	1,653	0.0033710
10934	489,461	1,647	0.0033649
10948.78	478,929	1,700	0.0035496
10963.57	490,125	1,721	0.0035113
10978.36	486,045	1,576	0.0032425
10993.15	489,729	1,607	0.0032814
11007.94	496,287	1,720	0.0034657
11023.99	489,113	1,542	0.0031526
11038.78	491,297	1,585	0.0032262
11053.57	492,519	1,542	0.0031308
11068.36	490,471	1,502	0.0030624
11083.15	487,603	1,546	0.0031706
11097.94	489,567	1,604	0.0032764
11112.73	490,501	1,531	0.0031213
11127.54	485,455	1,729	0.0035616
11142.32	482,825	1,654	0.0034257
11157.11	481,187	1,601	0.0033272
11171.9	473,579	1,683	0.0035538
11186.69	484,703	1,675	0.0034557
11201.48	483,568	1,704	0.0035238
11216.27	484,913	1,630	0.0033614
11231.06	477,668	1,622	0.0033957
11245.84	481,697	1,556	0.0032302
11260.63	471,899	1,729	0.0036639
11275.42	479,923	1,659	0.0034568
11290.21	477,519	1,634	0.0034219
11305	477,993	1,834	0.0038369
11319.79	478,805	1,809	0.0037782
11334.58	472,103	1,648	0.0034908
11349.36	491,143	1,548	0.0031518
11364.15	486,647	1,534	0.0031522
11378.94	489,445	1,595	0.0032588
11393.73	480,988	1,541	0.0032038
11408.52	480,066	1,618	0.0033704
11423.95	475,791	1,591	0.0033439

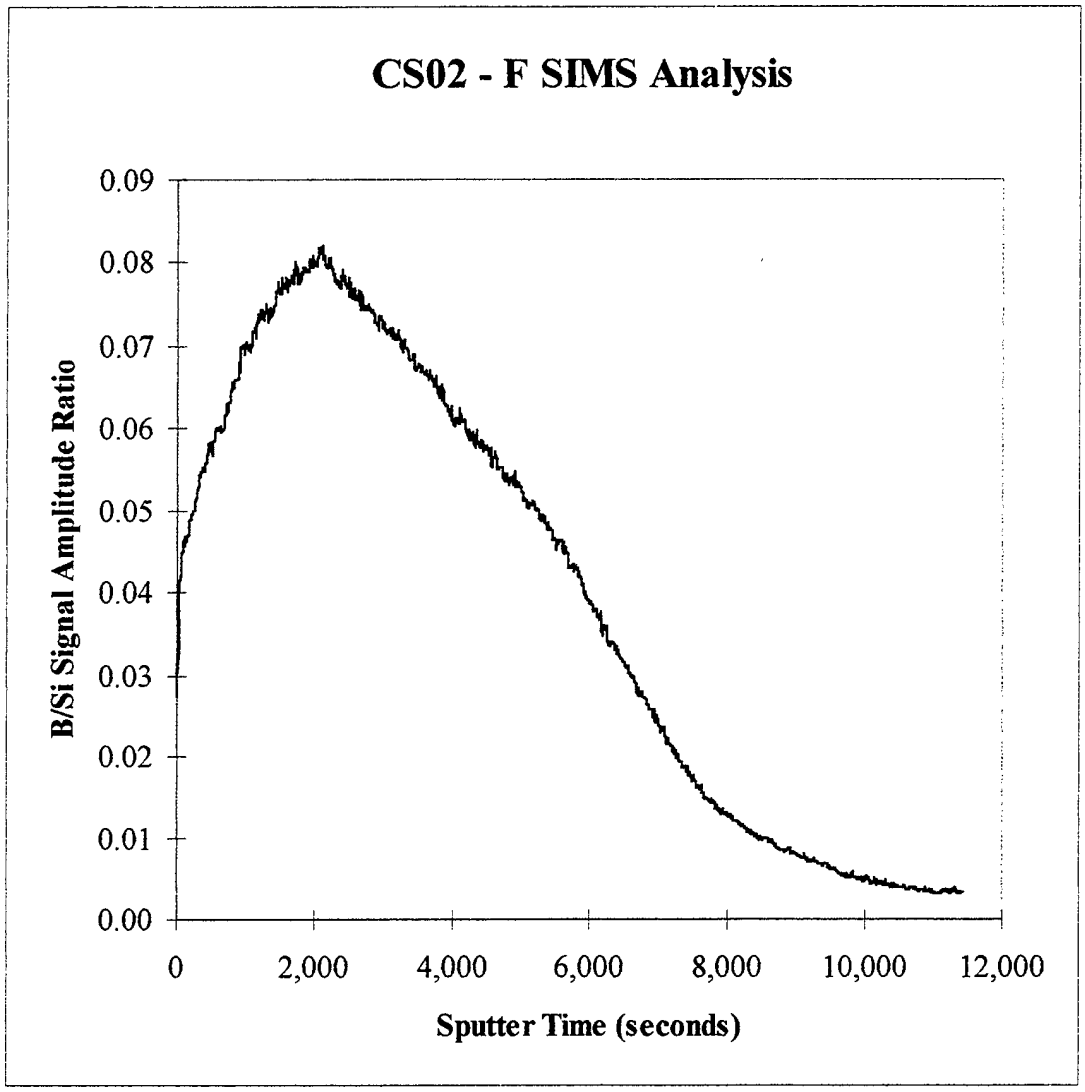
CS02 - F SIMS Analysis
B/Si Signal Amplitude Ratio
0.09
0.08
0.07
0.06
0.05
0.04
0.03
0.02
0.01
0.00
0
2,000
4,000
6,000
8,000
10,000
12,000
Sputter Time (seconds)

BIBLIOGRAPHY

J. M. Baribeau and S. J. Rolfe, "Characterization of Boron-Doped Silicon Epitaxial Layers by X-ray Diffraction," Appl. Phys. Lett., vol. 58, pp. 2129-2131, 1991.

C. Cabuz, K. Fukatsu, T. Kurabayashi, K. Minami and M. Esashi, "Microphysical Investigations on Mechanical Structures Realized in p+ Silicon," Journal of Microelectromechanical Systems, vol. 4, pp. 109-117, 1995.

W. Chu and M. Mehregany, "A Study of Residual Stress Distribution Through the Thickness of p+ Silicon Films," IEEE Transactions on Electron Devices, vol. 40, pp. 1245-1250, 1993.

X. Ding, W. H. Ko and J. M. Mansour, "Residual Stress and Mechanical Properties of Boron-Doped p+ Silicon Films," Sensors and Actuators, vol. A21-A23, pp. 866-871, 1990.

J. W. Edington, Practical Electron Microscopy in Materials Science, N. V. Philips' Gloeilampenfabrieken, sections 2 and 3, 1976.

V. N. Erofeev and V. I. Nikitenko, "Mobility of Dislocations in Silicon Containing Substitutional and Interstitial Impurities," Sov. Phys. - Solid State, vol. 13, pp. 116-120, 1971.

R. B. Fair, "Boron Diffusion in Silicon - Concentration and Orientation Dependence, Background Effects, and Profile Estimation," J. Electrochem. Soc., vol. 122, pp. 800-805, 1975.

H. Holloway, "Curvature in Boron-Doped Silicon and Other Compositionally Graded Single Crystals," J. Appl. Phys., vol. 75, pp. 2297-2299, 1994.

H. Holloway and S. L. McCarthy, "Determination of the Lattice Contraction of Boron-Doped Silicon," J. Appl. Phys., vol. 73, pp. 103-111, 1993.

A. M. Lin, D. A. Antoniadis and R. W. Dutton, "The Oxidation Rate Dependence of Oxidation-Enhanced Diffusion of Boron and Phosphorus in Silicon," J. Electrochem. Soc.: Solid-State Science and Technology, vol. 128, pp. 1131-1137, 1981.

S. Lippold and J. Podlesny, WYKO Surface Profilers Technical Reference Manual, WYKO Coporation, p. 1-3, 1995.

X. J. Ning and P. Pirouz, "Dislocations in Heavily Boron-Doped Silicon," Institute of Physics Conference Series, vol. 117, pp. 205-210, 1991.

X. J. Ning, P. Pirouz, M. Mehregany and W. Chu, "Cross-Sectional TEM Studies of Heavily Boron Doped Silicon," TRANSDUCERS '91. 1991 International Conference on Solid-State Sensors and Actuators. Digest of Technical Papers, pp. 755-758, 1991.

K. E. Peterson, "Silicon as a Mechanical Material," Proc. IEEE, vol. 70, pp. 420-456, 1982.

S. Prussin, "Generation and Distribution of Dislocations by Solute Diffusion," J. Appl. Phys., vol. 32, pp. 1876-1881, 1961.

N. D. Thai, "Concentration-Dependent Diffusion of Boron and Phosphorus in Silicon," J. Appl. Phys., vol. 41, pp. 2859-2866, 1970.

J. Wang, Q. Xu, F. Lu, H. Sun and X. Wang, "Effects of Rapid Thermal Annealing on Heavily Boron Doped Silicon Epitaxial Layers," Mat. Res. Soc. Symp. Proc., vol. 355, pp. 637-642, 1995.

J. Wang, Q. Xu, J. Yuan, F. Lu and H. Sun, "Effect of Rapid Thermal Annealing on the Strain Relaxation in Heavily Boron Doped Silicon Epitaxial Layer," J. Appl. Phys., vol. 77, pp. 2974-2977, 1995.

J. Washburn, G. Thomas and H. J. Queisser, "Diffusion-Induced Dislocations in Silicon," J. Appl. Phys., vol. 35, pp. 1909-1914, 1964.

S. Wolf and R. N. Tauber, Silicon Processing for the VLSI Era, Volume 1: Process Technology, Lattice Press, p. 244, 1986.

REFERENCES

1. K. E. Peterson, "Silicon as a Mechanical Material," Proc. IEEE, vol. 70, pp. 420-456, 1982.

2. H. Holloway and S. L. McCarthy, "Determination of the Lattice Contraction of Boron-Doped Silicon," J. Appl. Phys., vol. 73, pp. 103-111, 1993.

3. S. Wolf and R. N. Tauber, Silicon Processing for the VLSI Era, Volume 1: Process Technology, Lattice Press, p. 244, 1986.

4. N. D. Thai, "Concentration-Dependent Diffusion of Boron and Phosphorus in Silicon," J. Appl. Phys., vol. 41, pp. 2859-2866, 1970.

5. R. B. Fair, "Boron Diffusion in Silicon - Concentration and Orientation Dependence, Background Effects, and Profile Estimation," J. Electrochem. Soc., vol. 122, pp. 800-805, 1975.

6. A. M. Lin, D. A. Antoniadis and R. W. Dutton, "The Oxidation Rate Dependence of Oxidation-Enhanced Diffusion of Boron and Phosphorus in Silicon," J. Electrochem. Soc.: Solid-State Science and Technology, vol. 128, pp. 1131-1137, 1981.

7. K. Wu, Unpublished Data - MIT Department of Materials Science and Engineering.

8. S. Prussin, "Generation and Distribution of Dislocations by Solute Diffusion," J. Appl. Phys., vol. 32, pp. 1876-1881, 1961.

9. J. Washburn, G. Thomas and H. J. Queisser, "Diffusion-Induced Dislocations in Silicon," J. Appl. Phys., vol. 35, pp. 1909-1914, 1964.

10. X. J. Ning and P. Pirouz, "Dislocations in Heavily Boron-Doped Silicon," Institute of Physics Conference Series, vol. 117, pp. 205-210, 1991.

11. X. J. Ning, P. Pirouz, M. Mehregany and W. Chu, "Cross-Sectional TEM Studies of Heavily Boron Doped Silicon," TRANSDUCERS '91. 1991 International Conference on Solid-State Sensors and Actuators. Digest of Technical Papers, pp. 755-758, 1991.

12. V. N. Erofeev and V. I. Nikitenko, "Mobility of Dislocations in Silicon Containing Substitutional and Interstitial Impurities," Sov. Phys. - Solid State, vol. 13, pp. 116-120, 1971.

13. J. M. Baribeau and S. J. Rolfe, "Characterization of Boron-Doped Silicon Epitaxial Layers by X-ray Diffraction," Appl. Phys. Lett., vol. 58, pp. 2129-2131, 1991.

14. X. Ding, W. H. Ko and J. M. Mansour, "Residual Stress and Mechanical Properties of Boron-Doped p+ Silicon Films," Sensors and Actuators, vol. A21-A23, pp. 866-871, 1990.

15. W. Chu and M. Mehregany, "A Study of Residual Stress Distribution Through the Thickness of p+ Silicon Films," IEEE Transactions on Electron Devices, vol. 40, pp. 1245-1250, 1993.

16. H. Holloway, "Curvature in Boron-Doped Silicon and Other Compositionally Graded Single Crystals," J. Appl. Phys., vol. 75, pp. 2297-2299, 1994.

17. J. Wang, Q. Xu, F. Lu, H. Sun and X. Wang, "Effects of Rapid Thermal Annealing on Heavily Boron Doped Silicon Epitaxial Layers," Mat. Res. Soc. Symp. Proc., vol. 355, pp. 637-642, 1995.

18. J. Wang, Q. Xu, J. Yuan, F. Lu and H. Sun, "Effect of Rapid Thermal Annealing on the Strain Relaxation in Heavily Boron Doped Silicon Epitaxial Layer," J. Appl. Phys., vol. 77, pp. 2974-2977, 1995.

19. C. Cabuz, K. Fukatsu, T. Kurabayashi, K. Minami and M. Esashi, "Microphysical Investigations on Mechanical Structures Realized in p+ Silicon," Journal of Microelectromechanical Systems, vol. 4, pp. 109-117, 1995.

20. S. Lippold and J. Podlesny, WYKO Surface Profilers Technical Reference Manual, WYKO Coporation, p. 1-3, 1995.

21. J. W. Edington, Practical Electron Microscopy in Materials Science, N. V. Philips' Gloeilampenfabrieken, sections 2 and 3, 1976.